UNIVERSITÉ DE SHERBROOKE
Faculté de génie
Département de génie civil

SEISMIC BEHAVIOR OF HYDRO- QUÉBEC ACCESS UNDERGROUND STRUCTURES IN LIQUEFIABLE SOIL

Comportement Sismique Des Structures Souterraines D'accès D'Hydro-Québec Dans Le Sol Liquéfiable

by

Ahmed Omar Kamel MAHMOUD

A dissertation submitted in partial fulfillment
of the requirements for the degree of
Doctor of Philosophy
Civil Engineering
(Geotechnical Engineering)

Thèse de doctorat
Génie civil

Sherbrooke (Québec), Canada

January 2020

MEMBRES DU JURY

Prof. Mourad KARRAY
Directeur

Prof. Mathieu NUTH
Rapporteur

Simon GRENIER ING., Ph.D.
Évaluateur

Mahmoud N. HUSSIEN ING., Ph.D.
Évaluateur

RÉSUMÉ

Les réseaux de transport, de communication et d'énergie deviennent de plus en plus complexes. La possibilité que deux réseaux ou plus occupent une même emprise ou se croisent augmente à mesure que les réseaux se développent. En raison de ce problème, les gouvernements ont commencé à passer du transfert de ces services du sol vers le sous-sol par le biais de canaux souterrains qui se croisent dans des structures enterrées. L'entretien et le remplacement de cette structure sont très coûteux et peuvent dépasser le coût de sa construction. Par conséquent, l'étude et la protection de ces structures souterraines des risques potentiels devient impératif afin de les préserver. Le risque sismique est l'un des risques les plus importants. Il pourrait endommager ces structures et les mettre hors de service. En effet, de grands tremblements de terre pourraient faire flotter ou fissurer ces structures. Dans cette étude, des modèles numériques de différences finies (FD) de structures souterraines typiques enfouies dans des sols sableux ont été construits en adoptant l'approche à base d'énergie en tant que modèle constitutif de sol à l'aide du code informatique FLAC^{3D}. Le modèle numérique a été validé par comparaison entre les différents résultats expérimentaux antérieurs. La présente étude est consacrée à l'étude de la performance des structures souterraines sous charges sismiques compatibles avec les cinq zones sismiques du Québec. De plus, trois séismes différents en termes de contenu fréquentiel, ont été utilisés pour étudier l'effet du contenu fréquentiel dans le sol et le comportement de la structure. De plus, deux cas d'étude ont été simulés pour étudier le comportement sismique sous un séisme réaliste compatible avec le Code national du bâtiment du Canada de 2015. Le comportement sismique de la structure comprenait la réponse à l'accélération, la pression de l'eau interstitiel, le déplacement de soulèvement de la structure et les forces internes de la structure ont été analysées. De plus, dans cette étude, les différentes méthodes d'atténuation mentionnées ci-dessus ont été utilisées pour contrôler la pression interstitielle entourant la structure, empêchant ainsi le soulèvement de la structure et la mettant hors service.

Mots clés: structure souterraine; différences finies; liquéfaction; zones sismiques; contenu de fréquence; pression interstitielle; PGA; méthode simplifiée; CHBDC; atténuation.

ABSTRACT

Transportation, communications, and energy networks are growing in complexity. The possibility of two or more networks occupying a common right-of-way or intersecting increases as the networks grow. As a result of this problem, governments have begun to shift the transfer of those services from above ground to the underground through underground tubes converge at buried structures. Maintenance and replacement of these structures are very expensive and it can exceed the cost of their constructions. Consequently, the study and the protection of these underground structures from the potential risks become imperative in order to preserve them. Seismic risk is one of the most risks, that could damage these structures and get them out of service. In fact, strong earthquakes could lead to float or crack through these structures. In this study, rigorous three-dimensional numerical finite different (FD) analyses of typical underground structures buried in sandy soils were carried out by adopting the energy-based approach as a constitutive model of soil using the computer code, FLAC^{3D}. The adopted numerical models were validated against various previous experimental results. The main objective of the present study is to investigate the performance of the underground structures under seismic signals compatible with the five seismic zones of Québec. Moreover, three earthquakes with different frequencies were used to study the effect of the frequency content on the soil and structure behavior. Moreover, two study cases were simulated to investigate the seismic behavior under realistic earthquakes compatible with the 2015 National building code of Canada. The seismic behavior of the soil-structure model included acceleration response, excess pore water pressure, structure uplift displacement, and structure internal forces were analyzed. Also, in this study, different mitigation methods were used to control excess pore water pressure surrounding the structure, thus preventing uplift of the structure and putting it out of service.

Keywords: underground structure; finite-difference; liquefaction; seismic zones; frequency content; excess pore pressure ratio; PGA; simplified method; CHBDC; mitigation.

REMERCIEMENTS

Toutes les louanges et la gratitude à Allah le Tout Miséricordieux, le Très Miséricordieux. Avec toute ma gratitude, je souhaite exprimer ma profonde gratitude à tous ceux qui ont rendu cette recherche possible. L'auteur est redevable au Dr. Mourad KARRAY pour sa supervision, ses conseils et ses critiques constructives à toutes les étapes du programme de recherche. Son encouragement et sa volonté d'aider de toutes les manières possibles sont grandement appréciés.

Je suis également très reconnaissant au Dr. Mahmoud N. HUSSIEN pour ses encouragements à poursuivre sur cette question, son aide précieuse pour la planification, la modélisation numérique et l'analyse, ainsi que pour les heures de discussions sur le sujet et pour me guider tout au long du processus.

Mes remerciements particuliers vont également au Dr Mohamed CHEKIRED, ing. Carole BESSETTE et ing. Livius JINGA d'Hydro-Québec pour leurs soutiens.

Nos sincères remerciements vont également à prof. Mathieu NUTH, ing. Simon GRENIER et ing. Mahmoud N. HUSSIEN pour leurs précieuses suggestions et commentaires critiques qui ont permis de faire avancer la thèse.

Enfin, je voudrais exprimer ma gratitude à mes parents, ma femme (mon amour Eman) et mes fils (Omar et Moaz), dont le soutien et les encouragements constants m'ont aidé à traverser les moments difficiles de ce programme. Je leur suis profondément reconnaissant pour leur amour, leur compréhension et leur inspiration. Sans leurs bénédictions et leurs encouragements, je n'aurais pas pu terminer ce travail.

TABLE OF CONTENTS

LIST OF TABLES

LIST OF FIGURES

LIST OF SYMBOLS

Symbol	Definition
v_{s1} (m/s)	Normalized shear wave velocity
v_s (m/s)	Shear wave velocity
σ'_{v0} (MPa)	Initial vertical effective stress
σ'_v (MPa)	Vertical effective stress
G_0 (MPa)	Initial shear modulus at a confining pressure of 100 kPa
K_0 (MPa)	Initial bulk modulus at a confining pressure of 100 kPa
ρ_d (kg/m^3)	Soil dry density
ϕ_f (°)	Failure angle of friction
k (m/s)	Soil permeability
n	Porosity
α	Calibration liquefaction parameters
β	Calibration liquefaction parameters
a_x	Calibration liquefaction parameters
a	Hysteretic fitted-parameters
b	Hysteretic fitted-parameters
x_0	Hysteretic fitted-parameters
y_0	Hysteretic fitted-parameters
E_s (GPa)	Structure Young modulus
υ_s	Structure Poisson ratio

ρ_s (kg/m^3)	Structure density
k_s *(GPa/m)*	Shear interface stiffness
k_n *(GPa/m)*	Normal interface stiffness
$\delta°$	Friction angle of the interface surface
Ts	Tensile bond strength
K_w *(GPa)*	Water modulus
γ	Soil shear strain
Dr (%)	Soil relative density
W_s	Energy dissipated divided by the initial vertical stress
R_u	Excess pore water pressure ratio
CSR	Cyclic stress ratio
σ_v'	Vertical effective stress
λ	The input earthquake wavelength
ΔL	Maximum element height
Z_{min}	Smallest width of an adjoining zone in the normal direction
f_{min}	Natural frequency of oscillation
ζ	Rayleigh damping ratio
Δ_1	Maximum uplift displacement of underground structures
Δ_2	Soil settlement surround structure

LIST OF ACRONYMS

Abbreviation	Definition
FE	**F**inite **E**lement
FD	**F**inite **D**ifference
FLAC	**F**ast **L**agrangian **A**nalysis of **C**ontinua
FLAC^{3D}	**F**ast **L**agrangian **A**nalysis of **C**ontinua in **3D**
FF	**F**ree **F**ield
PGA	**P**eak **G**round **A**cceleration
PGV	**P**eak **G**round **V**elocity
TxSS	**T**riaxial **S**imple **S**hear
DSS	**D**irect **S**imple **S**hear
EPWPR	**E**xcess **P**ore **W**ater **P**ressure **R**atio
FS	**F**actor of **S**afety
C_f	**C**orrection **F**actor
AASHTO	**A**merican **A**ssociation of **S**tate **H**ighway and **T**ransportation **O**fficials
CHBDC	**C**anadian **H**ighway **B**ridge **D**esign **C**ode
CCMTA	**C**anadian **C**ouncil of **M**otor **T**ransport **A**dministrators
BM_{st}	**B**ending **M**oment due to **S**tatic loading
BM_{dy}	**B**ending **M**oment due to **dy**namic loading
SF_{st}	**S**hear **F**orce due to **S**tatic loading
SF_{dy}	**S**hear **F**orce due to **dy**namic loading

CHAPTER 1. INTRODUCTION

1.1. Overview

Geotechnical structures buried near the ground surface have a wide range of applications, from small-scale pipelines such as means of gas transmission, telecommunications, water supply, and sewerage pipelines, to large-scale infrastructures including tunnels for various transportation systems. These structures are becoming more and more prevalent in the modern world because of the decreasing availability of ground space due to the fast-growing population (Yue and Li 2007). In other words, underground infrastructures, serving for transport (e.g., highway tunnels and subway metro), utility (e.g., gas and water pipelines) and storage purposes (e.g., fuel storage and water tanks) have been a widespread alternative to what in redeveloping urban spaces to ease land congestion pressures. However, in the event of an earthquake, the functionality of these structures could be put in to risk especially when they were constructed in potentially liquefied soils (Chian and Tokimatsu 2012). In fact, the uplift phenomenon of buried structures has been abundantly reported following several earthquakes. For example, during the 2004 earthquake in Niigata-ken Chuetsu, Japan, more than 1400 manholes were uplifted causing serious lifeline problems. Many other earthquakes (e.g., the 2004 Niigata Chuetsu, the 2007 Noto Hanto, and the 2007 Niigata Chuetsu-Oki) caused serious damage to buried structures in the form of uplifting manholes and settlement of pavement above backfill soil for pipes (Yoshida et al. 2008). The Haiti 2010 Earthquake, in particular, resulted in severe destruction of essential systems (e.g., transportation and lifeline systems) leading to a 60% loss of the nation's infrastructure (DesRoches et al. 2011).

In Canada, the majority of public underground structures, unfortunately, included no modern seismic engineering knowledge during the design and construction as almost 60% of them were put in place before 1960 (CSCE 2003). For this particular reason, Canada's public infrastructures appear highly vulnerable following decades of underinvestment and would be severely challenged by relatively large earthquakes (Kovacs 2010). The 2010 Central Canada earthquake of a 5.0-magnitude occurred in Central Canada on 23 June and resulted

in spectacular damage to many buildings and lifelines. As a consequence, part of Quebec Route 307 was closed due to a partial bridge collapse near Bowman. Near the epicenter, many of the telephone networks were out. The O-Train Trillium Line in Ottawa was shut down until 5 pm, and the Agence métropolitaine de transport shut down four of five commuter trains in Montréal for a similar period of time in order for lines to be inspected (USGS. 2010).

1.2. Definitions of the problem

At present, underground pipes and structures are significantly used to transfer life utilities such as water supply and telecommunications and electricity. For example, in Québec, Hydro-Quebec had installed more than 30 thousand of typical underground structures over the province to transform the electricity for the housing through power cables during the last decades. The typical Hydro-Quebec underground structure is a cuboid concrete chamber (4.0 x 2.0 x 3.0 m) that is used to supply homes by electricity. This structure connected with side concrete tubes as shown in Figure 1.1. These structures could be damaged as a result of severe shakes. Replacing these structures is in fact very expansive and maybe disrupted life. Underground structures are designed to resist the surround loads from the ground and freezing pressures to the expected earthquakes loading (i.e., compatible with the Québec region). An important risk could menace the buried structure's safety which occurs indirectly from seismic loading which is structure uplift. The structure uplift due to soil liquefaction is one of the most dangerous hazards that lead to the underground structure out of service. Excess pore water pressure can lead to floating the structure. This type of risk is more significant in the high seismic zones where the structures were designed to withstand the above-mentioned conventional loads. Therefore, the challenge facing engineers is to design underground structures that can resist all hazards. In this study, the acceleration response, excess pore pressure, structure uplift and internal forces of underground structures have been carefully studied according to the different study parameters.

Figure 0.1 Typical Hydro-Québec underground structure.

1.3. Objective of research

The design of underground structures to resist seismic loadings is a very complicated issue that requires rigorous consideration of different elements that contribute to the performance of underground structures under seismic loading. Thus, the three-dimension computer code Fast Lagrangian Analysis of Continua (FLAC^{3D}) has been utilized in this study to create a three-dimensional (3D) model to comprehensively investigate this complex soil-structure interaction problem under seismic loading. This model is capable of predicting the structure's response in terms of straining actions as well as the structural deformations under different earthquakes. Soil stresses, as well as pore pressures generated during the excitations, could be also predicted.

The objectives of this study can be summarized as follows:

i. Study the seismic behavior of underground structures embedded in liquefied soil under different earthquakes compatible with the regions of Québec using a new soil constitutive model;

ii. Validate the soil constitutive model (energy-based approach) using previous experimental results;

iii. Estimate empirical equation to determine the factors that lead to underground structure failure;

iv. Ensure the possibility of using the empirical equation in standard codes to determine the underground structure internal forces;

v. Comparing different methods used to mitigate the underground structure uplift due to soil liquefaction to choose the most economical method.

1.4. Methodology

The current research is devoted to investigating the performance of Hydro-Quebec underground structures under seismic loads compatible with Eastern Canada Seismology. 3D FD models of underground structure buried in liquefied sandy soils were constructed through the computer code FLAC^{3D} by adopting the energy-based model. Numerical models used throughout this study have been validated using single soil element simulations and compared successfully with typical results from other numerical and experimental models. Moreover, two case studies of underground structures constructed in two different sites within the Quebec province have been employed to illustrate the applicability of the current numerical model to assess traditional design approaches of underground structures in question. Also, different mitigation methods have been used to reduce the pore water pressure ratio under the structure and decrease the uplift displacement. Results from the soil-structure interaction analyses with the different ground retrofit schemes were evaluated.

1.5. Thesis Chapters

This thesis is sectioned into the following chapters:

- **Chapter 1 "Introduction"**: includes problem overview; problem definitions; objectives and methodology of research.
- **Chapter 2 "Literate Review"**: summarizes the state of the art on the behavior of underground structure due to seismic loading. Some examples of infrastructure failure due to liquefaction reviewed in this chapter. Also, methods of modelling and constitutive models of liquefied soil had been illustrated. Plus, some mitigation methods of the underground structure against uplift had been mentioned.
- **Chapter 3 "First scientific journal paper submitted":** In this chapter, the seismic behavior of access underground structure embedded in sandy deposit was analyzed using the three-dimensional (3D) finite differences (FD) program FLAC^{3D} emphasizing on their structural behaviors under different earthquakes compatible with the five seismic hazard regions of Québec. The energy-based approach that can simulate the material cyclic behavior through the estimation of the pore water pressure built-up was incorporated in the numerical code as a constitutive model of the soil, while linear structural elements were used to model underground structures.
- **Chapter 4 "Second scientific journal paper submitted":** A numerical modelling was carried out to investigate the structural and soil performances under three different historical earthquakes with similar durations but with different frequency contents. The PGA of these earthquakes were modified to 0.25, 0.5, and 1.0 g to study the amplitude factors. Also, two study cases in different soil profiles have been studied.
- **Chapter 5 "Third scientific journal paper submitted":** The study investigates the performance of Hydro-Québec's typical underground access structures under seismic loads. The chapter introduces different structure uplift to mitigate methods to prevent putting it out of the service. These methods depended on the following approaches: I) Dissipate or decrease the excess pore water pressure beneath the underground structure; II) Increase the vertical effective stress under the structure; III) Increase the underground structure resistance

against uplift. Different mitigation methods were investigated and compared with the maximum allowable uplift to choose the recommended method.

❖ **Chapter 6 "Conclusions and recommendation"**: summarizes the general conclusions of this thesis, including the conclusions and contributions in each chapter, the limitations as well as the recommendations for additional researches.

CHAPTER 2. LITERATURE REVIEW

2.1. General Background

Canada in general and Quebec in particular face several types of problems as a result of the transfer of electricity to homes above the ground through overhead lines. Much of the destruction has been recorded throughout history because of the destruction of storms to the ground power lines (Fig.2.1). For example, in 1998, a lot of steel electrical pylons and wooden utility poles were crushed and crumpled due to freezing rain that occurred in Quebec (Fig.2.2), further damaging the power supply and hampering the return of electricity (Lecomte et al. 1998). To avoid this type of problem, it is now a common practice to transfer the electricity inside underground lines which is passing through access underground structures. In fact, the underground structures improve the landscape and protect electrical equipment from bad weather. Another important reason for using underground structure in the transfer of public services is the lack of green spaces, especially in large, busy cities. So, using underground structures lead to providing space for other benefits.

In Quebec, during the last few decades, 11% of the overhead lines had been changed to below ground lines over the province. At present, there are more than 30,000 access underground structures (Figs. 2.3 and 2.4). The construction of such lines and structures is very expensive however replacing these structures because of getting out service after earthquake occurring is more expensive (Guérin et al. 2016). For this reason, it is of importance to properly design these lines and structures against potential earthquakes.

Figure 0.1 Overhead power lines fail due to a windstorm.
(https://www.cbc.ca/news/canada/british-columbia/south-coast-ferries-service-1.5012922)

Figure 0.2 Power outages due to a snowstorm.
(https://www.accuweather.com/en/weather-news/how-to-survive-a-power-outage-in-winter/70000039)

Figure 0.3 Transfer the electricity power cables inside underground lines.
(https://www.hydroquebec.com/projects/beaumont-dorchester-line/works.html)

Figure 0.4 Underground chamber for electricity transfer.
(https://www.hydroquebec.com/projects/beaumont-dorchester-line/works.html)

2.2. Underground Structure Failure due to Earthquake.

2.2.1. Earthquakes in Canada

An earthquake is the shaking of the earth's surface from the movement of rock along a fault line beneath the Earth's surface. In Canada, there are more than 4,000 earthquakes every year, most of them are impalpable. The principal regions for seismic activity in Canada are the coast of British Columbia, the Cordillera region, the Arctic, and the eastern provinces and the eastern seaboard (Cassidy et al. 2010). In eastern Canada, there is seismic activity throughout the northern Appalachians, the series of M5 events in the Miramichi region of New Brunswick in 1982 being an example. More concentrated zones occur at the mouth of St Lawrence, in the St Lawrence Valley near La Malbaie in Charlevoix County and in western Québec. The Charlevoix zone is the site of most of the larger events in eastern Canada (Adams and Basham 1989). The earliest recorded earthquake in Canada took place on 5 February 1663which occurring in the Charlevoix–Kamouraska region in Québec, at a probable magnitude of 7. The earthquake was felt over much of eastern North America as shown in Fig. 2.5. It also prompted landslides along the St. Maurice, Batiscan and St. Lawrence rivers. On 28 February 1925, M6.2 earthquake was felt throughout eastern Canada and the northeastern U.S. The epicenter for this quake was in Québec's Charlevoix–Kamouraska region. Homes in communities along the St. Lawrence River were damaged, as were several prominent buildings, including the Québec City's railway station (Marsh 2001). At present, the 1988 Saguenay earthquake struck Quebec (Canada) with a moment magnitude of 5.9 on November 25. It is one of the largest recorded earthquakes in eastern Canada and eastern North America during the 20th century. The earthquake was felt by hundreds of thousands and damaged some buildings. It could be felt as far as Toronto. This earthquake caused little property damage and no loss of life. However, this event made it possible to highlight the fragility of certain buildings as well as the sensitivity of the pavements to the ground movements. The damage observed is specifically in Quebec and Montreal. Strong earthquakes in the region look like Québec where a large number of rivers surrounded by saturated loose grain size soil could lead to earthquake liquefaction (Lamontagne et al. 2007).

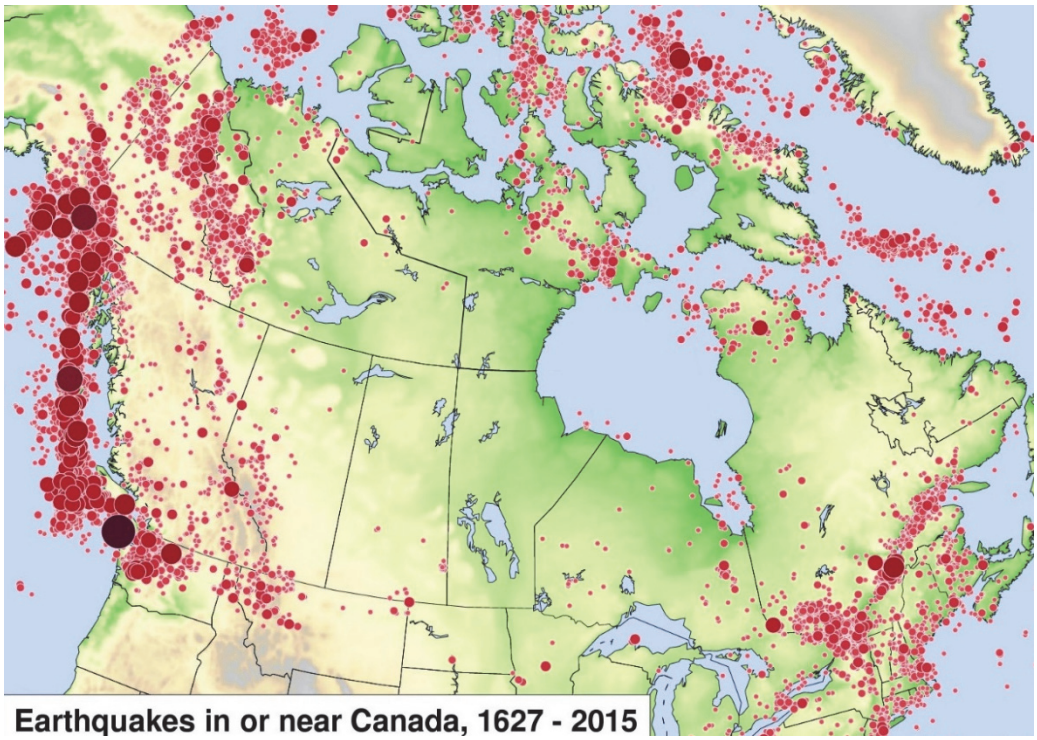

Figure 0.5 Locations of last earthquakes in Canada.
(http://www.seismescanada.rncan.gc.ca/historic-historique/caneqmap-en.php**)**

2.2.2. Soil Liquefaction

Soil liquefaction is most often occurring in saturated or partially saturated loose sand or silt soil. The soil substantially loses its stiffness in response to an applied stress such as shaking during an earthquake or other sudden change in stress condition, in which soil that is ordinarily a solid behaves like a liquid. This is because loose sand tends to compress when a load is applied. When the soil is saturated by water then water fills the void ratio between soil particles. In response to soil compressing, the pore water pressure increases and the water attempts to flow out from the soil to zones of low pressure (usually upward towards the ground surface). However, if the loading is rapidly applied and large enough, or is repeated many times (e.g. earthquake shaking) such that the water does not flow out before the next cycle of load is applied, the water pressures may build to the extent that it exceeds the force (contact pressure) between the soil particle that keep them in contact. The increase of the excess pore water pressure leads to a decrease in the effective vertical stress of the soil. This loss of soil stress causes it to lose its strength (the ability to transfer shear stress) and convert the soil from the solid-state to the liquid state.

Although the effects of liquefaction have been long understood, engineers took more notice after the 1964 Niigata earthquake and the 1964 Alaska earthquake. It was a major factor in the destruction in San Francisco's Marina District during the 1989 Loma Prieta earthquake, and in Port of Kobe during the 1995 Great Hanshin earthquake. More recently liquefaction was largely responsible for extensive damage to residential properties in the eastern suburbs and satellite townships of Christchurch, New Zealand during the 2010 Canterbury earthquake and more extensively again following the Christchurch earthquakes that followed in early and mid-2011 (Cubrinovski et al. 2010). On 28 September 2018, an earthquake of 7.5 magnitudes hit the Central Sulawesi province of Indonesia. Resulting soil liquefaction buried the suburb of Balaroa and Petobo village in 3 meters deep mud. The government of Indonesia is considering designating the two neighborhoods of Balaroa and Petobo, that have been totally buried under mud- as mass graves (Sassa and Takagawa 2019).

2.2.3. Example of Underground Structure Failure

Underground structures are constrained by the surrounding soil and cannot move independently so are not generally subject to significant dynamic amplification effects. They are affected by deformation of the surrounding ground and by inertia forces acting on the structure. Rectangular underground structures experience transverse deformations due to earthquake-induced shear strains in the surrounding soil. The deformation of the cross-section is usually more critical in design than the axial or curvature deformations induced along the axis of the structure (Wood 2004). The analytical solution of the rectangular underground structure indicates that the structure deformation is dependent on the stiffness ratio between the structure and the ground and on the shape of the structure, which is given by the ratio between its length and height (Huo 2005). For example, in 1995, a great earthquake (Kobe earthquake) occurred in the region of southwestern Japan by a moment magnitude of 6.9. During the earthquake, more than 30 columns of the central section of the station completely collapsed as shown in Fig. 2.6. About 100 m of National Highway No. 28 above the Daikai Station had settled by up to 3 to 4 m, over a width of 30 m as shown in Fig. 2.7.

Figure 0.6 Columns of the central section of the station complete failure (Uenishi and Sakurai, 2000).

Figure 0.7 Daikai Station Collapse.
(https://resources.realestate.co.jp/ja/living/earthquake-building-codes-and-technology-in-japan-jp).

Another example, the 2016 Kumamoto earthquake was a shallow earthquake in Kyushu, Japan with a magnitude of 7.3. This earthquake caused severe damage to the superstructure and substructure in the epicentral region. Six bridges and a tunnel were found damaged due to earthquake. Tawarayama tunnel (Fig.2.8) suffered from an axial seismic loading for about 250 m from the tunnel portal. The cause of compression of the tunnel was thought to be a surface fault movement in the right lateral component, which was confirmed at the damaged location. Cracks appeared on both sidewalls of lining concrete. Large chunks of concrete came off the lining joint. (Shirahama et al. 2016).

Figure 0.8 Damage of the Tawarayama tunnel.
(http://learningfromearthquakes.org/2016-04-15-kumamoto-japan/11-resources/61-overview-of-damage-to-roads-and-bridges-in-nishihara-area-2).

There are several reports on the devastations of underground structures caused by seismic loadings. Among others, Tokimatsua et al. (2012) presented a comprehensive overview of the geotechnical aspects of the building damage due to the 2011 Tohoku Pacific Earthquake, based on field reconnaissance made after the earthquake. His study showed extensive soil liquefaction that occurred along the coast of Tokyo Bay. Underground facilities, such as manholes, emergency water tanks and parking lots were uplifted (Fig. 2.9), tap water and sewerage systems were damaged, roads had dents and utility poles were toppled. The liquefaction induced floating of sewer manhole during an earthquake causes serious damages to the function of the sewer system. In addition, the uplift of manholes poses hazards to the traffic of ambulances and obstructs the rescue activities as it was reported by Koei (2014).

Substantial damage to buildings and underground structures have been reported after the magnitude 7.1 earthquake and its aftershocks in the Christchurch's central city and eastern suburbs. Significant liquefaction affected infrastructure as shown in Fig. 2.10. Figure 2.11 shows the uplift of a manhole at West Takanosu, Shiraishi City, which reaches 1.15 m. Since the ground subsided along the sewage line, fill at the construction of the sewage line is supposed to have liquefied. In the 2010 Maule Earthquake, in Chile, the uplifting of the underground structures (manholes and underground tanks) were reported, and the underground tank in San Pedrodel Valle was uplifted by approximately 1.2 m, as shown in Fig. 2.12 (Kang et al. 2014).

Figure 0.9 Uplift of underground parking Lot-Chuetsu Earthquake

(Tokimatsua et al. 2012).

Figure 0.10 Uplift of Petrol tank - Christchurch Earthquake
(http://www.civildefence.govt.nz/Assets/Uploads/images/gas-station-tanks.jpg)

Figure 0.11 Uplift of a manhole – Tohoku Earthquake (Yamaguchi et al. 2012).

Figure 0.12 Uplifted sewage tank after the2010 Maule, Chile, earthquake (Kang et al. 2014).

2.3. Soil-Structure Modelling Methods

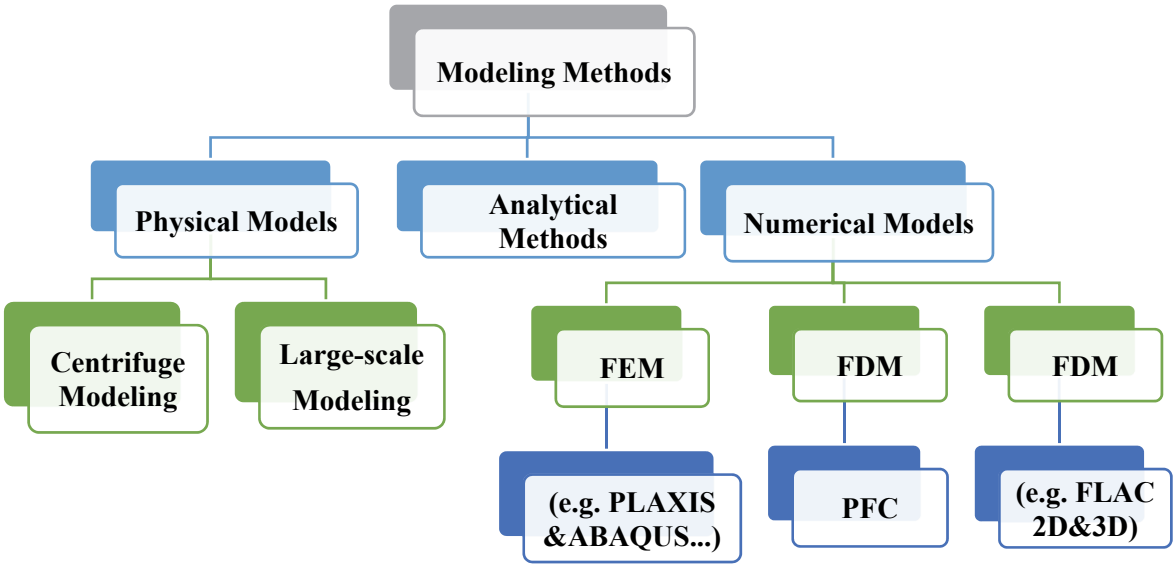

2.3.1. Physical (Experimental) Modelling.

Considering the importance of underground structures, the behavior of these structures has been investigated in detail in the literature mainly through geotechnical centrifuges. In the course of these investigations, some practical methods of predicting uplift displacement of buried structures and surface settlements of backfill have been also developed and validated using centrifuge results (Koseki[a] et al. 1997; Ling et al. 2003; Sasaki and Tamura 2004; Chou et al. 2011; Tobita et al. 2011; Kang et al. 2009; Kang[a&b] et al. 2013; Zhou et al. 2015).

In fact, geotechnical centrifuges have been widely used to perform small-scale model tests of geotechnical structures. On a reduction scaling of N value, it is possible to reproduce the same level of effective confining stress with a prototype ground. If the tests are conducted with the centrifugal acceleration of N.G (where g is gravity acceleration), the scaling law for the centrifuge tests for N.G is summarized in Table 2.1 (Kang 2010). For example, Ling et al. (2003) prepared the ground with Nevada sand and shaken with a sinusoidal wave at an amplitude of 0.5g to study soil liquefaction occurring. The centrifuge model test was performed on saturated sand deposits with a shallowly buried structure model on the

geotechnical centrifuge. The loose saturated sand backfills placed around the underground structure were considered to be liquefiable (Chou et al. 2011). Many factors can be used in the experiments (e.g. groundwater levels, the magnitude of input accelerations, the duration time of shaking, the relative densities of backfill and the soil, etc.) to assess its impact of liquefaction and uplift of underground structures (Tobita et al. 2011). A series of dynamic centrifugal model tests can be conducted to investigate the effects of several factors on the uplift movement of underground structure (Sasaki and Tamura 2004). Kang[a&b] et al. (2013) found that excess pore water pressure is one of the contributing factors to the magnitude of the manhole uplift. The photograph of the centrifuge test (Figure 2.13) shows that the top of the underground structure emerged on the surface of the sand layer after shaking. Uplift of the structure initiated after the surrounding sand layer had attained liquefaction (Zhou et al. 2015).

2.3.2. Numerical Modelling.

Many works are reported on numerical analyses of the seismic behavior of underground structures constructed in-ground, especially liquefiable soils. When the surrounding soil of the underground structure is liquefied, large deformations happen to lead to the increase of the internal stresses and deformations of the structure. The uncoupled method and the coupled method are two kinds of numerical methods that are usually used to analyze the response of an underground structure under seismic loads (Wang et al. 2005). Coupled is more realistic but even more complicated where it uses both flow simulation and mechanical deformation modelling in the same step. On the other side, it needs two separate steps in order to be done. Xia et al. (2010) investigated the seismic response of an underground structure in saturated deposits using a fully coupled dynamic finite element method. Khoshnoudian and Shahrour (2002) studied this problem using the (u-p) formation of the elastoplastic constitutive model, which can reproduce liquefaction of loose soils under undrained loading paths (displacement for solid phase and pore-pressure for the fluid phase).

Table 0.1 Scaling law for the centrifuge tests for N.G (after Kang 2010).

Quantity	Scale	Quantity	Scale
Length	N	Stiffness	1
Density	1	Permeability	N
Time	N	Pore pressure	1
Frequency	N^{-1}	Fluid pressure	1
Acceleration	N^{-1}	EI	N^4
Velocity	1	EA	N^2
Displacement	N	B.M.	N^3
Stress	1	Shear force	N^2
Strain	1	Axial force	N^2

Using the program (dynamic Finite Element code DYNA Swandyne-II), Liu and Song (2005) incorporated a generalized plasticity model that can simulate the soil liquefaction and generate the excess pore water pressure of sandy soils. Lu et al. (2005) and Jung[a] et al. (2013) used a two-dimensional, finite element (FE) continuum model with a Mohr–Coulomb (MC) to evaluate soil– pipeline interaction for the uplift in granular soil. Kang et al. (2014) have used the Finite-Element Analysis of Liquefaction Program (FLIP) program to study the seismic response of underground structures built in liquefiable soils. Azadi[a&b] and Hosseini (2010) assessed the topic through the use of the Finn model incorporated in the FLAC software which can assess the liquefaction effects for the soil. He and Chen (2011) and Yang and Wang (2012) simulated the pore water pressure until liquefied of sand by Finn model based on the Mohr-Coulomb model under dynamic load in FLAC^{3D} software. Bao et al. (2017) conducted a numerical model using a two-phase fully coupled distinct element code. This code incorporates a particle-fluid fully coupling finite element-finite difference (FE-FD) method to determine the movement of the soil and underground structure as shown in Figure 2.14. Lui and Song (2006) and He and Chen (2011) assumed the boundary between the soil deposit and the bedrock was fixed. In order to prevent the reflection of waves in the model and make the boundaries act as adsorbent boundaries, it is recommended to use the free field boundary condition. Liu and Song (2005) tested many trials using different element sizes to ensure that the seismic events from the base could be adequately transmitted. Also, it found that the width of the tied boundaries of the model must be large enough so that the structure isn't affected by the reflected vibration.

Figure 0.13 Observed Uplift of the structure model (after Zhou et al. 2015)

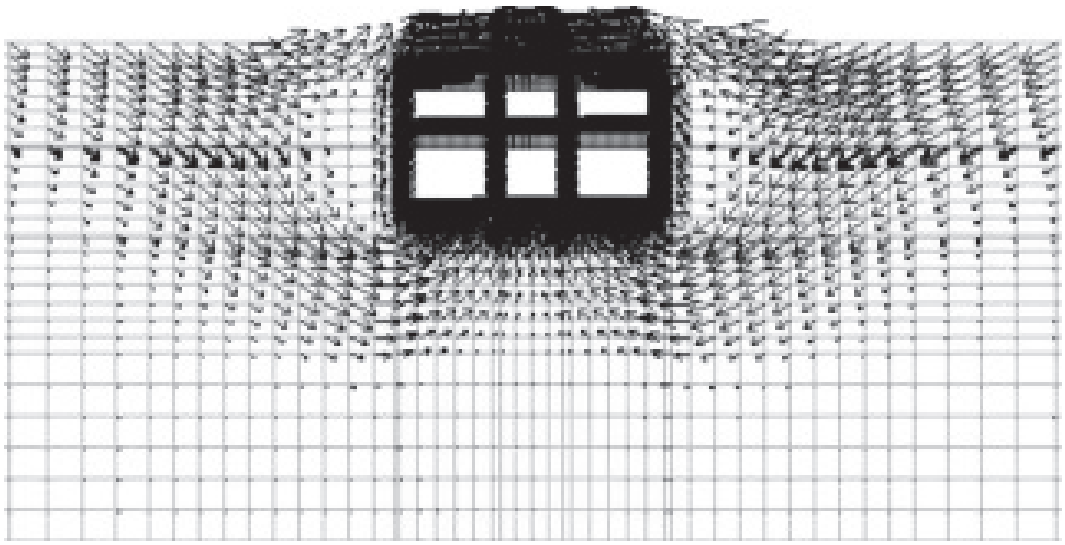

Figure 0.14 Particle velocity vectors (after Bao et al. 2017)

In this study, in the static analysis, the soil simulated by Mohr–Coulomb model to compute gravity stresses. The base boundary was fixed both horizontally and vertically and the side boundaries were fixed horizontally. Then, in the dynamic analysis, the horizontal seismic load was applied at the base boundary. The side boundaries were released and replaced by a free field boundary condition. The soil represented by the equivalent-linear model (hysteretic damping) in addition to the liquefaction model (energy-based approach).

Material Damping

The linear, non-linear and equivalent-linear methods are the most useful to calculate the stress-strain behavior in soil subjected to static or seismic loads. The equivalent-linear method does not directly capture any nonlinear effects because it assumes linearity during the solution process; strain-dependent modulus and damping functions are only taken into account in an average sense, in order to approximate some effects of nonlinearity (damping and material softening). For dynamic analysis, the damping in the numerical simulation should reproduce in magnitude and form the energy losses in the natural system when subjected to dynamic loading. In soil and rock, natural damping is mainly hysteretic. FLAC contains an optional form of damping (called hysteretic damping) that incorporates strain-dependent damping ratio and secant modulus functions, allowing direct comparisons between the equivalent-linear method and the fully nonlinear method. The hysteretic damping formulation is not intended to be a complete constitutive model. The hysteretic damping is used in conjunction with the other damping schemes, such as Rayleigh damping or local damping. Rayleigh damping is unpopular with code users because it often involves a drastic reduction in time step and a consequent increase in solution time. Qiao et al. (2008) and Yang and Wang (2012) used the hysteretic damping option in FLAC to simulate soil damping due to dynamic loads. In this study, the hysteretic damping (SIG4) is adopted to simulate soil damping. Also, Rayleigh damping is used (at low levels: e.g., 0.2%) to take off high-frequency noise.

2.4. Liquefaction Simulation Methods

There are different methods that could represent the soil liquefaction process. From screening criteria method to determine the possibility of liquefaction occurring. And empirical methods and simplified methods used to make an evaluation of soil liquefaction potential that's have become popular among practicing engineers. These methods use deterministic relations to develop bounds or boundary curves to imply the occurrence of liquefaction and the safety against. However, due to the complexity of the problem, several analytical and numerical methods have been developed to estimate earthquake-induced liquefaction (Javadi et al. 2006).

2.4.1. Screening Criteria Method

Empirical screening criteria are one of the most common which can be utilized to evaluate the soil liquefaction occurring. These criteria are used in the United States of America (USA), Japan, and China. The screening criteria are limited to determining the probability that liquefaction will be triggered for a given earthquake. Post-earthquake data, field results and/or geotechnical laboratory test data are most commonly utilized to evaluate and develop criteria (Green and Ziotopoulou, 2015). The criteria are based on geologic history, soil shear stiffness, particle size distribution, water content, Atterberg limits, and CPT/SPT indices. "Chinese Criteria" was the first liquefaction susceptibility screening criteria used in the USA (Wang 1979; Seed and Idriss 1982; Marcuson et al. 1990; Koester 1992; Robertson & Wride 1998; Andrews and Martin 2000; Moss and Chen 2008). Seed et al. (2003) propose other criteria that can define the significant loss of strength and stiffness due to cyclic pore pressure generation. As with the Seed et al. (2003) criteria, the Bray and Sancio (2006) propose criteria for liquefaction susceptibility of fine-grained soils. The Boulanger and Idriss (2006) develop criteria state which provides improved guidance for selecting engineering procedures for estimating potential strains and strength loss during seismic loading. The Japanese Criteria for liquefaction susceptibility for port and harbor facilities are shown in Figure 2.15 (Iai et al. 1986, 1989). The criteria for liquefaction are only based on grain size distribution.

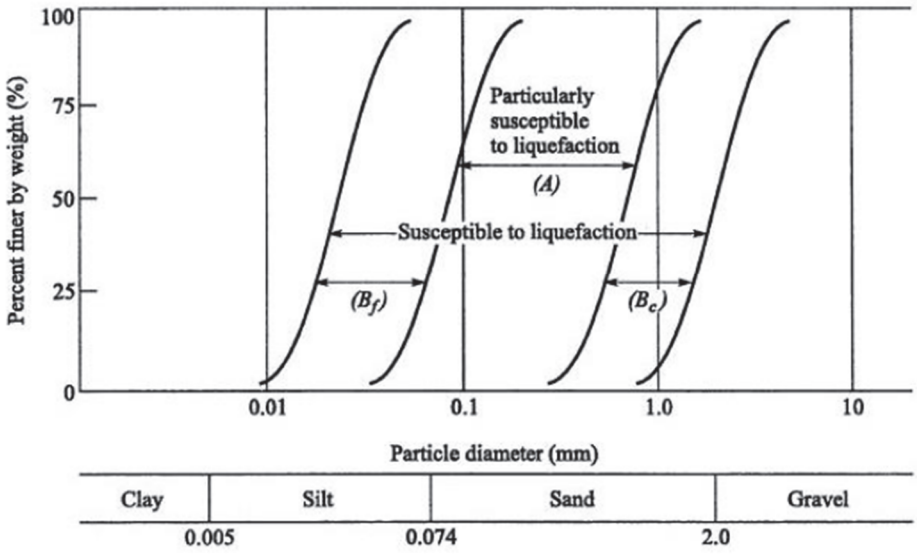

Figure 0.15 Japanese liquefaction susceptibility criteria (Iai et al. 1986, 1989).

2.4.2. Simplified Empirical Method.

Many earthquakes around the world have led to soil liquefaction. Therefore, it is necessary to study this phenomenon. Seed and Idriss (1971) developed a simplified procedure based on laboratory and field tests to evaluate the liquefaction potential, which was defined by a safety factor calculated by the ratio of the cyclic resistance ratio (CRR) to the cyclic stress ratio (CSR). Thereafter, this procedure was modified and improved, in particular by Seed and Idriss (1982), Seed et al. (1983), Seed et al. (1985), and Youd et al. (2001). In the first step, from dynamic shaking, the dynamic shear stress history τ_{cyc} or and vertical effective stress (σ'_{vo}) can be calculated according to the following equation:

$$\mathrm{CSR} = 0.65 \times \left(\frac{\tau_{\mathrm{cyc}}}{\sigma'_{\mathrm{vo}}}\right) = 0.65 \times \left(\frac{a_{\max}}{g}\right) \times \left(\frac{\sigma_{\mathrm{v0}}}{\sigma'_{\mathrm{vo}}}\right) \times r_d \qquad [5]$$

where σ_{v0} is the vertical total stress of the soil at the depth studied, σ'_{v0} is the vertical effective stress of the soil at the depth studied, a_{max} is the peak horizontal ground surface acceleration, and r_d is the shear stress reduction factor. The next step in this method is to find the cyclic resistance ratio (CRR) for the soil which based on Standard Penetration Test blows $(N_1)_{60}$. This can be determined by using an empirical base curve drawn from the liquefaction catalog for an earthquake with magnitude 7.5. Next, the value of CRR should be adjusted for the applied earthquake by multiply the value in the magnitude scale factor. Excess Pore water pressure is not computed in this method but it is indirectly accounted for the soil liquefaction safety factor. If the CRR of the soil is less than or equal CSR generated by the earthquake, liquefaction is assumed to occur in this location.

2.4.3. Advanced Method

The soil liquefaction of the ground is one of the most important subjects in Earthquake Engineering. Liquefaction occurs due to the increase of pore water pressure accompanied by a decrease of vertical effective stress and shear modulus. Both experimental and numerical models have been used to study the soil liquefaction phenomenon. For numerical methods to simulate the liquefaction behavior of sandy ground, there are various types of formulations based on the numerical method and the constitutive equation for soils. There are two main methods in numerical models in soil mechanics. One is based on total stress, and the other is

based on the effective stress. The most advantageous type of continuum models is the fully-coupled effective stress models. These models directly predict the tendency of soil to dilate or contract in response to each load increment. This results in the generation or reduction of pore pressure depending on whether the strain is contractive or dilative. These models are often the most difficult to calibrate and verify since the stiffness and pore pressure response of these models depend on the accurate prediction of volumetric strains at each load increment. The effects of pore water flow can often be considered when using a fully coupled model. Although coupling groundwater flow and dynamic mechanical response require an extremely complex analysis procedure, the effects of pore pressure migration or dissipation can be significant in some cases. Some well-known models implemented in FLAC software will be summarized in the following. On another hand, there are three main estimation approaches to evaluate the soil liquefaction: (1) stress-based procedures, (2) strain-based procedures, and (3) energy-based procedures (Green 2001).

Stress-Based Pore Pressure Models

Stress-based models are used primarily for soils subject to changes in effective stresses due to cyclic loading. For stress loading, the cyclic shear strain is replaced by the normalized cyclic shear stress and the void ratio. Seed[a] et al. (1975) developed an empirical, closed-form solution to calculate excess pore-water pressure ratio (R_u) which is inconsiderate to the relative density of soil and initial effective confining stress. Some examples of constitutive models based on the stresses list below.

WANG model is a fully coupled effective stress, bounding-surface hypo-plasticity model for (cohesionless) soil (Wang, 1990). The model formulation includes a non-circular pyramidal failure (bounding) surface, a loading surface, a surface of phase transformation (at which contractive behavior changes to dilative during shearing), and a critical state surface (defining an ultimate state in which the sand deforms at constant volume under constant stress). The model calibrated by using the relation curve between cyclic stress ratio, number of cycles to liquefaction (Wang 2001).

UBCSAND model is an incremental elastic-plastic model, which is controlled by changes in the effective stress ratio. The UBCSAND model was introduced by Puebla et al. (1997), Beaty and Byrne (1998). The model was developed based on plasticity theory and observations from laboratory tests on sands at the University of British Columbia (Byrne et al., 2004; Beaty and Byrne 2011). The model is in use on multiple large-scale projects. The elastic strains for this model are a function of changes in either the shear or normal effective stress. The relationship between stresses and strain is controlled by the shear and bulk moduli. Both moduli are isotropic and non-linear, meaning they are a function of the current mean stress.

Strain-Based Pore Pressure Models

Cyclic shear loading can induce significant volumetric compression strains in near-saturated sands which can result in induce pore pressure rise and liquefaction (Byrne 1991). For strain-controlled cyclic loading, excess pore pressure depends on the number of cycles, the cyclic shear strain, and the effective consolidation stresses. According to Martin and Finn (1975), the relation between irrecoverable volumetric strain and cyclic shear-strain amplitude is independent of confining stress.

Finn Model is used for simulating liquefaction uses Mohr-Coulomb failure criteria along with an assumed linear elastic-perfectly plastic stress-strain behavior. The linear elastic model is governed by the bulk and shear moduli which can be decreased through the analysis by the user to encounter losses of soil stiffness during liquefaction. Pore water pressure generation is modeled by computing volumetric strains induced by the cyclic shear strains using a formulation given by Byrne (1991).

Energy-Based Models (Current Model).

The energy-based approach is a model that can use to simulate soil liquefaction and predict the change in the pore-water pressure developed in the soil from the energy dissipated in the soil during cyclic loading (Polito et al. 2013). In the beginning, Martin et al. (1975) found that there is a relation between the built-up excess pore-water pressure (ΔU) and the soil volumetric change (ΔV) through the modulus of elasticity (E) as following:

$$\Delta U = E \times \Delta V \quad [1]$$

Also, Nemat-Nasser and Shakooh's (1979) proved that the energy required to increase pore pressure of sand is related to the dissipated energy per unit volume calculated from the hysteresis loops. The amount of energy dissipated in the soil (ΔW) is correlated to the volumetric change (ΔV) by means of constant (A). And, consequently, related to the excess pore-water pressure (ΔU) be as follows:

$$\Delta U = E \times A \times \Delta W \quad [2]$$

Davis and Berrill (1982) and Berrill and Davis (1985) proposed an empirical equation to relate of (ΔU) from (ΔW) by entering the vertical effective stress(σ_v'):

$$\frac{\Delta U}{\sigma_{v'}} = \alpha * \left(\frac{\Delta W}{\sigma_v'}\right)^{\beta} \quad [3]$$

where α and β are constant parameters that depend on soil properties and can be determined from laboratory tests using cyclic shear tests. This model has been successfully applied to laboratory data and field case studies (Sunitsakul 2004). This method has not been widely adopted in numerical modelling. Subsequently, Karray et al. (2015) have updated the equation formula and proposed an energy-based model to computed excess pore water pressure ratio (R_u) from cyclic shear stress-strain hysteresis loop:

$$R_u = \alpha * \left(\frac{-Ws^{0.5}}{a_x}\right)^{\beta} \quad [4]$$

where Ws is the energy dissipated per unit volume of soil divided by the initial effective confining pressure which can be determined by integrating area bound by stress-strain hysteresis loops, a_x is a variable parameter depend on soil type. Fig. 2.16 shows a typical shear stress-strain curve of soil subjected to cyclic loading. The energy dissipated per unit volume in one cycle of cyclic loading can be represented by the area of the hysteresis loop and then the excess pore water ratio can be calculated. Whereby calculating the shear strain (γ) and cyclic stress ratio (CSR) of each step, the energy dissipated of soil can be calculated by the following equation:

$$W_s = \sum \Delta W_s = \sum \left(\frac{CSR_{i+1} + CSR_i}{2}\right) * (\gamma_{i+1} - \gamma_i) \quad [5]$$

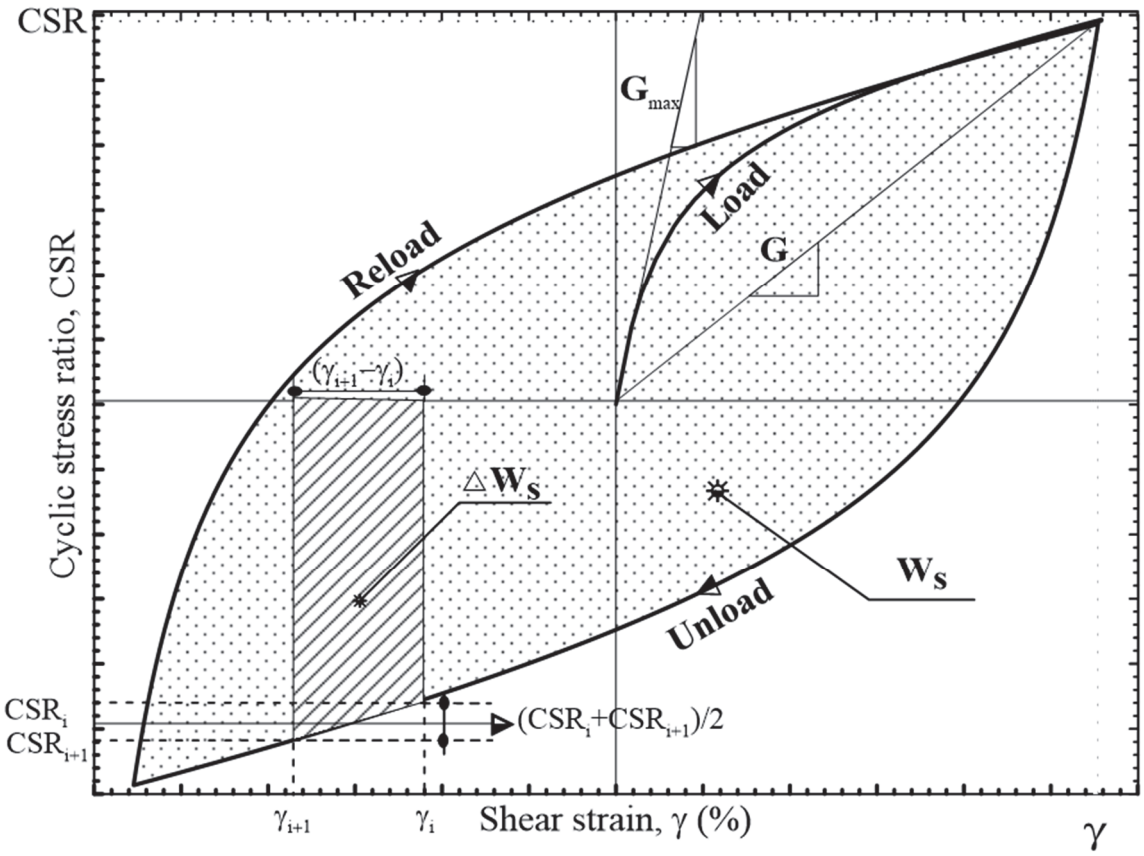

Figure 0.16 Dissipated energy for a soil sample in cyclic shear test determined by stress-strain hysteresis loops (Karray et al, 2015)

Comparing Between Models Using One Element

One zone element is used to validate the energy-based model modeled with an experimental shear test and three other liquefaction constitutive models (Finn, Wang, and UBCSAND) used in the software FLAC. This element consists of fully saturated sand soil (Bulk modulus=4.5 GPa. and shear modules=44 MPa.). It's fixed against the motion at the base. Shear velocity loading is applied to the two top nodes in the horizontal direction as shown in Fig. 2.17. Figure 2.18. shows the pore pressure build-up in a single element. It can be seen that the excess pore water pressure ratio reaches one which leads to the effective stress reaches zero after about 20 cycles of shaking where the soil is completely liquefied.

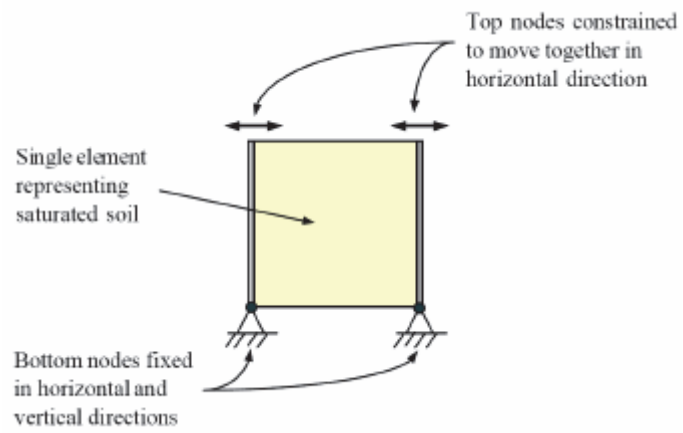

Figure 0.17 One element model by using FLAC

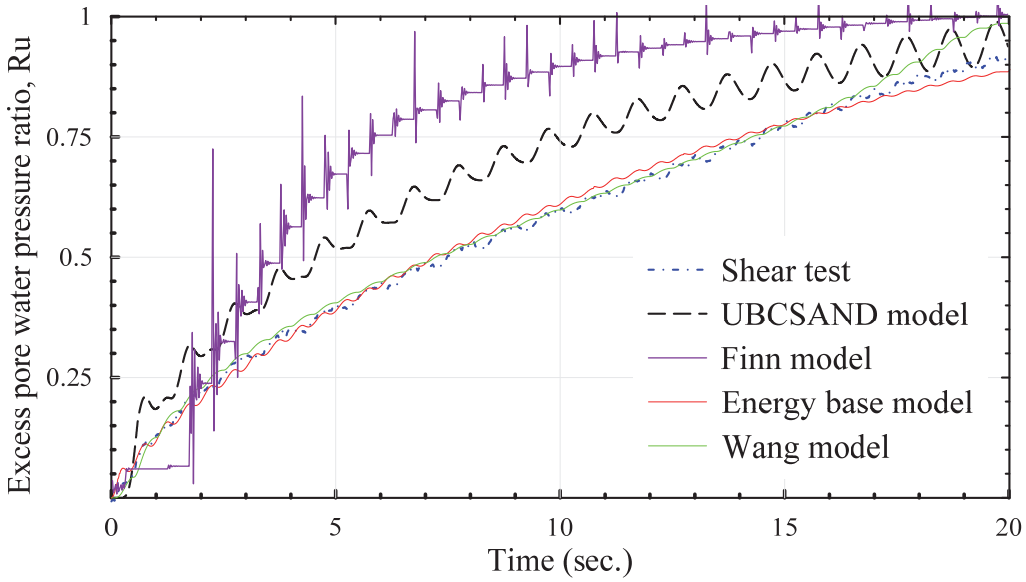

Figure 0.18 Comparison of different models predicted excess pore pressure ratios

2.5. Uplift Mitigation Methods.

Underground structures such as electric chambers are vulnerable to liquefaction hazards. Floatation of these structures takes place when the buoyancy force generated in the liquefied subsoil exceeds the gravity weight of the structure and soil in addition to surround friction forces. To protect these underground structures from possible earthquakes in risk regions, structure uplift mitigation measures are urgently required. There are many methods to mitigate structure uplift. These methods rely on the following mean approaches which are: 1) dissipation or decrease the excess pore water pressure beneath the underground structure;

2) increase the effective vertical stress under the structure; 3) increase the underground structure resistance against uplift; 4) reduce the seismic shear loading earthquake-induced. These approaches could be pursuance by events some changes in the model parameters (structure geometry and surrounding soil properties). The following literature review describes the studies conducted to mitigate the underground structure failures caused by earthquake-induced soil liquefaction. The countermeasures against soil liquefaction and structure failure included: 1) improve the structure surrounding soil (eg. compact the sand beneath and around the buried structures, add gravel drain walls along the sides of the structures); 2) increase the vertical stresses under the structure (eg. Add solid base and connect the structure with heavy loads); 3) protect the structure against seismic loading by surround protections (surround geogrid and vertical sheet piles); 4) change structure geometry (eg. increase the depth of the buried structure, increase the unite weight of the structure, and use anther structure shape has more float resistance).

2.5.1. Improve the Surround Soil

The traditional mitigation methods such as densification of backfill sand, water dissipation by using gravel, and sandy soil solidification by cementation were suggested after the Niigata Earthquake in 2004 (Technical Committee on Earthquake Resistant Design of Sewage Lifelines, 2004). Satisfactory performances of these measures have been reported after several actual earthquakes although minor damages were reported (Technical Committee on Earthquake Resistant Design of Sewage Lifelines, 2008). On the other hand, for a large project, some conventional measures such as cut off the wall or surround sheet piles which require a considerable time and economic resources could be used, which hinders the feasibility of these methods in the small project (Otsubo[a] et al. 2016).

Surround Sand Compaction

These loose saturated sand soil could encounter bearing compress beyond tolerable limits under static or failures due to earthquake-induced liquefaction. To eliminate such failures, loose granular soils require densification to enhance their engineering properties (Bo et al. 2014). The principle of the densification method is to increase the density and resistance of

soil against liquefaction occurring by reducing the void ratio of the soil particles and increase the soil shear stiffness (JGS, 1998). There are several methods to improve the soil against liquefaction. The most common methods are: 1) Compaction pile method; 2) Vibration method; 3) Dynamic compaction method (Fig. 2.19). Several previous studies utilize soil densification to limit the excess pore water pressure. For example, Yasuda (2005) proposed ground densification on the surround of the underground structure to mitigate possibility structure uplift. Jung[b] et al. (2013) used high-density material or increased the density of existing material surrounding the structure to limit the generation of pore water produced by soil liquefaction. Tobita et al. (2011) compacted the trench backfill surround and beneath the manhole to protect the structure against uplift. Cheuk et al. (2008) found that the value of uplift displacement of the underground structure is depended on the particle size and density of deposited soil. Yang et al. (2004) improve the ground by densifying the soil using Vibro-replacement stone columns along both sides of the tunnel.

Dissipation Using Drainage Gravel

Excess pore water dissipation methods are one of the most popular methods currently being employed to protect the underground structure against liquefaction. Changing the drainage conditions of the liquefiable soil under the structure so that the excess pore water pressure could quickly be dissipated. Excess pore water dissipation is a method to mitigate the uplift of infrastructure by enables to protect the structure from the liquefaction by dissipating the increasing of pore pressure through gravel drains or any other grain material as shown in Fig. 2.20. Here is some review of previous studies utilizing this method. Sasaki and Taniguchi (1982), drained the buildup of pore water pressure under and beside the structure caused by earthquake loading by using a gravel drain treatment adjacent to the structure. Orense et al. (2003) used recycled concrete crushed stones as gravel drain materials to dissipate the excess pore water pressure surround and under the buried structure. Yang et al. (2004) found that enhanced drainage using seismic gravel drains adjacent to were effective in remediation of earthquake-induced structure uplift.

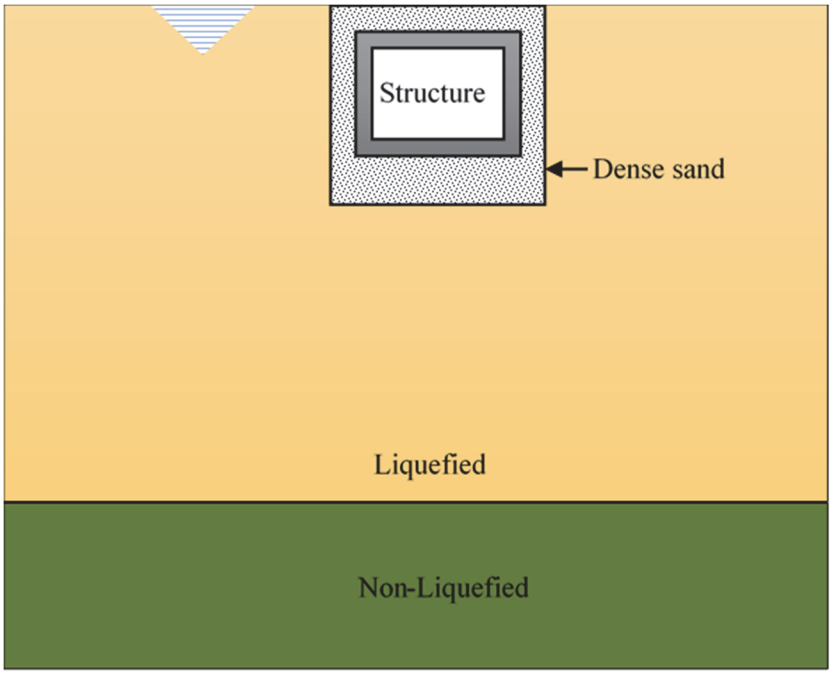

Figure 0.19 Compaction surround sand to increase the density.

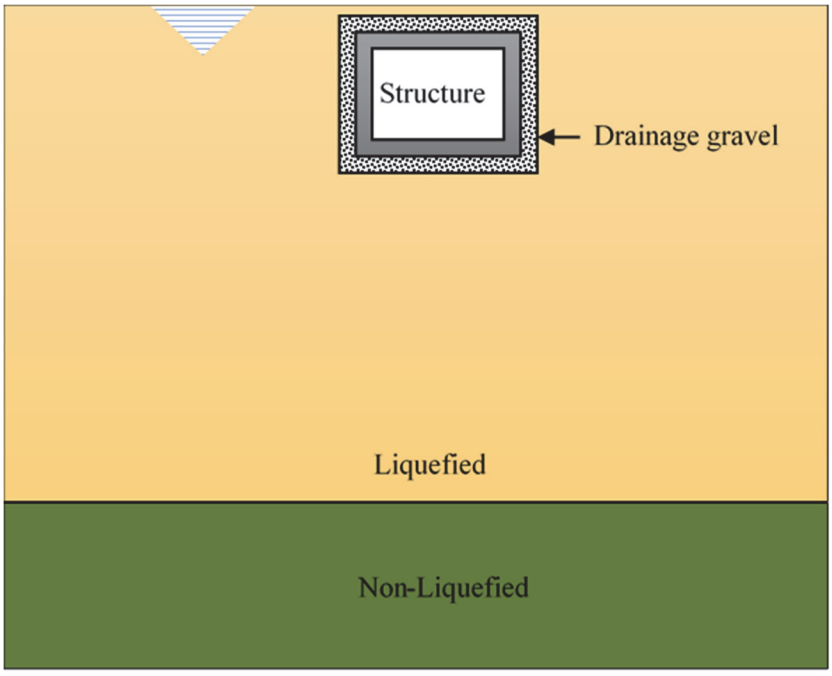

Figure 0.20 Drainage material surround the underground structure.

2.5.2. Increase the vertical stresses

The excess pore water pressure ratio (R_u) is the ratio between the excess pore water pressure and the vertical effective stress. Reducing the excess pore water pressure ratio can be implemented by decrease the excess pore water pressure as previously mentioned or increase the vertical effective stress which will be clarified currently. This method depends on increasing the pressure under the structure be adding heavy concrete weights under or surround the structure.

Solid Base Layer

Soil solidification is a method can be used to stabilize the soil by increasing its liquefaction resistance (Fig. 2.21). The non-liquefied weight gain layer is covered on the liquefiable soil layer by pressurization to increase the effective stress of the liquefiable soil layer and improve the anti-liquefaction ability of soil. The objective of this method is to reduce the liquefaction of a loose, saturated, fine sand based on the cementation concept. Liquefaction measures based on solidification include the deep mixing method, compaction grouting, jet grouting, and premixing method. For the field studies, the jet grouting method, applied for several projects in North America, was discussed in detail by Welsh and Burke (1991) and Welsh (1997). Also, in the laboratory, Bao et al. (2017) injected the soil with cement to strengthen the soil. It found that the reinforcement beneath the structure could restrain the pore water pressure of soil beneath the structure and reduce structure uplift obviously.

Surround Overweight

Castiglia et al. (2017) stabilized pipelines in liquefiable soils using heavy concrete weighting which leads to increase the vertical effective stress under the pipelines and limit its uplift (Fig. 2.22).

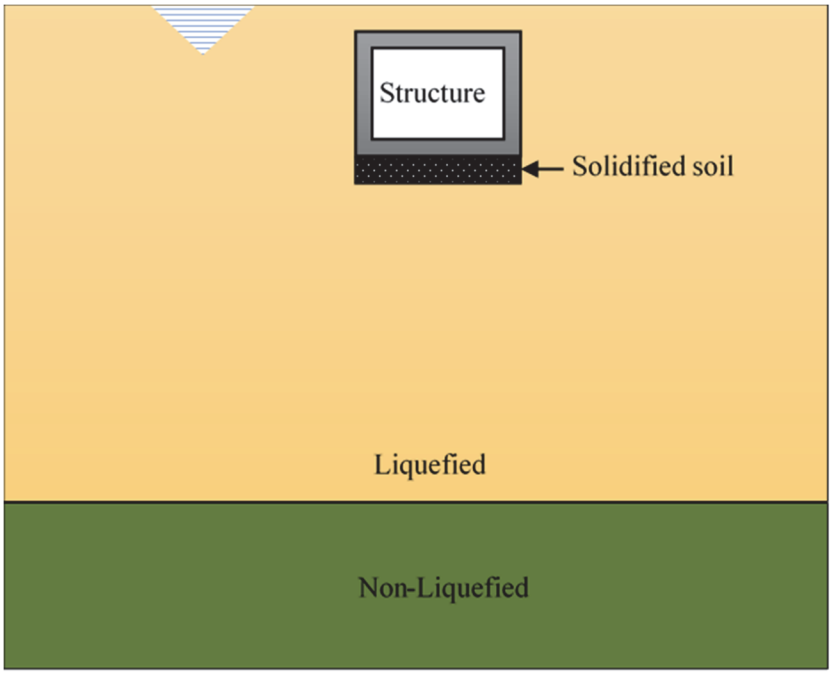

Figure 0.21 Solidification liquefaction soil by mixing with cement.

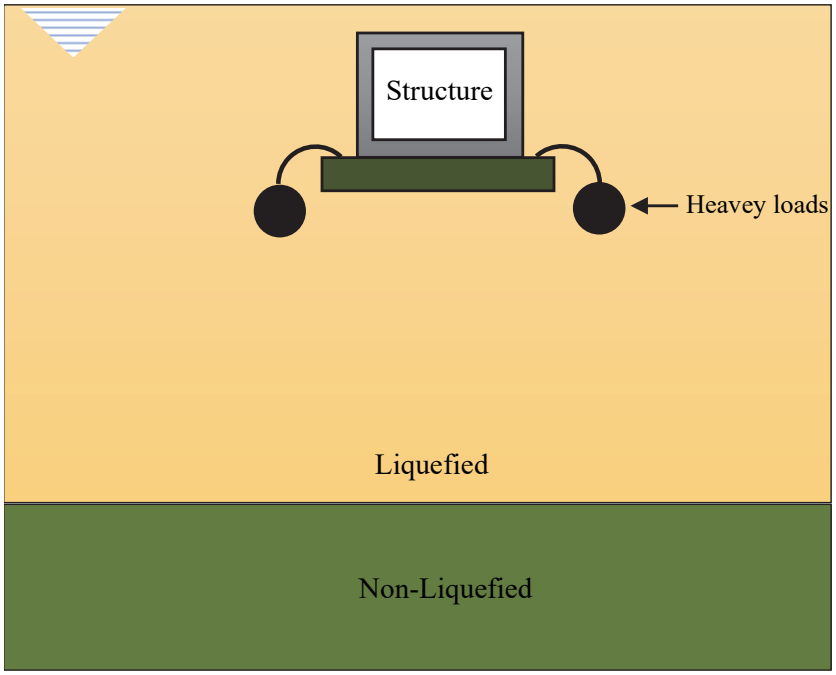

Figure 0.22 Increase the structure vertical stresses using surround concrete weights.

2.5.3. Suppression of Surround Stress

This method prevents or decreases of liquefaction occurring or structure damaging with a sheet piles (Fig. 2.23) or surrounding geogrid (Fig. 2.24) to restricting shear stresses during earthquakes. The first time this phenomenon was observed was in the 1964 Niigata earthquake, where the building encloses to sheet piles did not suffer from damages (JGS, 1998). Yasuda et al. (2004), Lui and Song (2006) and Rasouli et al. (2015) mitigate the uplift of the underground and the settlement of super surface structures due to seismic liquefaction by the installation of sheet-pile walls around the foundation. Tupa and Palmeira (2007), Palmeira and Andrade (2010), and Palmeira and Bernal (2015) used the geosynthetic material to mitigate pipeline flotation.

2.5.4. Change Structure Architecture

The development of structure architecture is a more economical method to reduce the uplift of buried structures than soil improvement. However, in many projects, changing the structure geometry (depth or dimensions) is not permissible.

Increase Burial Depth

Increasing the soil layer above the underground structure by increasing the buried depth is one of the most important methods for increasing the safety of structures against flotation (Fig. 2.25). Saeedzadeh and Hataf (2011) found that the burial depth in sands has an important role to reduce uplift is more important. Chian et al. (2014) carried out structure at different buried depths to investigate floatation failure. Liu and Song (2005) increased the depth of the buried structure which increases the vertical effective stress and confining pressure.

Change Structure Geometry

Increasing structure unit weight by increasing the structure walls thickness or change the structure shape by increase structure width or using pyramidal frustum shape (Fig. 2.26) could be used to decrease the structure uplift. Although that method is expensive, it increases the stiffness of the structure and the ability to carry more dynamic loading. This method could be used if there is no method from the above can be implemented.

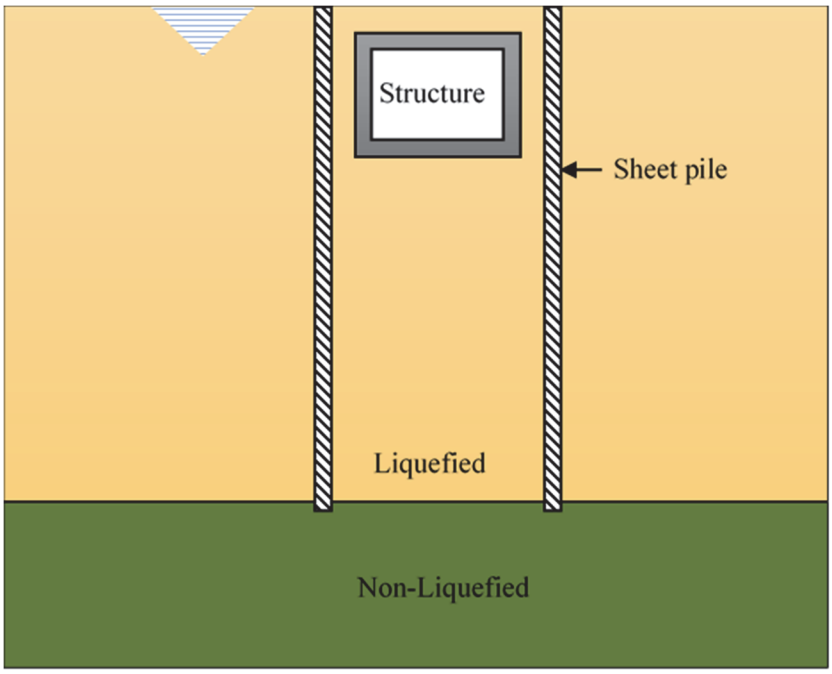

Figure 0.23 Protection underground structure from uplift using sheet pile.

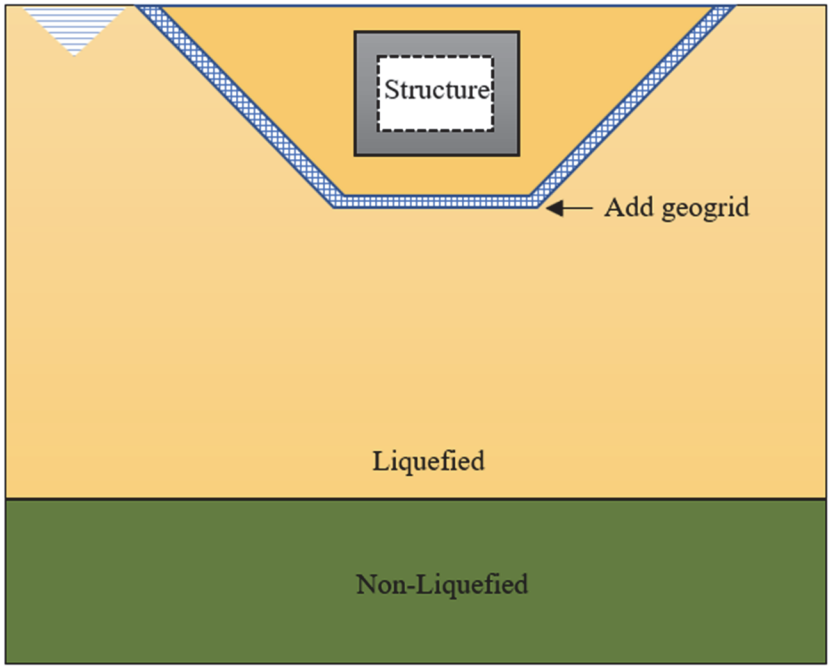

Figure 0.24 Protection underground structure using surround geogrid.

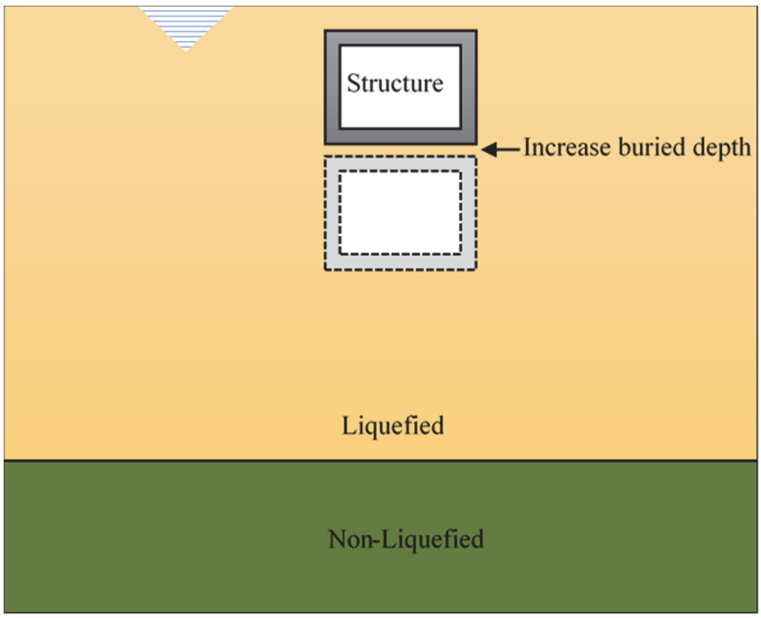

Figure 0.25 Protection underground structure from uplift by increase structure buried depth.

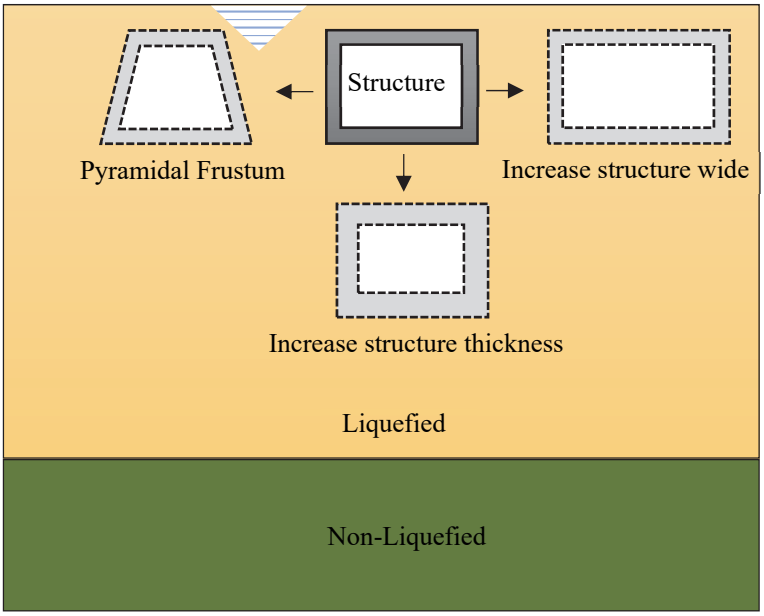

Figure 0.26 Protection underground structure from uplift by change structure shape.

CHAPTER 3. ZONES SISMIQUES AU QUÉBEC

Ahmed O. Mahmoud: Ph.D. student, Department of Civil Engineering, Université de Sherbrooke Sherbrooke, Québec, Canada.

Mahmoud N. Hussien: Researcher, Department of Civil Engineering, Université de Sherbrooke, Sherbrooke, Québec, Canada.

Mourad Karray: Professor, Department of Civil Engineering, Université de Sherbrooke, Sherbrooke, Québec, Canada.

Mohamed Chekired: Researcher, Institut de Recherche d'Hydro-Québec, Varennes ,Québec, Canada.

Carole Bessette: Direction Encadrement réseau et planification, Hydro-Québec, Montréal, Québec, Canada.

Livius Jinga: Direction Encadrement réseau et planification, Hydro-Québec, Montréal, Québec, Canada.

Date de soumission : Octobre 2019

État de la soumission : en évaluation par le comité de lecture de la revue.

Revue: Tunnelling and Underground Space Technology.

Titre français: Mise en œuvre de l'approche basée sur l'énergie comme un modèle constitutif du sol dans les analyses sismiques des structures souterraines.

Titre English: Implementation of the energy-based approach as a soil constitutive model in seismic analyses of underground structures.

Résumé: Au Québec, plus de 30 000 structures souterraines d'accès ont été installées dans la province au cours des dernières décennies pour les câbles de logement, les télécommunications et les transformateurs. Malgré les coûts énormes associés au remplacement de ces structures en cas de dommages ou de problèmes de fonctionnement suite à des dépôts naturels tels que des tremblements de terre, la conception et la construction de telles structures ne font pas l'objet de connaissances approfondies en ingénierie sismique. Dans cet article, le comportement sismique des structures souterraines d'accès enchâssées dans des dépôts sableux a été analysé à l'aide du programme FLAC^{3D} de différences finies (3D) en trois dimensions (3D), en soulignant leurs défaillances structurelles sous différents tremblements de terre compatibles avec les cinq régions à risque sismique du Québec. L'approche basée sur l'énergie, capable de simuler le comportement cyclique du sol par l'estimation de la pression de l'eau dans les pores, a été intégrée au code numérique en tant que modèle constitutif du sol, tandis que des éléments structurels linéaires ont été utilisés pour modéliser des structures souterraines. Les résultats numériques ont montré que le changement des caractéristiques sismiques en fonction de la zone sismique du Québec avait un effet prononcé sur le rapport de pression de l'eau dans les pores en excès généré dans le sol entourant la structure. L'évolution du taux de pression d'eau interstitielle en excès s'est révélée compatible avec l'augmentation du flux d'énergie du séisme. Les résultats ont également mis en evidence l'effet de la charge sismique sur les forces internes structurelles (à savoir, la force de cisaillement et le moment de flexion). Il a été constaté que les forces internes de la structure souterraine ne sont pas toujours proportionnelles aux accélérations a la base du model, en revanche, une réduction significative des forces internes a été constaté avec l'augmentation des charges sismiques à certains endroits tels que la dalle de base de la structure. Les résultats ont ensuite été utilisés pour construire des équations de conception à utiliser directement pour évaluer les valeurs de conception des forces de cisaillement dynamiques et des moments de flexion au niveau de sections critiques de ce type de structures souterraines.

Mots-clés: structure souterraine; différences finies; liquéfaction; rapport de pression interstitielle en excès; forces internes.

Abstract: In Québec, there are more than 30,000 access underground structures that had been installed over the province during the last few decades for housing power cables, telecommunications, and transformers. Despite the huge costs associated with replacing these structures in case of their damage or unserviceability following natural events such as earthquakes, there is no profound seismic engineering knowledge being included in the design and the construction of such structures. In this article, the seismic behavior of access underground structures embedded in sandy deposits was analyzed using the three-dimensional (3D) finite differences (FD) program FLAC^{3D} emphasizing their structural failures under different earthquakes compatible with the five seismic hazard regions of Québec. The energy-based approach that can simulate the material cyclic behavior through the estimation of the pore water pressure built-up was incorporated in the numerical code as a constitutive model of the soil, while linear structural elements were used to model underground structures. Numerical results showed that changing the earthquake characteristics according to the seismic zone of Québec has a pronounced effect on the excess pore water pressure ratio generated in the soil surrounding the structure. The trends of the increase in the excess pore water pressure ratio were found to be compatible with the increase of the earthquake's energy flux. The results have also evaluated seismic loading effect on the structural internal forces (i.e., shear force and bending moment). The results showed that the internal forces of the underground structure are not always raised with the increase of the input accelerations, however, there is a significant reduction in the internal forces with the increase in seismic loadings in some locations such as the base slab of the structure. The results were then utilized to develop design equations to be directly employed to assess design values of dynamic shear forces and bending moments at critical sections of this type of underground structure.

***Keywords*:** underground structure; finite difference; liquefaction; seismic zone; excess pore pressure ratio; internal forces.

3.1. Introduction

Buried geotechnical structures from small-scale pipelines to large-scale infrastructures including tunnels and subway metro are becoming more and more prevalent in the modern world because of the land congestion pressures associated with the fast-growing population (Broere 2016, Tobita, et al. 2011). Several structural damages from weather change constitute another reason for the recent widespread of underground constructions. For instance, about 1,000 steel electrical pylons and 35,000 wooden utility poles were crushed and crumpled in 1998 due to freezing rain that occurred in Québec (Lecomte et al. 1998). These damages and malfunctions suggested the transfer of electricity inside underground lines that pass-through access underground structures. In fact, the use of such underground structures improves the landscape and protects electrical equipment from bad weathering to the extent that over 10% of the overhead lines had been transferred to underground lines over the province of Québec during the last few decades. This transfer of electrical lines was accompanied by the installation of more than 30,000 access underground structures. The construction of these lines and structures is a very expensive matter however replacing these structures as a result of getting out of service following natural events such as earthquakes is more expensive (Guérin et al. 2016) and represents a serious economic burden to the province.

The history of failure of underground structures is filled with various examples, where many earthquakes (e.g., the 2004 Niigata Chuetsu, the 2007 Noto Hanto, and the 2007 Niigata Chuetsu-oki) caused serious damage to these structures (Yoshida et al. 2008). The Haiti 2010 Earthquake, in particular, resulted in severe destruction of essential systems (e.g.,

transportation and lifeline systems) leading to a 60% loss of local infrastructure (DesRoches et al. 2011). The 1995 Kobe earthquake caused about 100 m of the National Highway above the Daikai Station to settle by up to 4 m, over a width of 30 m which led to damage to the subway system in Kobe city (Tokimatsua et al. 2012). Substantial damages to buildings and underground structures have been reported after the 2011 Christchurch earthquake and its aftershocks in the Christchurch's central city and eastern suburbs (Potter et al. 2015). Uplifting of underground structures such as manholes and underground tanks were reported after the 2010 Maule Earthquake in Chile (Kang et al. 2014). These serious damages have highlighted the importance of understanding the seismic behavior of underground structures, and consequently many studies have discussed the issue through analytical (Tobita et al. 2012), numerical (e.g., Byrne et al. 2004; Yang et al. 2004; Gazetas et al. 2005; Liu et al. 2006; Azadi[a&b] and Hosseini 2010; Zhai, et al. 2014; Zhou et al. 2015; Zhuang et al. 2015; Hu et al. 2018; Wang et al. 2019], and experimental (e.g., Ling et al. 2003; Cheuk et al. 2009; Kang et al. 2009; Chou et al. 2011; Kang[b] et al. 2013; Zhou et al. 2014) modelling. However, there is no enough knowledge on the performance (e.g., straining action and uplift displacement) of these structures especially the new installed Québec access underground structures under earthquake loadings with different characteristics. The current study is devoted to the investigation of the performance of an access underground structures under seismic loads compatible with the five seismic zones of Québec shown in Fig. 3.1. To this end, three-dimensional (3D) finite different (FD) models of structures buried in sandy soils were constructed through the 3D computer code (FLAC^{3D}) (Itasca 2013) adopting the energy-based approach as a constitutive model of the soil.

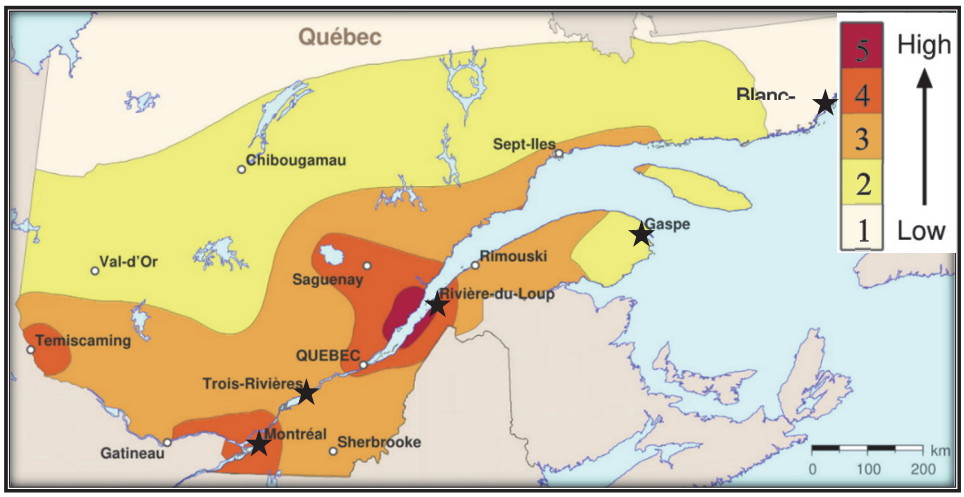

Figure 0.1 A simplified seismic hazard map in Québec (Natural Resources Canada, 2015).

These models were excited with different real and synthetic earthquakes compatible with the five seismic zones of Québec. Before presenting the results of the numerical modelling with respect to the effect of the earthquake characteristics on the seismic response of underground structures, this article presents a detailed description of the adopted numerical model and the utilized energy-based soil constitutive model. A special section has been placed on the validation of the adopted numerical model against available experimental results.

3.2. Finite Difference Modelling

There are several finite-element (FE) and finite difference (FD) programs that can adequately model soil-structure interaction problems but a little of these programs can simulate soil liquefaction that requires the differential equations of the solid and fluid phases to be coupled. The two- (2D) and three-dimensional (3D) FD, FLAC programs (Itasca 2013), are of these codes that can implement coupled effective-stress models. The computer program FLAC^{3D}, in particular, is extensively utilized in engineering practice to investigate the seismic response of underground structures in liquefiable and non-liquefiable grounds and it has been used herein to simulate the seismic behavior of Québec access underground

structures. The soil was loose saturated Ottawa sand which is one of the most recommended liquefied soil and was utilized in several previous studies. The soil layer was assumed to be 10 m thickness overlaid a rigid rock. The properties of the used Ottawa sand and its particle size distribution are described in Table 3.1. The underground structure in question is a typical Hydro-Québec chamber (4.0 x 2.0 x 3.0 m) with two different diameter manholes (i.e., D = 0.6 and 1.0 m) located at the top slab of the structure as shown in Fig. 3.2. Figures 3.2 (a and b) show the elevation (on x-y plane)) and plane (on x-y plane) views of the chamber with the surrounding soil zones. The structure and the two manholes are simulated by linear structural elements. The height of the soil elements affects the transmission of high-frequency shear waves. For this reason, the height of the elements was limited to a maximum height, ΔL (Kuhlemeyer and Lysmer 1973), which is smaller than one-tenth of the wavelength of the input wave.

$$\Delta L \leq \frac{\lambda}{10} \qquad [1]$$

where λ is the wavelength associated with the highest frequency of the input earthquake. The soil element size is selected at 0.5 x 0.5 x 0.5 m around the structure and gradually increases as it goes outward as shown in Figs. 3.3.

3.3. Constitutive Model of The Soil (Energy-Based Approach)

When a saturated cohesionless soil layer is subjected to an earthquake or strong shaking, it tends to decrease in volume producing an increase in the pore water pressure accompanied by a significant decrease in its shear strength and it behaves like a liquid (Figueroa et al. 1994). During soil liquefaction, most of the shear energy of the motion is dissipated.

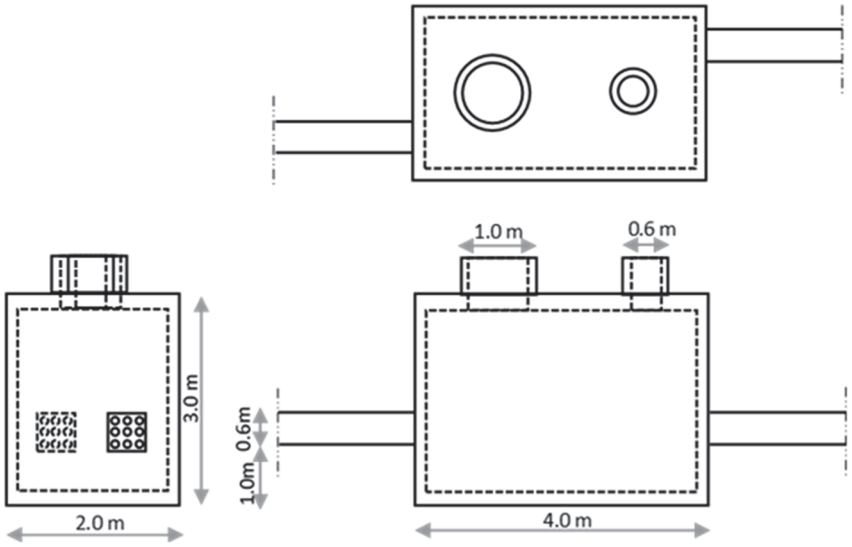

Figure 0.2 Dimensions of a typical Hydro-Québec chamber.

Seed and his colleagues at the University of California at Berkeley developed an energy-based pore pressure generation model as an alternative to the well-known stress-based model (Booker et al. 1976). The motivation for the development of this model was to enable them to use the dissipated energy as a measure of soil liquefaction resistance (Seed et al. 1983). Nemat-Nasser and Shokooh (1979) assumed that the pore water pressure build-up is directly related to the amount of seismic energy dissipated in the unit volume of soil. The excess pore water pressure ratio (R_u) can be then estimated from the cyclic energy per unit volume of the soil as demonstrated by Berrill and Davis (1985) and Davis and Berrill (1982). More recent laboratory test results obtained from the stress and strain-controlled cyclic shear tests by Karray et al. (2015) confirmed that the dissipated energy per unit volume during cyclic loading is closely connected to the generated excess pore water pressure, and the developed relationship between dissipated energy and excess pore pressure ratio can be expressed as (Cubrinovski and Ishihara 2001):

$$R_u = \alpha \left(\frac{W_s^{0.5}}{a_x} \right)^{\beta} \qquad [2]$$

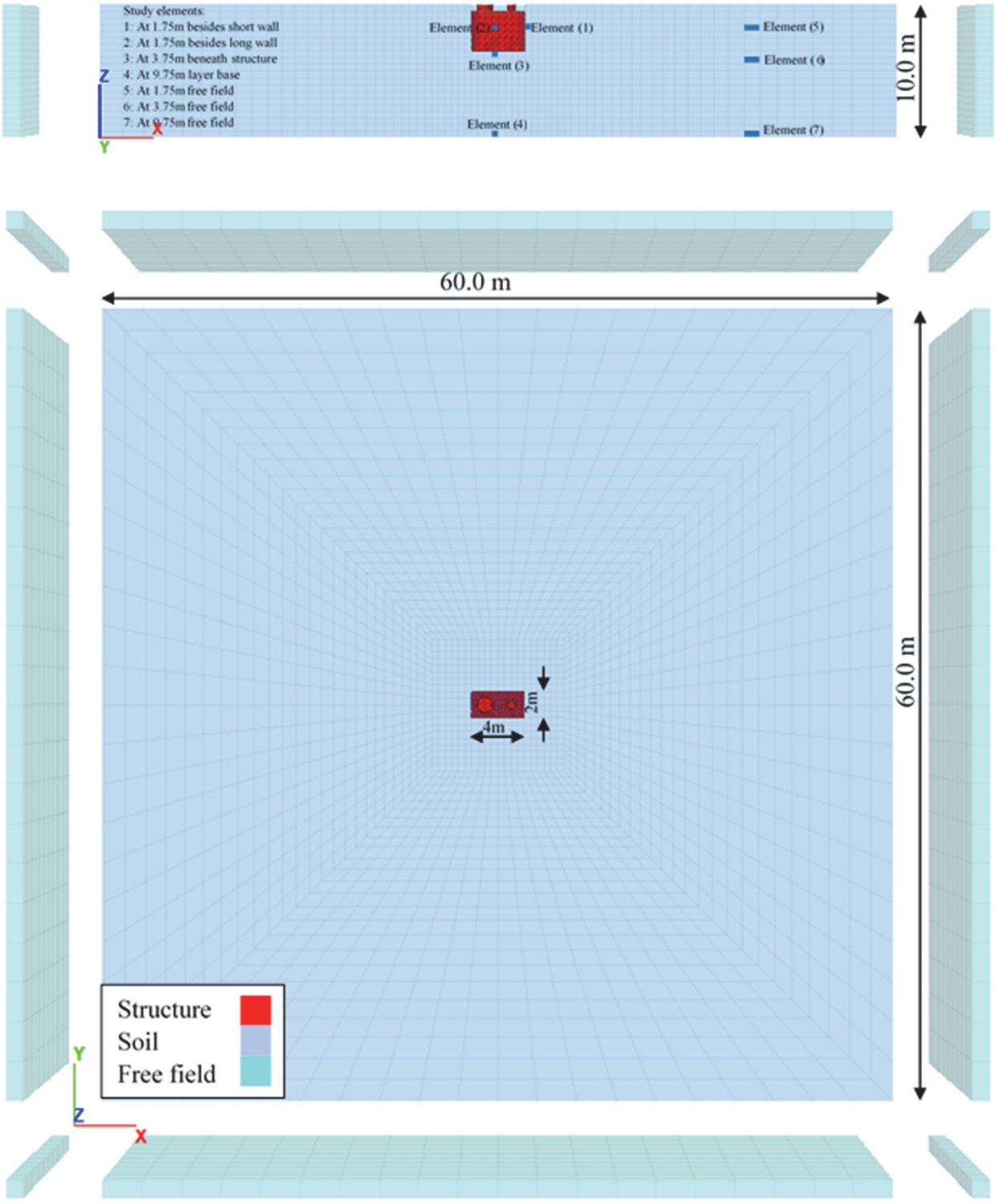

Figure 0.3 (a) section elevation (view on x-z plane); (b) plane view (top view on x-y plane) of the numerical model.

where W_s is the energy dissipated per unit volume of soil divided by the initial effective confining pressure which can be determined by integrating the area bound by stress-strain hysteresis loops as shown in Fig. 3.4; α, β, and a_x are parameters depend on the tested soil. The area enclosed by the stress-strain hysteresis loop is proportional to cyclic energy dissipation. The accumulative dissipated energies can be calculated by accumulating the dissipated energy in consecutive cycles.

In this study, the numerical analyses were performed in two stages. In the first stage (self-weight static analysis), the soils were represented by the elastic constitutive model implemented in FLAC^{3D} and in-situ stresses were developed in the model due to gravity. Following this phase, the strains and displacements within the model were reset to zero. In the second stage (seismic analysis), the soils were represented using the Mohr-Coulomb model as implemented in FLAC^{3D} and liquefaction behavior is simulated using the energy-based approach constitutive model (Eq. 2) calibrated with cyclic simple shear tests. In the first phase, the base boundary between the soil deposit and the bedrock was assumed to be fixed in both horizontal and vertical directions. However, the lateral boundaries are assumed to be fixed in horizontal directions. Also, the ground surface was assumed to be flat and free of loadings. As an extreme case, the underground water level is assumed at the ground surface. In the second stage, the free field (FF) conditions were employed to release the horizontal restraints of the side boundaries (Fig. 3.3). The horizontal seismic load was applied at the rigid base boundary. Sand parameters used in the numerical analyses (Table 3.1) were determined based on the assumed relative density (% D_r) and stress-normalized shear wave velocity (V_{s1}) equal to 20% and 100 m/s, respectively. The shear wave velocity (V_s) can be then determined from V_{s1} as (Youd et al. 2001):

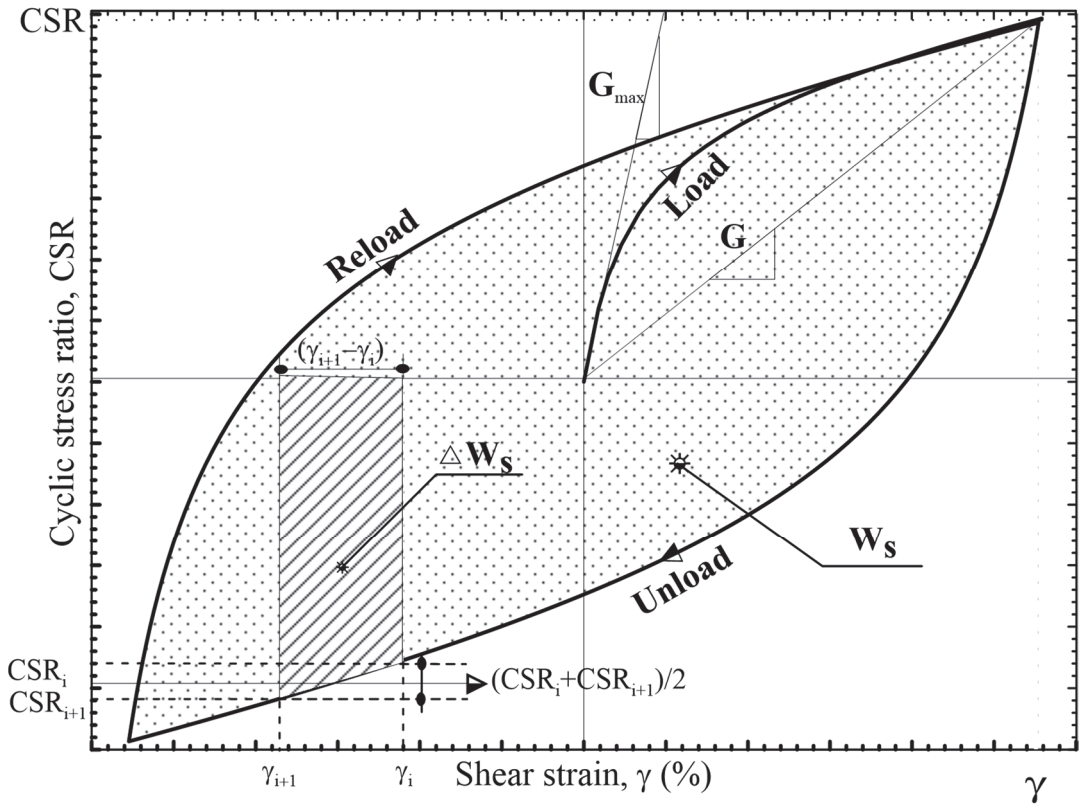

Figure 0.4 Dissipated energy per unit volume of a soil sample tested in a cyclic shear test determined by integrating the area bound by the stress-strain hysteresis loop.

$$V_s = V_{s1} \times \left(\frac{\sigma_v^{'}}{P_a} \right)^{0.25} \quad [3]$$

G_0 and K_0 are the elastic parameters used in the first phase of numerical analyses. The maximum shear modulus (G_0) was determined based on the value of V_s from the elastic relationship between the G_0 and V_s; $G_0 = \rho \times V_s^2$, where ρ is the soil density. By assuming a Poisson ratio (υ) of 0.33, the bulk modulus of soil (K_0) can be determined from G_0. Following the dynamic analysis, the hysteretic-type model is developed by noting that the S-shaped curve of modulus versus the logarithm of cyclic strain can be represented by a cubic equation, with zero slopes at both low strain and high strain. The secant modulus (G_s) can be calculated from the following equation (Hardin and Drnevich, 1972):

$$G_s = y_0 + \frac{a}{1 + e^{\frac{x_0 - L}{b}}} \quad [4]$$

Where L is the logarithmic shear strain and the fitted parameters (a, b, x_0, y_0) of the sigmoidal (SIG4) model were selected to produce shear modulus degradation and damping curves, of the sand deposit. The SIG4 model was adopted to fit the shear modulus degradation (Fig. 3.5a) and damping (Fig. 3.5b) curves of the sand during dynamic loading to the experimental curves suggested by Seed and Idriss (1970). The fitted parameters of the SIG4 model were selected such that they produce shear modulus degradation and damping curves, respectively at the sand upper and lower limits provided by Seed and Idriss (1970) as shown in Fig. 3.5. Additionally, a Rayleigh damping ratio of 0.2% and minimum frequency (f_{min} = vs/4H) equal 2.5 Hz which was used to ensure the stability of the numerical solution process at low strain levels and remove high frequency.

3.4. Calibration and validation constitutive model

Before describing the results of the seismic analyses of underground structures, the applicability of the adopted energy-based approach to study the soil behavior under cyclic loading has been carried out through the simulation of cyclic simple shear test on a sand quarry at Canada named as Ottawa Sand F-65. The sand parameters used in the numerical simulation are listed in Table 3.1. These parameters were determined based on the known relative density of the soil (D_r = 20%). In the analysis, shear stress is applied to the top of a soil element having a fixed base and free top as a sine wave with a 50 kPa amplitude and 1.0 Hz frequency. The results of the analysis are compared to the simple shear test results in terms of shear strain path and excess pore water pressure ratio response. The comparative results presented in Fig. 3.6 indicates that the current energy-based model has the capability to reasonably simulate the cyclic behavior of sand.

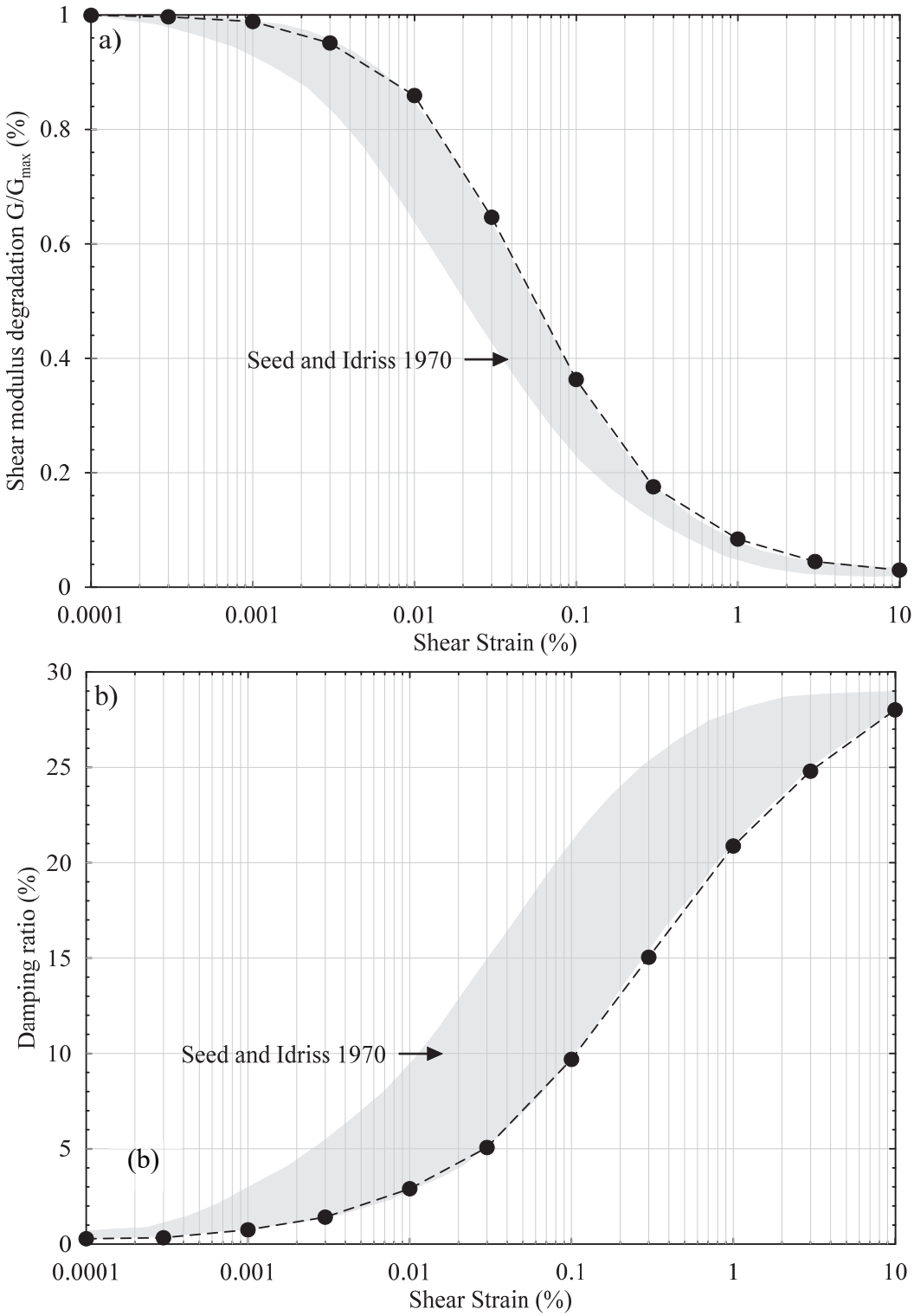

Figure 0.5 (a) Shear modulus reduction; (b) damping ratio curves for sandy soil compared with Seed and Idriss (1970).

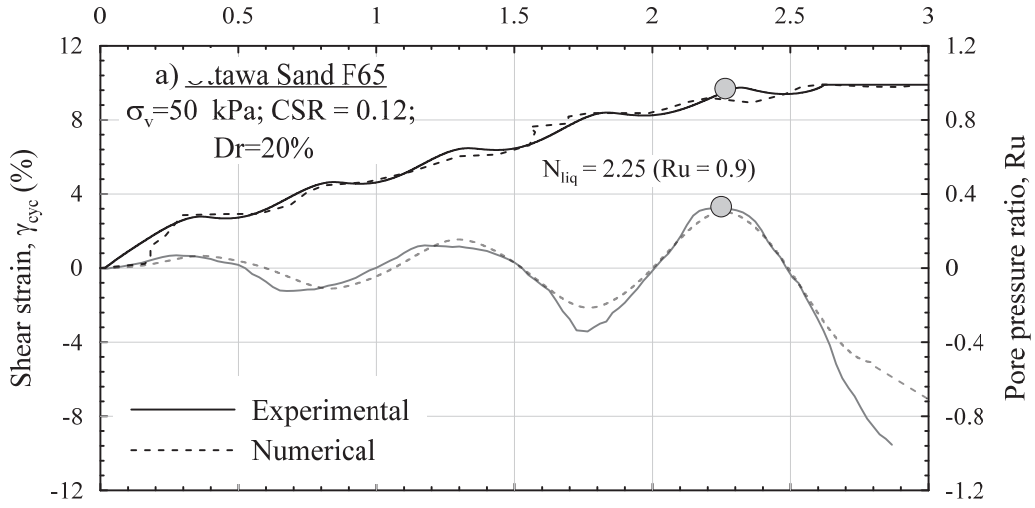

Figure 0.6 Comparison between cyclic direct shear test results and current numerical simulations (a) Loose sand (relative density = 20%).

The applicability of the used soil constitutive model in particular and the adopted numerical model in general to the analysis of the seismic behaviour of underground structure is examined by the simulation of centrifuge experiments conducted by Chian et al. (2014), to be called previous study, on seismic performance of a circular tunnel embedded in a uniform horizontal fully saturated sand. The centrifuge experiments were created using a window box. A sine wave acceleration with amplitude = 2.2 m/s^2 and frequency = 0.75Hz was applied as a seismic load. In the analysis, the dimensions of the zone elements were selected at 0.5 × 0.5 × 0.5 m (Fig. 3.7a). The same numerical parameters were used to simulate the soil behavior in the numerical analyses conducted in this study. The structure is assumed to be elastic material with young modulus and Poisson's ratio of 30 GPa and 0.2, respectively (Liu and Song 2005). From Figs. 3.7b and 3.7c, it can be found that the build-up of excess pore water pressure ratios (R_u) computed at the spring of the tunnel and the model base are very close to their measured counterparts. Also, the final predicted movements were in good agreement with the measured data from the centrifuge tests. And therefore, it could be concluded that the numerical model adopted in the investigation is capable of simulating the structure seismic behavior.

3.5. Numerical results and discussion

In recent decades, the seismic analysis of above and underground structures using seismic hazard maps has been an important design practice for engineers. Through the National Building Code of Canada, seismic hazard maps have been developed and updated for design structures based on 2% in the 50-year probability of exceedance (Adams and Atkinson 2003). In this map, the Province of Québec was divided into five main zones (from 1 to 5) according to the severity of the earthquake (Fig. 3.1). Every zone has a limit to the seismic value to design the structures. Usually, the spectral acceleration value of every region used to find out the extent of the expected intensity of earthquakes. Figure 3.8a shows the spectral acceleration of five cities in Québec located in the five different zones. In the numerical analyses, a realistic earthquake (Saguenay 1988) (Fig. 3.8b) which is one of the largest recorded earthquakes in Eastern Canada and Eastern North America during the 20th century is used as an input motion. The earthquake amplitude was multiplied by different factors to be compatible with the various zones as shown in Table 3.2. The input accelerations of the different zones were applied at the model base in the longitudinal direction of the structure (X-dir.) which is more soften than the short direction. The acceleration response, excess pore pressure and internal forces of underground structures have been carefully studied in the different cases. However, the uplift displacement has not been discussed herein as there is no occurrence of full liquefaction and the excess pore water pressure ratio did not reach unity. At such value, the structure begins to move (Liu and Song 2005; Kang[b] et al. 2013; Chian et al. 2012).

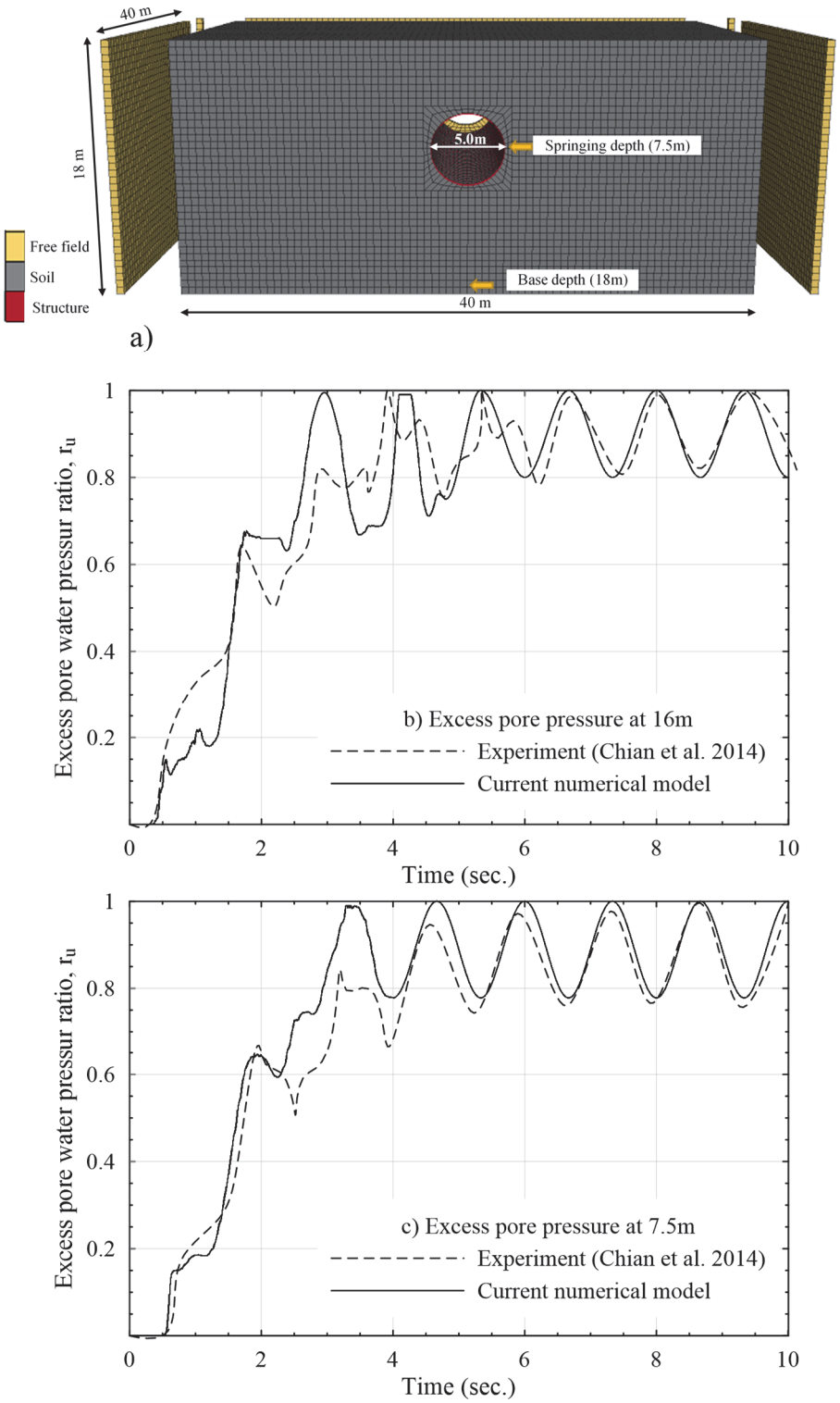

Figure 0.7 (a)Layout of the numerical validation model of Chian et al. (2014); (b) excess pore water pressure ratio time histories at base depth; (c) excess pore water pressure ratio time histories at spring level.

Table 0.1 Sand parameters used in the numerical simulation.

Static numerical parameters		Dynamic numerical parameters	
v_{s1} (m/s)	100	α	1.0
G_0 (MPa)	15	β	0.6
K_0 (MPa)	40	a_x	$0.92\gamma^{-0.455}$
ρ_d (kg/m^3)	1540	a	1
ϕ_f (°)	32.9	b	-0.55
k (m/s)	1e-5	x_0	-1.5
n	0.43	y_0	0.001

V_{s1}: normalized shear wave velocity; G_0: initial shear modulus at a confining pressure of 100 kPa; K_0: initial bulk modulus at a confining pressure of 100 kPa; ρ_d: dry density; ϕ_f: failure angle of friction; k: soil permeability; n: porosity; α, β and a_x: calibration liquefaction parameters; a, b, x_0 and y_0: hysteretic fitted-parameters; γ: soil shear strain.

Table 0.2 Different study zones and different applied earthquake characteristics.

Location characteristics		Earthquake properties		
Zone	Location	Multiply factor	Arias intensity (cm/sec)	PGA (g)
1	Blanc-Sablon	0.5	0.46	0.025
2	Gaspé	1.0	1.83	0.05
3	Trois-Rivières	2.0	7.3	0.10
4	Montréal	3.0	16.5	0.15
5	Rivière-du-Loup	6.0	65.9	0.30

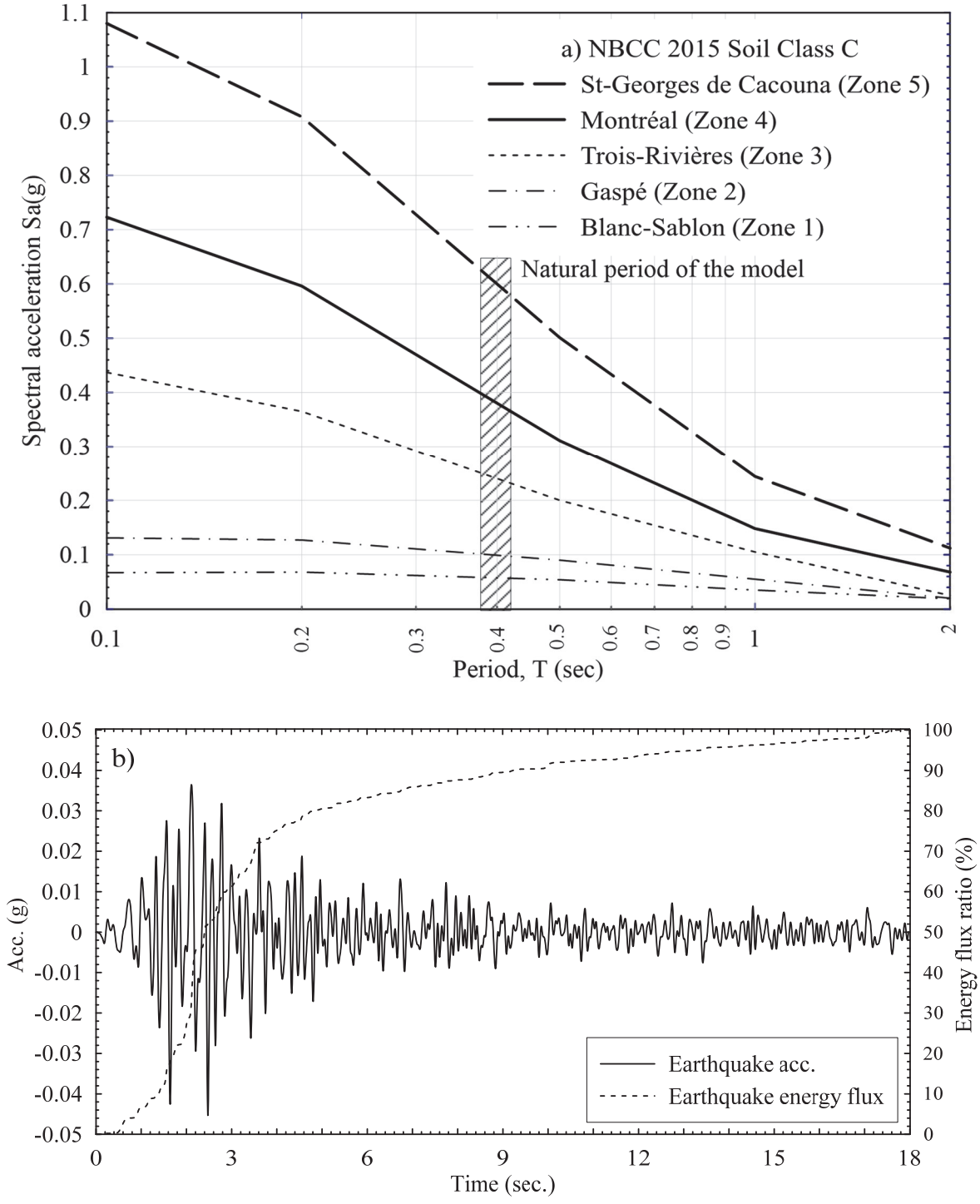

Figure 0.8 (a) spectral accelerations of different seismic zones in Quebec, (b) acceleration time history of the 1988 Saguenay earthquake.

3.5.1. Acceleration response

Figures 3.9 shows the time histories of the acceleration response to different earthquakes compatible with the seismic zones (1-5) of Québec at different locations (i.e., at the base and at the ground surface in the free-field and above the structure) of the deposit. In the seismic zones 1 and 2, significant amplification occurred at the free-field ground surface accelerations compared to the slight changes of the ground surface accelerations above the structure. The difference in the acceleration amplifications is attributed to the filtering effect caused by the structure. In the seismic zones 3, 4 and 5, the soil became more softening due to the increase in the excess pore water pressure ratio as it will be discussed later. Therefore, it is found that there is a reduction in the ground acceleration both in the free-field and above the structure (Youd and Carter 2005).

The above results can be verified from Fig. 3.10 that pertains to spectral accelerations at the base and at the ground surface in the free-field and above the structure for the seismic zones 1 and 5. In zone 1, when the soil deposit is excited with relatively low-frequency excitations ($f < 3.3$ or $T > 0.3$), there are ground surface amplifications both in the free-field and above the structure, and the amplification of the ground surface acceleration above the structure begins to diminish with the increase of the excitation frequency until it is converted to a reduction at relatively higher frequencies as shown in Figs.3.10a. In zone 5 (Fig.3.10b), except for a relatively low-frequency excitation ($f < 1.5$ or $T > 0.7$) where there is no significant change in the acceleration amplitude, the amplitudes of the ground surface accelerations are significantly reduced both in the free-field and above the structure.

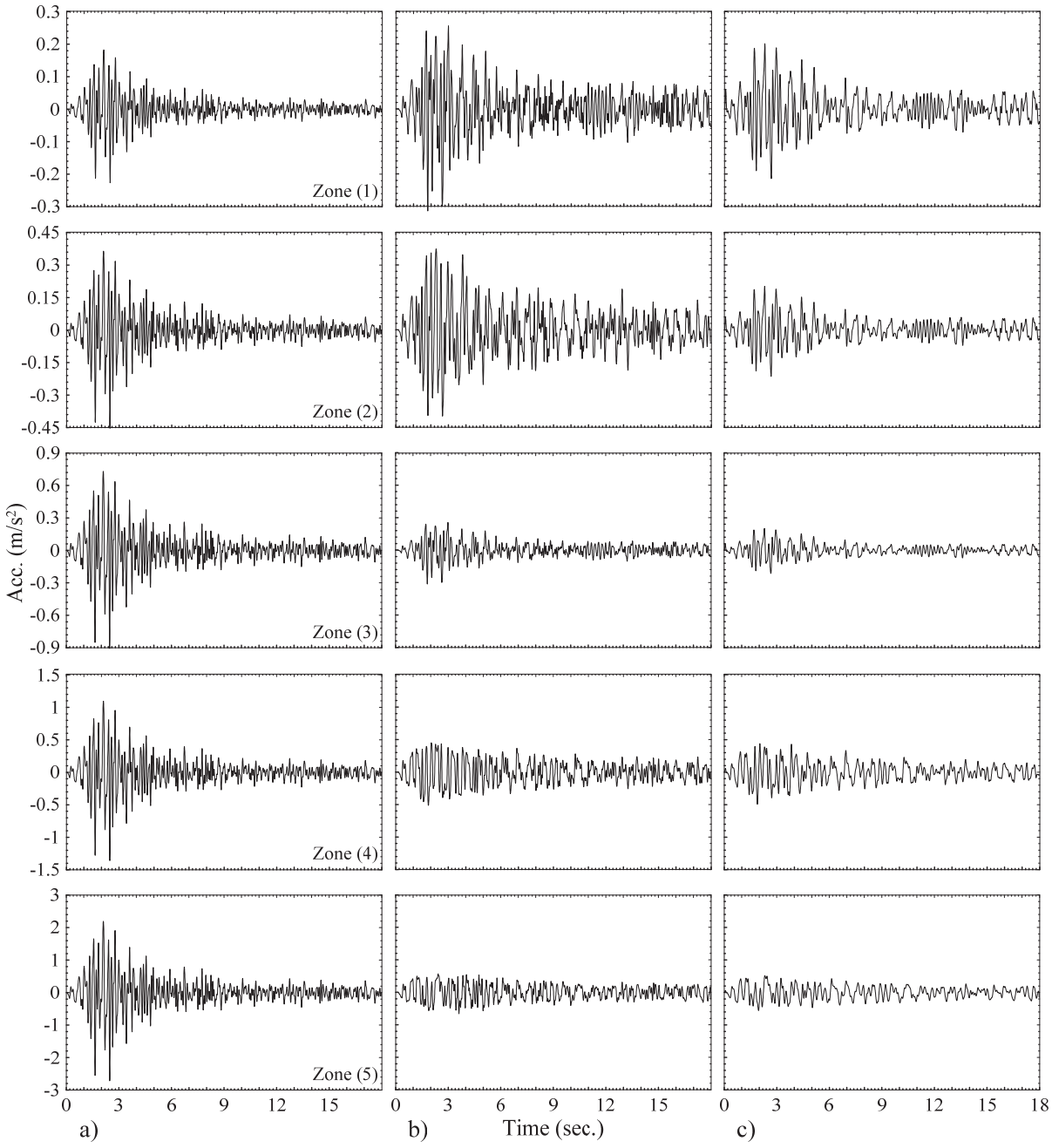

Figure 0.9 Time histories of the acceleration: a) at the base and; b) at the free-field ground surface; c) at the ground surface above the structure for the different zones.

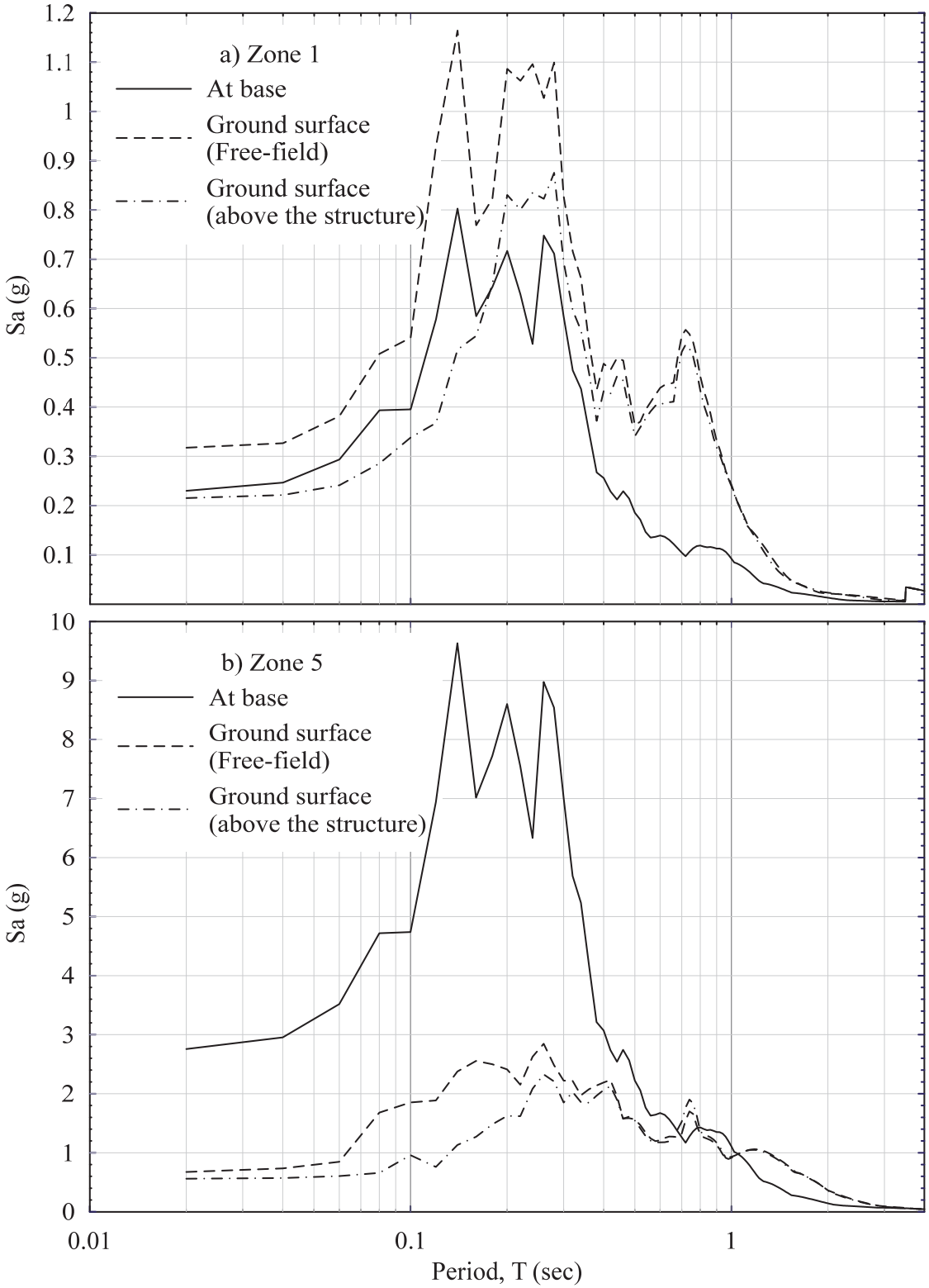

Figure 0.10 Spectral accelerations of the motions at the base and at the surface in the free-field and at the ground surface above the structure for zones: (a) 1 and (b) 5.

Figures 3.11 show the effects of the excitation amplitude (soil nonlinearity) on the acceleration response at ground surface both at the free-field (Fig. 3.11a) and above the structure (Fig. 3.11b). The theoretical transfer function in linear condition (Gazetas 1984) is used as a reference liner amplification and calculated as follows. The horizontal acceleration (a_0) is applied at the bedrock of homogenous soil deposit of thickness(H) and shear wave velocity (v_s) and soil damping (ζ). By using the one-dimension amplification theory, the output acceleration (a_1) at the ground surface can be calculated according to the following equation:

$$\frac{a1}{a_0} = \frac{2}{e^{iqH}+e^{-iqH}} \quad [5]$$

where i^2=-1 and$q = \frac{\pi}{2H\times\sqrt{1+2i\zeta}}$. In Fig. 3.11a, in the free-field case, it is found that the increase of the acceleration amplitude has two main effects: (a) it decreases the natural frequency of the soil deposit (natural period lengthening) due to the reduction of shear wave velocity (shear modulus) with acceleration amplitude (strain level); (b) it reduces the peak values because of the increase of soil damping with shear strain. These results are consistent with those established in the literature (e.g., Gazetas 1984, Hussien et al. 2018). These two effects are not noticeable in Fig. 3.11b where the presence of the structure significantly alters the ground surface response. More specifically, the structure acts as a kind of filter that absorbs significant excitation energy. As can be seen in Fig. 3.11b, the amount of energy-filtered by the structure depends on the excitation amplitude. For lower input motion (PGA = 0.25 m/s^2), the structure absorbs most of the input energy resulting in a transfer function (T.F.) greatly lower than the unity. At larger input motion (PGA = 3.00 m/s^2), it appears that the structure doesn't filter significant energy and the resulted filtered ground surface acceleration is not very far from the unfiltered acceleration at the free-field (Fig. 3.11a), which is compatible with Bao et al. (2017).

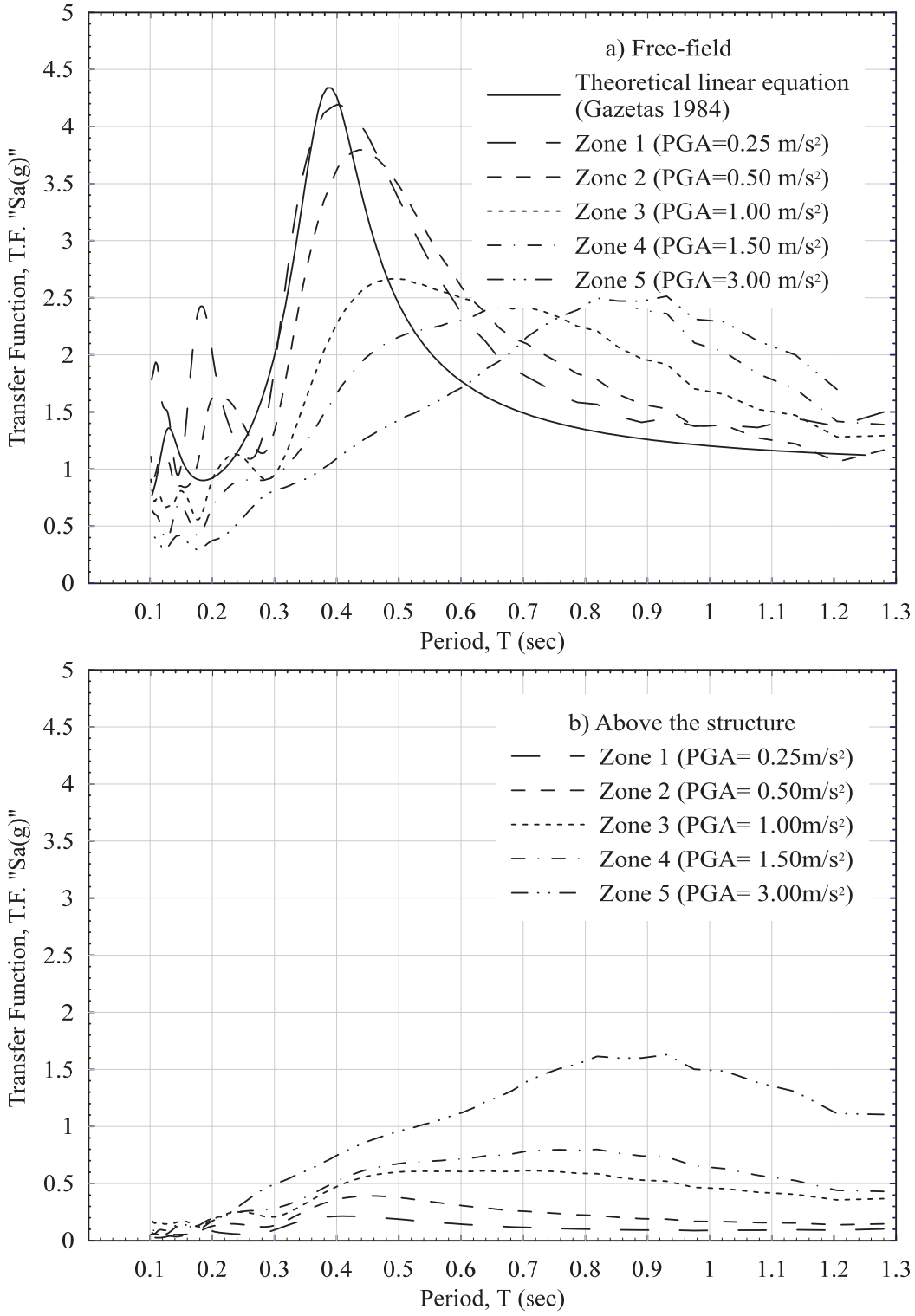

Figure 0.11 Transfer Function of the surface to the base acceleration: (a) at the free-field; (b) above the structure.

3.5.2. Excess pore water pressure ratio

Figures 3.12 show the variation of the excess pore pressure ratio of the soil beneath the structure and at the same depth at a different horizontal distance from the centerline of the structure for the different seismic zones. Fig. 3.12a, it can be seen that the excess pore water pressure ratio under the structure is more than that of the surrounding soil at the same level due to the pronounced reduction in the effective vertical stresses under the structure. Also, it is found that the excess pore water pressure ratio increases from 20% to 80% between zone 1 and zone 5. Figure 3.12a shows also that the excess pore water pressure ratios under the structure are approximately twice their values at the free-field. The diagram is not symmetric due to the direction of the propagating wave and the structure geometry. Figure 3.12b shows the build-up of excess pore water pressure ratio at 3.5m depth in the different seismic zones. It is found that the excess pore water pressure ratio increases steadily during the first 4 seconds in varying proportions for each zone after that the increase is of a small percentage; this trend of change in the pore water pressure is, in fact, compatible with the increase in the energy flux of the input earthquake motion (Fig. 3.8b). Figure 3.13 shows the excess pore water pressure ratio built-up in the seismic zone 4 at depths 1.75, 3.5, and 10m both in the free-field and close to the structure. Figure 3.13a illustrates that the excess pore water pressure ratio generated at 1.75 m depth in the free-field is generally lower than that developed adjacent to the short side of the structure at the same depth and it is in the meantime greatly higher than the developed ratio adjacent to the long direction. Similarly, Fig. 3.13b shows that the excess pore water pressure ratio generated under the structure (3.5 m depth) is higher than that developed in the free-field at the same depth. As expected, the excess pore water pressure ratio at or close to the bedrock level (depth = 10 m) is almost the same irrespective of whether the point in question is located under the structure or at the free-field region (Fig. 3.13c).

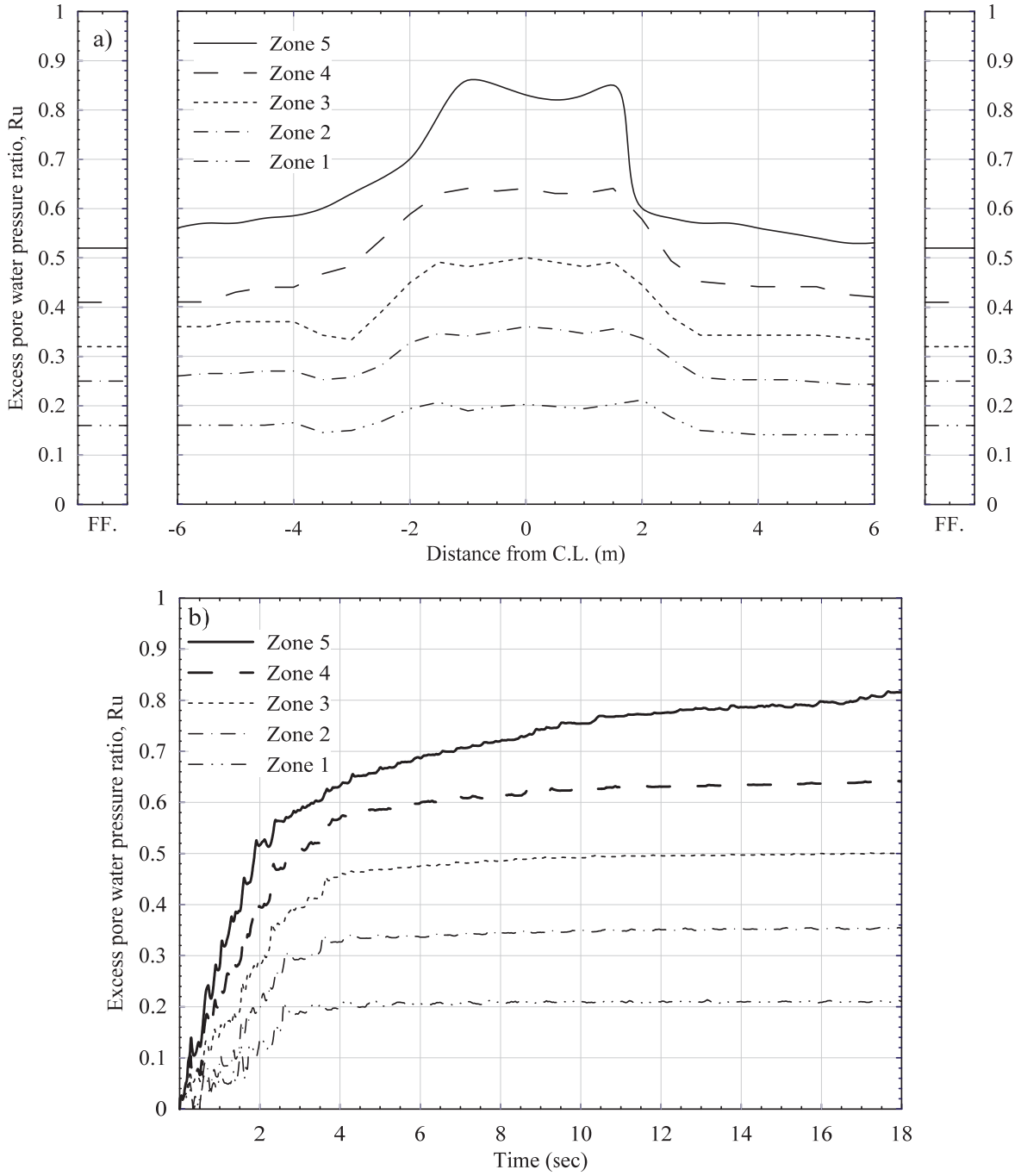

Figure 0.12 variation of the excess pore pressure ratio of the soil beneath the structure with different seismic zones: a) cross-section at the middle of the structure; b) excess pore water pressure time histories.

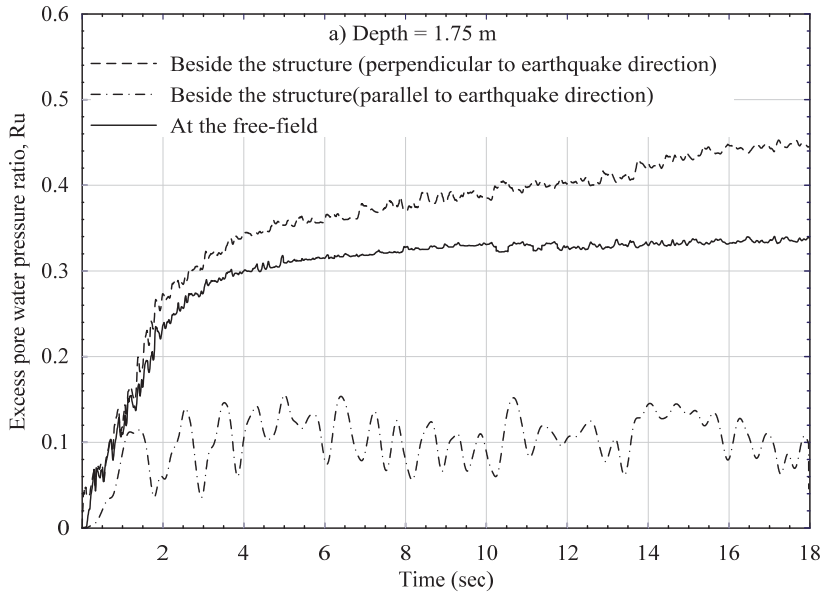
a) Depth = 1.75 m
Beside the structure (perpendicular to earthquake direction)
Beside the structure(parallel to earthquake direction)
At the free-field
Excess pore water pressure ratio, Ru
Time (sec)
0
0.1
0.2
0.3
0.4
0.5
0.6
2
4
6
8
10
12
14
16
18

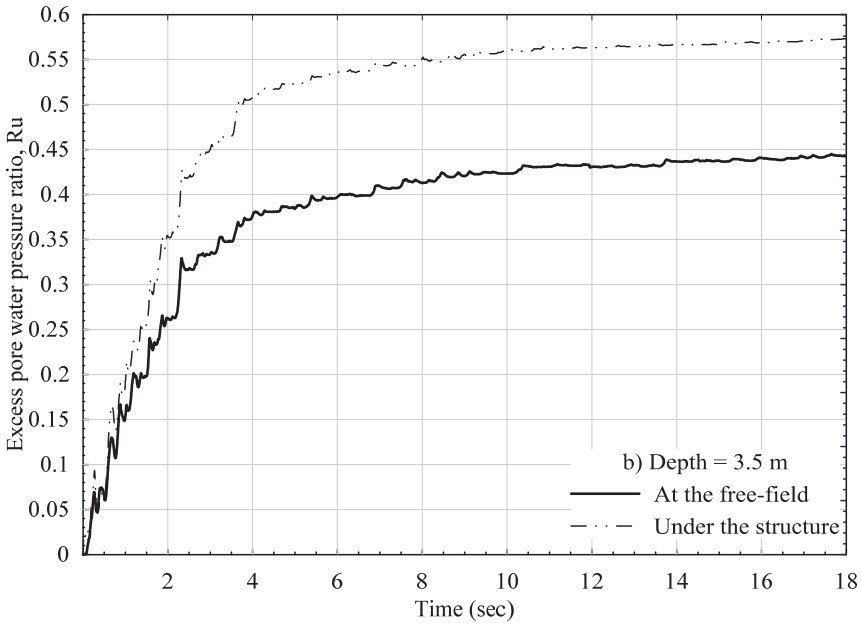
b) Depth = 3.5 m
At the free-field
Under the structure
Excess pore water pressure ratio, Ru
Time (sec)
0
0.05
0.1
0.15
0.2
0.25
0.3
0.35
0.4
0.45
0.5
0.55
0.6
2
4
6
8
10
12
14
16
18

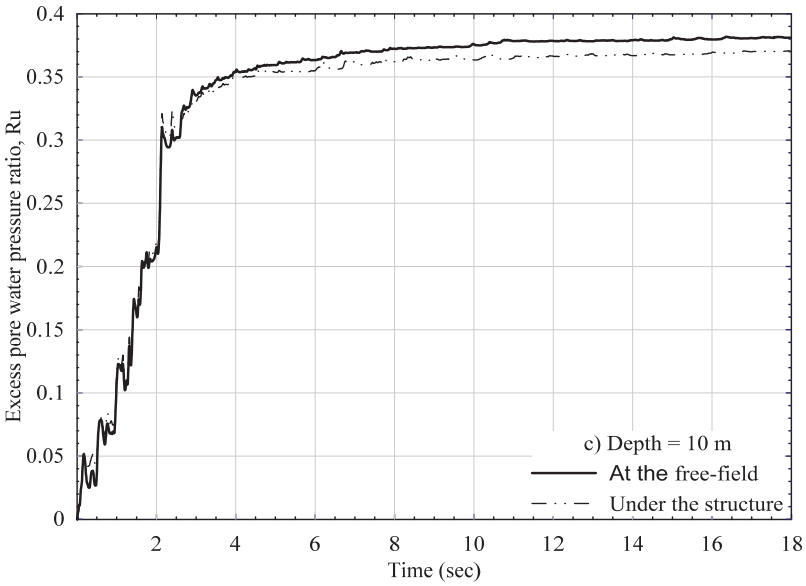

Figure 0.13 Comparison between the excess pore pressure ratio time histories of zone 4 in the free-field and the structure at: (a) 1.75m; (b) 3.5m; (c) 10m depth.

Figure 3.14 shows the excess pore water pressure ratio distribution at different cross-sections for the seismic zones 1, 3, and 5. It can be seen that the excess pore pressure ratio generated in the soil beneath the structure is relatively high compared to that generated elsewhere at the same depth due, as mentioned earlier, to the reduction in the effective vertical stresses under the structure. In the soil surrounding the structure, it is observed that the excess pore pressure ratio exhibits significant reduction beside the long side of the structure (parallel to the earthquake direction) and significant increase beside the short side of the structure (perpendicular to the earthquake direction) compared to the free-field soil at the same depth. The increase in the excess pore water pressure ratio beside the short side can be attributed to the inertial stresses (i.e., in the form of successive tension and compression stresses) transferred to the soil from the direct contact of the vibrated sides (short sides) of the structure with the surrounding soil. While the reduction in the excess pore water pressure ratio of the soil beside the long sides of the structure as a result of moving the soil beside the structure long side at the same structure velocity which leads to a reduction in the soil strain in this area and then decreases in the liquefaction ratio.

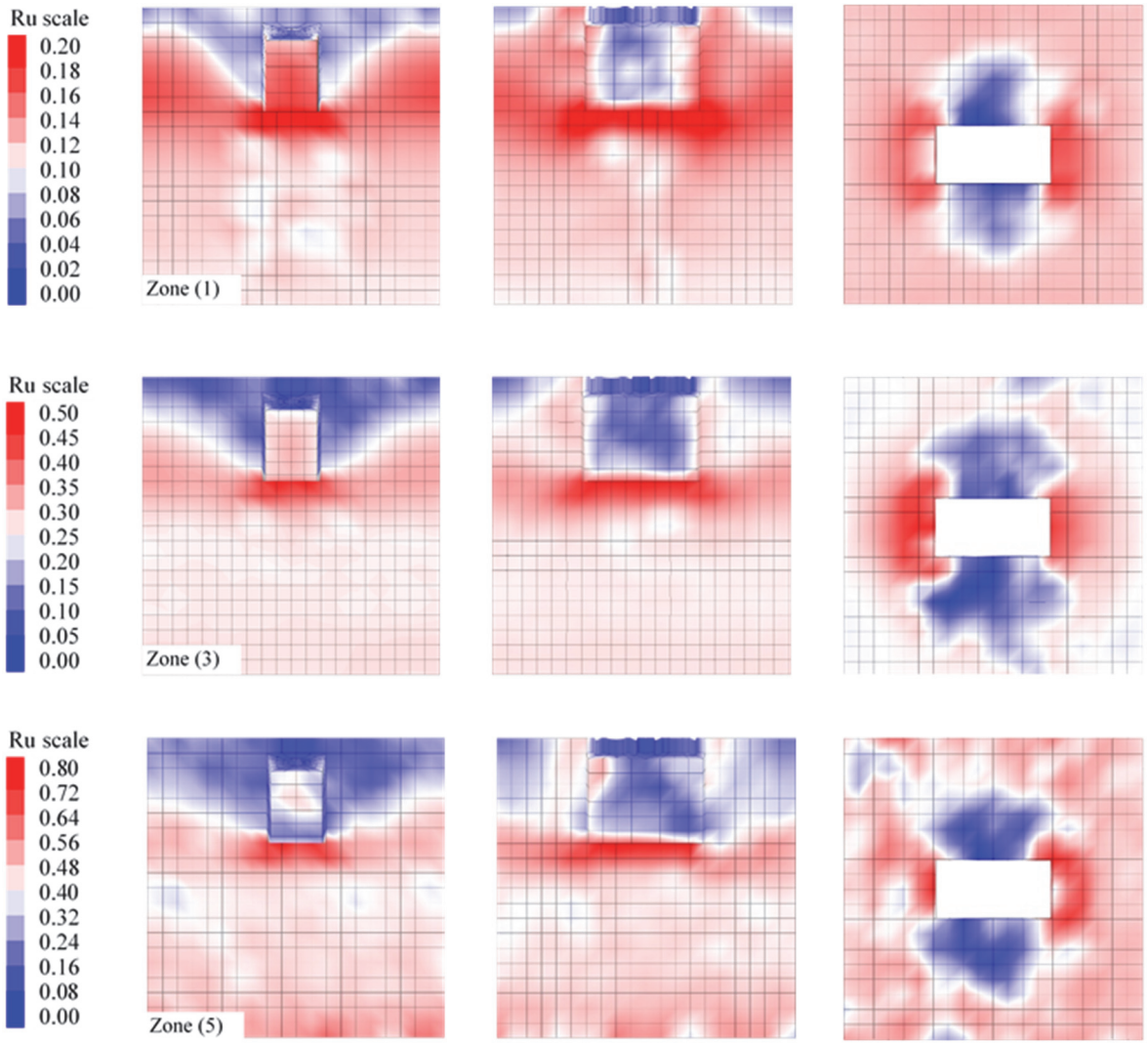

Figure 0.14 (a) Vertical section along the short side of structure(Y-Z); (b) Vertical section along the long side of the structure(X-Z); Horizontal section of the structure at 1 m depth (X-Y).

3.5.3. Internal forces of the underground structure

Similar to what have been established in the literature (e.g., Liu and Song 2005), the results of the current numerical study show that the maximum internal forces in the analyzed structures have occurred at the edges and members corners (Liu and Song 2005), and these seismic internal forces increase with the increase of the earthquake amplitude. Figures 3.15 shows the

bending moment distribution of the structural members at the same cross-sections presented in Figs. 3.15 for both cases before (static) and after (static +dynamic) the earthquake application assuming the loading condition of the seismic zone 5. It can be seen from Figs. 3.15 that the maximum moment at the static case occurs in the base slab of the Y-Z section with a value of 18.12 kN.m/m at the edge and a value of 11.4 kN.m/m at the middle of the slab. However, at the maximum seismic loading at 4 sec, it is found that the moment in the middle of the slab decreases to 7.1 kN.m/m and that in the sidewall increases from 7.4 to 11.6 kN.m/m, thus the sidewall has the maximum moment in the seismic case and the base slab has the maximum moment in the static case. The elements that have maximum bending moments in the three cross-sections as shown in Figs. 3.15a-3.15c have been further studied in Figs. 3.16. Figure 3.16a shows the increase and the decrease in the normalized dynamic bending moment (i.e., in Fig. 3.16a the dynamic bending moment (BM_{dy}) at a given section is normalized by the static moment (BM_{st}) at the same section) of the selected elements considering the loading conditions of the five seismic zones of Québec. It can be seen that the normalized bending moment increases in the long-side wall from about10-15% to 56-66% between the seismic zone 1 and 5. These increases are resulting from the increase in the lateral soil pressure due to the increase in the earthquake amplitude accompanied by the soil softening with the strain level attained. However, the increase of the normalized bending moment in the short wall did not exceed one-third of the value in the long wall. On the other hand, there is a reduction in the normalized bending moment of the based slab up to 38% with the increase of the earthquake amplitude (i.e., moving from the seismic zone 1 to 5). This reduction is, in fact, resulted from the reverse moment generated from the additional deformations and stresses in the side walls.

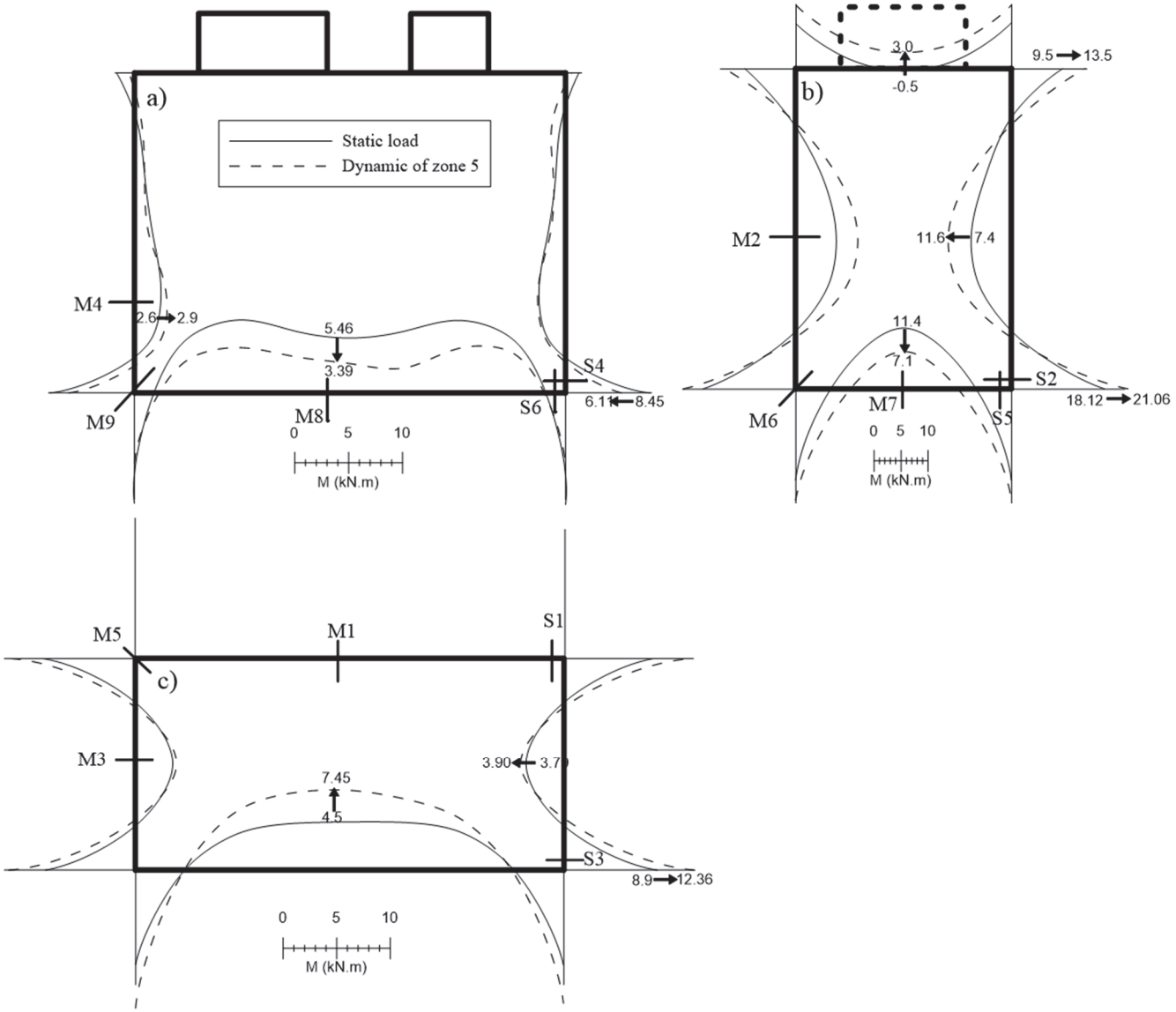

Figure 0.15 Bending moments in static and dynamic phases of analyses at a time of 4 sec in the considering the seismic zone 5: (a) X-Z section; (b) Y-Z section; (c) X-Y section at 2m depth.

Figure 3.16a portrays also the normalized bending moments in the corners of the structural elements. In the corner between long and short walls where there is an increase in the soil pressure in both walls with the increase of the earthquake amplitude, a condition that leads to an increase of the normalized bending moment at this edge. Likewise, in the base slab-long wall corner where the normalized bending moment increases with the increase of the seismic acceleration. This can be simply attributed to that the rate of the increment of the normalized bending moment in the long side wall is higher than the reduction rate of the normalized moment in the base slab and this reason can also explain the observed reduction in the normalized bending moment in the base slab-short wall corner. The same trends have been observed in shear forces as shown in Fig. 3.16b, where the increase in the pressure of the soil surrounding the sidewalls of the structure leads to increases of the shear forces in both long- and short-side walls. The extra deformations and stresses in the sidewalls give rise to generate deformations and stresses reverse the deformations resulting from the soil structure base slab interaction. Which in turn leads to reduction occurs to the shear forces in the base slab.

Figs. 3.17a-3.17b show the most important alteration in shear forces and bending moments due to the change in the spectral accelerations (Sa) in the Y-Z section. On the sidewalls, it is noted that shear forces at the edges and bending moments at the center increase linearly as Sa increases. However, for the bottom slab, they decrease linearly as Sa increases. The actual rate of change in the normalized shear forces (SF) and the normalized bending moments (BM) of the sidewall and the base slab with the change in Sa, shown in Figs. 3.17, can be expressed as:

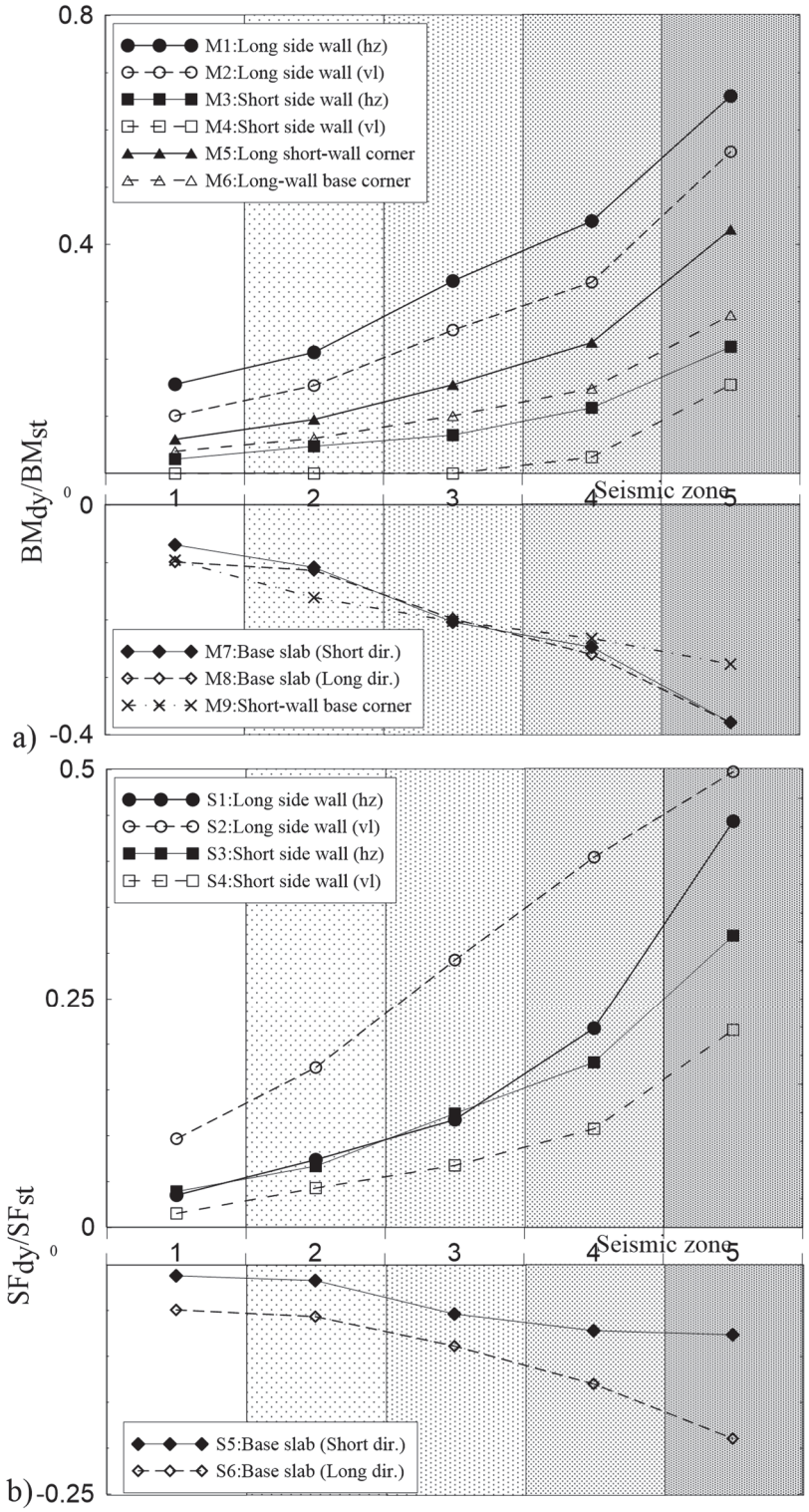

Figure 0.16 Change of the internal forces with the different seismic zones in: (a) bending moment; (b) shear forces.

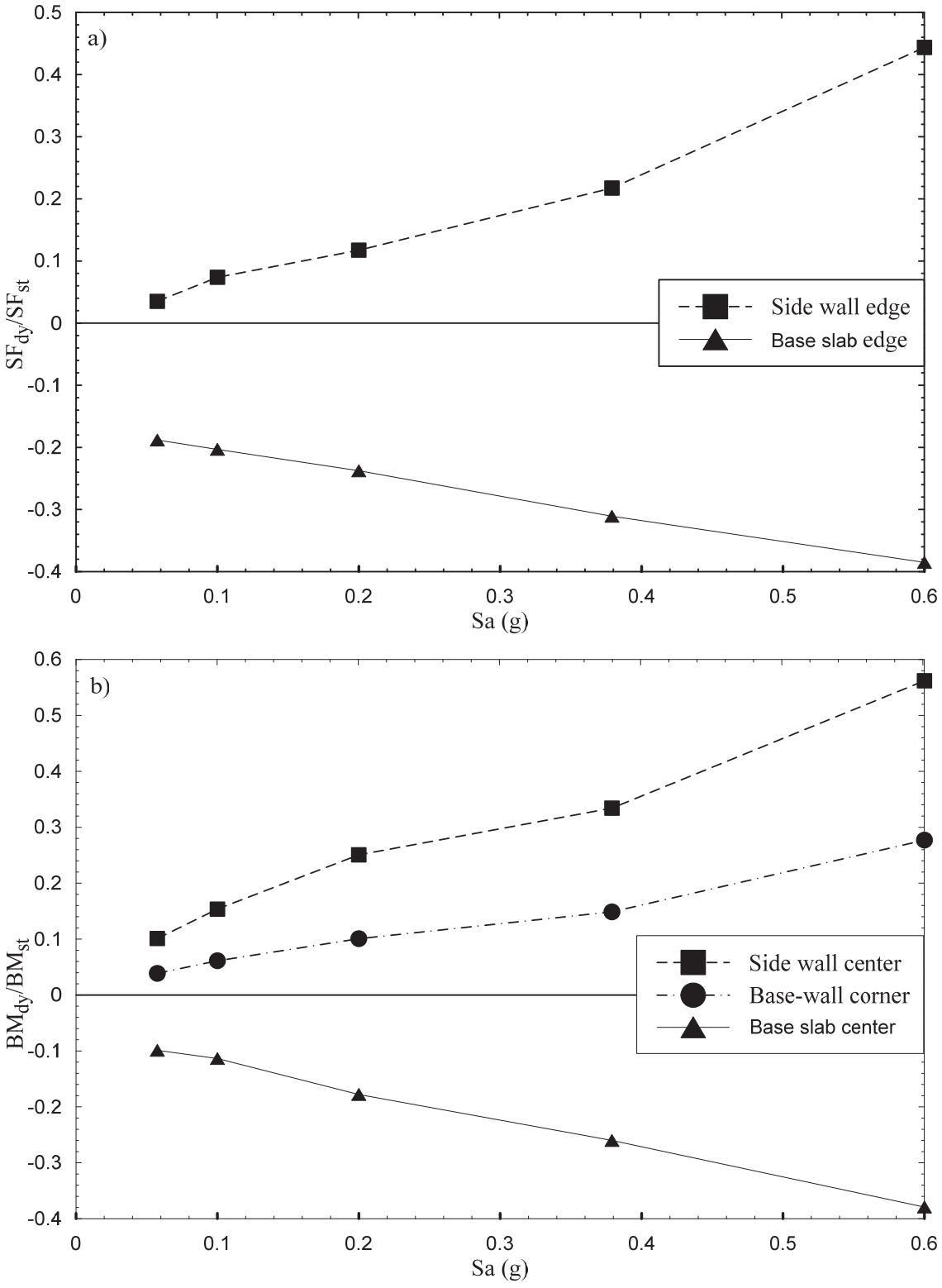

Figure 0.17 Effect of spectral acceleration of the different seismic zones on: (a) shear forces; (b) bending moments of Y-Z section.

For the sidewall:

$$(SF_{dy} / SF_{st}) = 0.72 \times Sa - 0.016 \quad [6]$$

$$(BM_{dy} / BM_{st}) = 0.80 \times Sa + 0.065 \quad [7]$$

For the base slab:

$$(SF_{dy} / SF_{st}) = -0.367 \times Sa - 0.167 \quad [8]$$

$$(BM_{dy} / BM_{st}) = -0.52 \times Sa - 0.067 \quad [9]$$

For the base-wall corner:

$$(BM_{dy} / BM_{st}) = 0.64 \times Sa + 0.021 \quad [10]$$

These equations can be used to estimate the dynamic straining actions at different critical sections of the structure based on the static values conventionally computed from simple static equilibrium analyses of the structure and the spectral accelerations (Sa) limits provided at the different seismic zones according to the deposit's characteristics as illustrated in Fig. 3.8a and loose saturated sand soil. In the case of stiffer or softer soil, the soil shear velocity will change and then the soil deposit natural frequency and its spectral acceleration need to recalculate.

3.6. Conclusion

Three-dimensional numerical analyses were conducted in this paper to study the seismic performance of access underground structure in the five seismic zones in Québec. The energy-based approach was used as a constitutive model to simulate the seismic behavior of the soil. The acceleration response, the excess pore pressure, and the internal forces of the underground structure (i.e., shear forces and bending moment) were investigated. From the numerical results, the following conclusions can be obtained:

1. At low-amplitude excitations, amplification of the ground surface accelerations in the free-field is higher than those occurring above the structure. However, at higher amplitude excitations, there is a general reduction in the ground surface acceleration both in the free-field and above the structure as a result of the increase in the excess pore water pressure ratio producing a softer behavior of the soil.

2. The trends of the increase in the excess pore water pressure ratio were found to be compatible with the increase of the earthquake's energy flux. And the excess pore pressure ratios under the structure are approximately twice their values at the free-field.

3. The excess pore pressure ratio increases along the side of the structure perpendicular to the earthquake direction compared to the free-field soil at the same depth. While the significant smaller increase in the R_u value was observed along the side of the structure parallel to the earthquake direction.

4. The numerical results obtained throughout the current study are utilized to construct design equations to be directly employed to assess design values of dynamic shear forces and bending moments at critical sections of this type of underground structure.

It should be noted that the results presented in this paper are valid for Hydro-Québec underground structure which is installed in Québec seismic zones, and the specific soil properties that were used. For any other installation structures, seismic zones and different soil conditions similar analysis should be performed.

CHAPTER 4. SÉISMES DE FRÉQUENCES DIFFÉRENTES

Ahmed O. Mahmoud: Ph.D. student, Department of Civil Engineering, Université de Sherbrooke Sherbrooke, Québec, Canada.

Mahmoud N. Hussien: Researcher, Department of Civil Engineering, Université de Sherbrooke, Sherbrooke, Québec, Canada.

Mourad Karray: Professor, Department of Civil Engineering, Université de Sherbrooke, Sherbrooke, Québec, Canada.

Mohamed Chekired: Researcher, Institut de Recherche d'Hydro-Québec, Varennes ,Québec, Canada.

Carole Bessette: Direction Encadrement réseau et planification, Hydro-Québec, Montréal, Québec, Canada.

Livius Jinga: Direction Encadrement réseau et planification, Hydro-Québec, Montréal, Québec, Canada.

Date de soumission : Décembre 2019

État de la soumission : en évaluation par le comité de lecture de la revue.

Revue: Soil Dynamics and Earthquake Engineering.

Titre français: Variabilité de la réponse de la structure souterraine à des séismes de caractéristiques variées.

Titre English: Variability in the underground structure’s response to earthquakes with varied characteristics.

Résumé: La liquéfaction du sol sous et autour des structures souterraines développées en raison de l'augmentation de la pression de l'eau dans les pores lors d'un événement sismique constitue l'une des principales causes dommageables de ces structures. L'accumulation de pression interstitielle lors de forts séismes entraînerait également un soulèvement important de la structure enterrée, ce qui aurait un impact direct sur sa fonctionnalité. Ce problème complexe d'interaction sol-structure constitue toujours un défi pour le praticien et les ingénieurs concepteurs, car il nécessite un examen rigoureux des aspects du problème liés à la modélisation géométrique et matérielle, ainsi que des caractéristiques des séismes utilisés dans les calculs. Dans cet article, le comportement sismique des structures souterraines d'accès enchâssées dans des dépôts sableux a été étudié à l'aide du programme de différences finies tridimensionnelles (3D) FLAC^{3D}. L'approche énergétique permettant de simuler la liquéfaction cyclique en estimant la pression de l'eau interstitielle accumulée a été intégrée au programme afin de modéliser le comportement du gisement sableux. Des éléments de structure de revêtement ont été utilisés pour modéliser la structure souterraine. Une modélisation numérique a été réalisée pour étudier les performances de la structure et du sol sous trois différents séismes historiques de durées similaires, mais avec des contenus de fréquence différents. Les PGA de ces séismes ont été modifiés à 0,25, 0,5 et 1,0 g pour étudier les facteurs d'amplitude. En outre, deux cas d'étude dans différents profils de sol ont été étudiés. On constate que l'effet du contenu fréquentiel sur la structure et le comportement du sol n'est pas moins important que l'effet du facteur d'amplitude et que, dans certaines situations, la l'accroissement de la fréquence des séismes entraîne une modification plus importante de la pression de l'eau dans le les forces internes structurelles que ferait l'amplitude du séisme.

Mots-clés: structure souterraine; différences finies; liquéfaction; contenu de fréquence; rapport de pression interstitielle en excès; PGA; méthode simplifiée; CHBDC.

Abstract: Soil liquefaction beneath and around underground structures developed due to the increase of the pore water pressure during a seismic event constitutes one of the most important damaging reasons for these structures. The build-up of pore water pressure during strong earthquakes would lead to a significant uplift of the buried structure which has a direct impact on its functionality. This complex soil-structure interaction problem always poses challenges to practitioners and design engineers as it requires a rigors consideration of geometrical and material modelling aspects of the problem as well as a proper assessment of earthquakes' characteristics used in the computations. In this paper, the seismic behavior of underground structures embedded in sandy deposits was studied using the three-dimensional (3D) finite differences (FD) program FLAC^{3D} adopting the energy-based approach to simulate the cyclic liquefaction of the soil. Liner Structural Elements were used to model the underground structure. Numerical modelling has been carried out to investigate the structural and soil performances under three different historical earthquakes with similar durations but different frequency contents. The PGA of these earthquakes were modified to 0.25, 0.5, and 1.0 g to investigate the amplitude factors. It is found that the effect of the frequency content on the structure and the soil behavior is not less important than the amplitude factor effect and in some situations, the increase of the earthquake frequency leads to more alter in the excess pore water pressure of the soil and consequently the structural internal forces than it would do the earthquake amplitude.

***Keywords*:** underground structure; finite-difference; liquefaction; frequency content; excess pore pressure ratio; PGA; simplified method; CHBDC.

4.1. Introduction

Geotechnical structures buried near the ground surface have a wide range of applications, from small-scale pipelines to large-scale infrastructures including tunnels and subway metro. These structures are becoming more and more prevalent in the modern world because of the decreasing availability of ground space due to the fast-growing population. In other words, underground infrastructures, have been a widespread alternative to what in redeveloping urban spaces to ease land congestion pressures (Yue and Li 2007). In another way, the transfer of the power to houses above the ground through overhead lines faces several types of damages as a result of weather changes represented by windstorms and frozen storms which is a bound-in Canada in general and Quebec in particular (Lecomte et al. 1998). For this reason, Hydro-Quebec starts to replace the overhead electricity lines by underground wires inside tubes. These tubes converge in typical Hydro-Quebec underground structures. Replacing those structures is very expensive so the structures should be designed against potential damages particularly earthquakes.

These underground structures are susceptible to damage during seismic loadings, especially those which are constructed underground in a liquefiable layer. There are several reports on the devastations of underground structures caused by earthquakes. Two damage types could occur to underground structures: i) failure of the structure due to raising in internal forces; ii) structure flotation due to the increment of the pore water pressure under the structure. Figures 4.1 show different examples of underground structure damages due to earthquakes. In 1995 through the Tohoku Pacific earthquake, about 100 m of National Highway above the Daikai Station had settled by up to 3 to 4 m, over a width of 30 m which leads to damage

to the subway system in Kobe city (Tokimatsua et al. 2012). Substantial damage to buildings and underground structures have been reported after the earthquake and its aftershocks in the Christchurch's central city and eastern suburbs (Kaiser et al. 2012). In the 2010 Maule Earthquake, in Chile, the uplifting of the underground structures (manholes and tanks) were reported, and the underground tank in San Pedrodel Valle was uplifted by approximately 1.2 m (Yasuda et al. 2010).

During seismic events, the underground structures are generally subjected to an uplift force due to an increase in the pore water pressures which leads to lowering their submerged unit weight compared to the surrounding soils. Numerical models and physical tests studied seismic behavior of underground structures including the potential uplift of these structures can be found in the literature (e.g., Ling et al. 2003; Cheuk et al. 2008; Kang et al. 2009; Kang[b] et al. 2013; Zhang and Chian 2019; Kutter et al. 2008; Haiyang et al. 2019; Kramer and Elgamal 2001; Wang et al. 2005; Byrne et al. 2004; Zhai et al. 2014; Zhou et al. 2014). The majority of these studies were focusing on the effect of peak ground acceleration of an earthquake (PGA) on the overall behavior of underground structures (e.g., Chen et al. 2019; Kang et al. 2014; Azadi[a&b] and Hosseini 2010; Bau et al. 2017; Liu and Song 2005; Liu and Song 2006; Tobita et al. 2011) as it was assumed that the PGA is the most significant element in the earthquake characteristics disregarding partially or completely other characteristics including the frequency content of the earthquake. In fact, few studies had discussed the frequency content effect of earthquakes on the underground structure’s response (Zhuang et al. 2015; Saeidzadeh and Hataf 2011; Paramasivam et al. 2019).

http://kobe117shinsai.jp/display_index/d026.php

http://www.civildefence.govt.nz/_Assets/Uploads/images/gas-station-tanks.jpg

Figure 0.1 Examples of underground structure damages due to earthquakes: a) Daikai Station failure (Niigata Earthquake); b) tank uplift (Christchurch Earthquake).

In this study, a 3D numerical model was devoted to the investigation of the performance of Hydro-Quebec underground structures under three different historical earthquakes (Table 4.1). The numerical modelling and material calibration, as well as the model verification,

are introduced first, then the obtained results in terms of both seismic soil and structure responses are presented.

4.2. Finite difference Program (FLAC^{3D})

There are several programs that can simulate soil-structure. Most of these programs are built from the finite element (FE) or finite difference (FD) methods. Many programs can model dynamic soil-structure problems, but few can simulate soil liquefaction as this requires the differential equations of the solid and fluid phases to be coupled. The three-dimensions (3D) FD program FLAC^{3D} is one of the available computer codes that can implement coupled effective-stress models (Itasca 2012). FLAC^{3D} offers an ideal analysis tool for the solution of 3D problems in geotechnical engineering (Unutmaz 2014). The computer code FLAC and FLAC^{3D} had been extensively utilized in engineering practice to investigate the seismic response of underground structures in liquefied and no liquefied grounds (e.g., Lin et al. 2013; Unutmaz 2014; Azadi[a&b] and Hosseini 2010; Yang et al. 2004).

4.3. Constitutive model of the soil (Energy-based approach)

The soil liquefaction of the ground is one of the most important subjects in Earthquake Engineering. Liquefaction occurs due to the increase of pore water pressure accompanied by a decrease of vertical effective stress and shear modulus. Both experimental and numerical models have been used to study the soil liquefaction phenomenon. Numerically, there are various types of formulations based on the used numerical tool and the constitutive equation of soils. There are two main methods in numerical models in soil mechanics: one is based on the total stress (UBCTOT model), and the other is based on the effective stress (UBCSAND

model). The effective stress models account for excess pore pressure liquefaction-induced changes during the seismic loading, whereas, the total stress models assume constant pore pressure during the dynamic analysis (Naesgaard 2011). On another hand, there are three main estimation approaches to evaluate the soil liquefaction: (1) stress-based procedures, (2) strain-based procedures, and (3) energy-based procedures (Green 2001). Seed and Idriss (1971) used an approximation to determine the cyclic shear stress to be developed due to earthquake loading. While Dobry et al. (1982) proposed another approach wherein a threshold shear strain is defined that can initialize plastic deformation and the consequent excess pore water pressure. On the other, Nemat-Nasser and Shokooh (1979) used the dissipated energy (area enclosed by the stress-strain history) of soil during seismic loading to find the excess pore water pressure buildup.

In particular, the energy-based approach is a model that can be used to simulate soil liquefaction and predict the change in the pore-water pressure developed in the soil from the energy dissipated in the soil during cyclic loading (Polito et al.2013). In the beginning, Martin et al. (1975) found that there is a relation between the built-up excess pore-water pressure (ΔU) and the soil volumetric change (ΔV) through the modulus of elasticity (E) as following:

$$\Delta U = E \times \Delta V \quad [1]$$

Nemat-Nasser and Shakooh's (1979) proved that the energy required to increase pore pressure of sand is related to the dissipated energy per unit volume calculated from the hysteresis loops. The amount of energy dissipated in the soil (ΔW) is correlated to the volumetric change (ΔV) by means of constant (A). And, consequently, related to the excess pore-water pressure(ΔU) be as follows:

$$\Delta U = E \times A \times \Delta W \quad [2]$$

Davis and Berrill (1982) and Berrill and Davis (1985) proposed an empirical equation to relate (ΔU) to (ΔW) by entering the vertical effective stress (σ_v'):

$$\frac{\Delta U}{\sigma_{v'}} = \alpha * \left(\frac{\Delta W}{\sigma_v'}\right)^{\beta} \quad [3]$$

where α and β are constant parameters depend on soil properties and can be determined from laboratory tests using cyclic shear tests. This model has been successfully applied to laboratory data and field case studies (Sunitsakul 2004). This method has not been widely adopted in numerical modelling. Subsequently, Karray et al. (2015) proposed an energy-based model to a computed excess pore pressure ratio (R_u) from stress-strain cyclic shear test results:

$$R_u = \alpha * \left(\frac{-Ws^{0.5}}{a_x}\right)^{\beta} \quad [4]$$

where Ws is the energy dissipated per unit volume of soil divided by the initial effective confining pressure which can be determined by integrating area bound by stress-strain hysteresis loops, the a_x parameter is a calibrated parameter depend on soil type. The liquefaction parameters (α, β, and a_x) can be determined from cyclic shear tests (e.g. Direct simple shear test, Triaxial shear test, Triaxial simple shear test, Torsion test). Fig. 4.2 shows a typical shear stress-strain curve of liquefied soil subjected to cyclic loading. The energy dissipated per unit volume in one cycle of cyclic loading can be represented by the area of the hysteresis loop and then the excess pore water ratio can be calculated. Whereby calculating the shear strain (γ) and cyclic stress ratio (CSR) of each step, the energy dissipated of soil can be evaluated by the following equation:

$$W_s = \sum \Delta W_s = \sum \left(\frac{CSR_{i+1} + CSR_i}{2}\right) * (\gamma_{i+1} - \gamma_i) \quad [5]$$

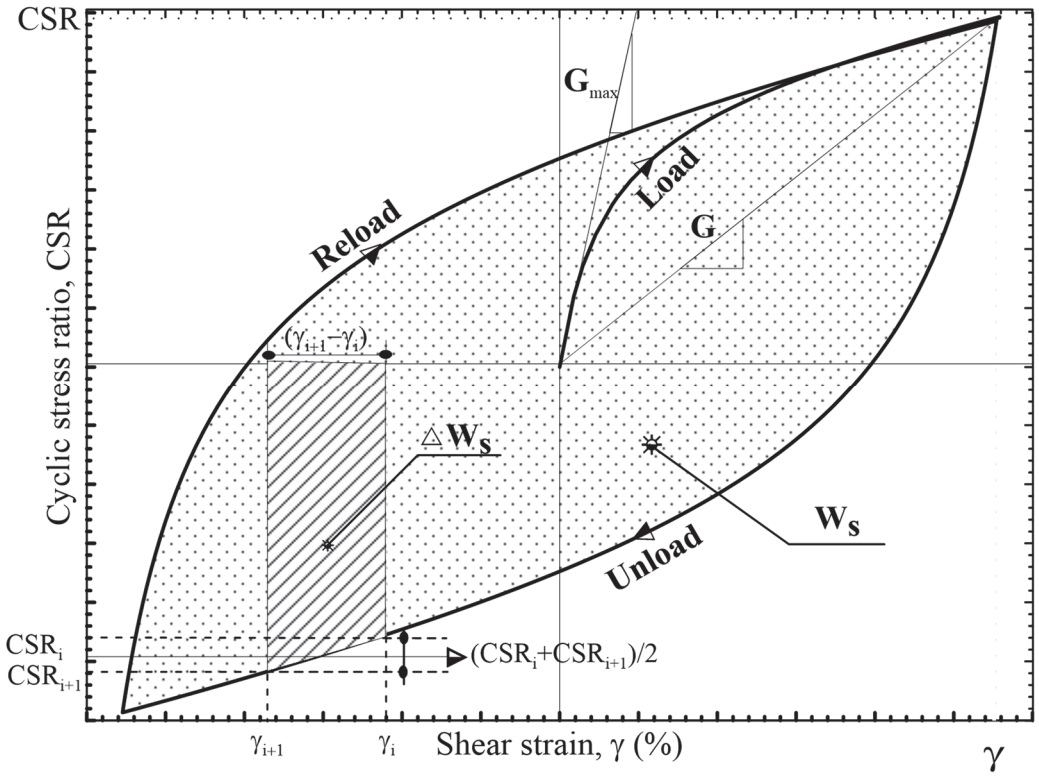

Figure 0.2 Dissipated energy per unit volume for a soil sample in a cyclic shear test determined by integrating the area bound by stress-strain hysteresis loops.

4.4. Numerical simulation

In this study, the numerical model was performed in two stages. In the first stage (self-weight static analysis), the soil and the structure were represented by the Mohr-Coulomb and elastic model implemented in FLAC^{3D} respectively. The static stresses were developed in the model due to gravity. Following this phase, the displacements within the model were reset to zero. In the second stage (seismic analysis), the soils were simulated using the energy-based approach constitutive model (Eq. 4) to determine the excess pore water pressure ration and perform liquefaction evaluation. The effect of liquefaction occurring on the acceleration response and structure internal forces and deformation also has been considered.

4.4.1. Structure and soil model

The seismic behavior of access underground structure and liquefaction of the surrounding soil was investigated. The underground structure under consideration is a typical Hydro-Quebec chamber (4.0x2.0x3.0m) with two different diameter manholes (i.e., D = 0.6 and 1.0m) located at the upper slab and 25cm wall and slab thickness. The structure buried depth was 0.5m as shown in Fig. 4.3a. The structure and the two manholes are simulated by Linear Structural Elements. Linear structural elements are three nodded, flat finite elements. In addition to providing the structural behavior of the shear-directed frictional interaction between the linear element and the soil grid. Also, in the normal direction (compressive and tensile forces) can be carried, and the liner may break free from the grid (Itasca 2012). The structure elasticity modulus (E_s) and Poisson ratio (υ_s) were assumed to be 30 GPa and 0.2, respectively (Liu and Song, 2005).

The general case soil was assumed to be loose sand soil with relative density (Dr=20%) and normalized shear wave velocity (V_{s1}=100m/s). The soil layer extended to 10m thickness overlaid a rock layer. Because the ground is a half-infinite space, enough width should be adopted to eliminate the influence of the artificial boundary. In this case, a domain of 60 m was used in the simulation, with the underground structure at the center as shown in Fig. 4.3b. The soil layer was assumed to be isotropic liquefiable sandy soil and simulated using Mohr-Coulomb and energy-based models in the static and dynamic stages respectively. The parameters for the soils used in this study are shown in Table 4.2.

Youd et al. 2001 determined the shear wave velocity of the soil (V_s) from V_{s1} as:

$$V_s = V_{s1} \times \left(\frac{\sigma_v^{'}}{P_a} \right)^{0.25} \qquad [6]$$

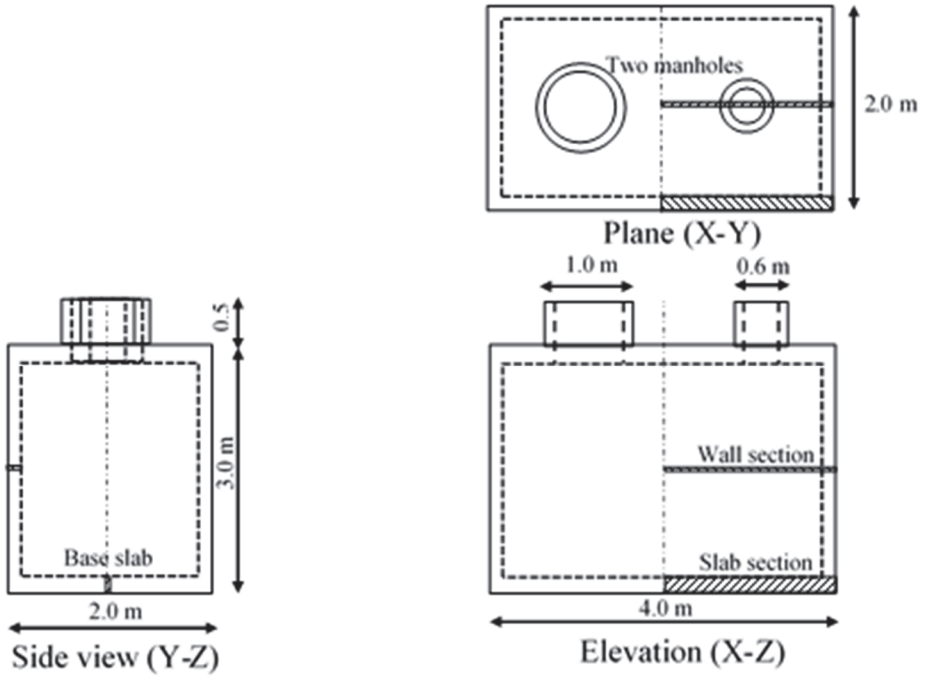

(a)

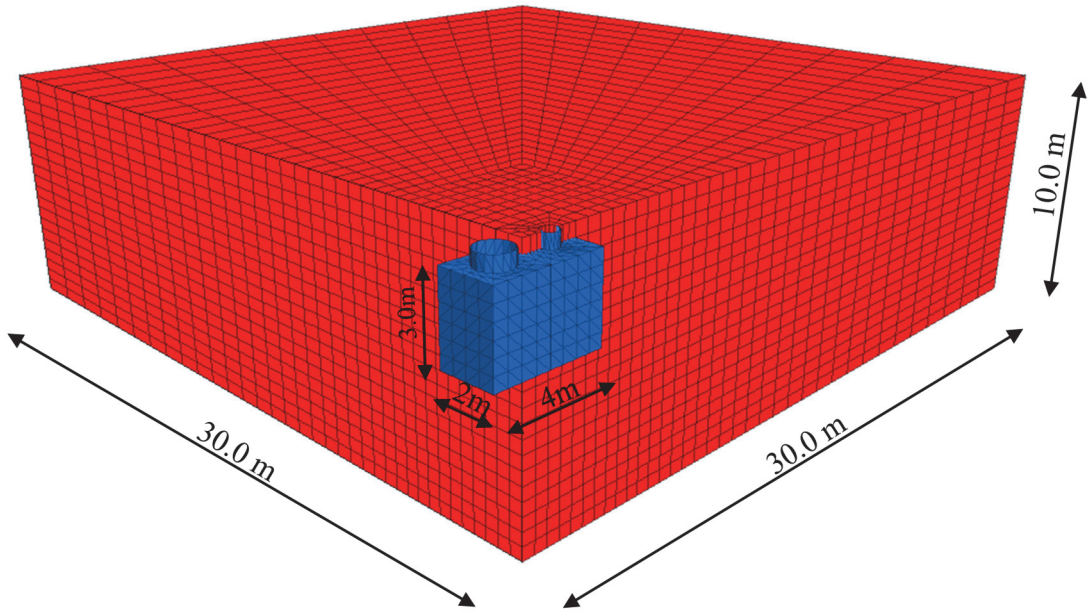

(b)

Figure 0.3 (a) Dimensions of a typical Hydro-Québec chamber; (b) model layout in 3D view and meshing.

The maximum shear modulus (G_0) and bulk modulus (K_0) of soil are the elastic parameters used in the first phase of numerical analyses. G_0 would be determined based on the value of V_s from the elastic relationship between the G_0 and V_s; $G_0 = \rho \times v_s^2$, where ρ is the soil density. By assuming a Poisson ratio ($\upsilon=0.33$), the K_0 could be determined. Also, two real soil profiles have been considered in this paper located in two different locations within Quebec, Canada. The first soil profile is located in Île-des-Sœurs where the soil deposits consist of three layers, of which the upper layer is liquefiable silty sand with the thickness of 3.25 m, under that a medium layer of liquefiable loose with a thickness of 1.0 m, and the lower layer is dense till with a thickness of 2.0 m. The underground water level was located at a depth of 3.5 m under the ground surface as shown in Fig. 4.4a. The other site is in Québec city. The soil profile includes 6 different soil layers with the groundwater table at 2m depth and extends to 40m over the bedrock as shown in Fig. 4.4b.

4.4.2. Boundary conditions

Two types of boundaries were chosen to simulate the model. First, in the static analysis to compute gravity stresses, the base boundary was assumed to be fixed both horizontally and vertically direction. However, the side boundaries were fixed only horizontally. Then, in the dynamic analysis, the horizontal seismic load was applied at the base boundary. The horizontal restraints of the side boundaries were released and replaced by the free field boundary condition.

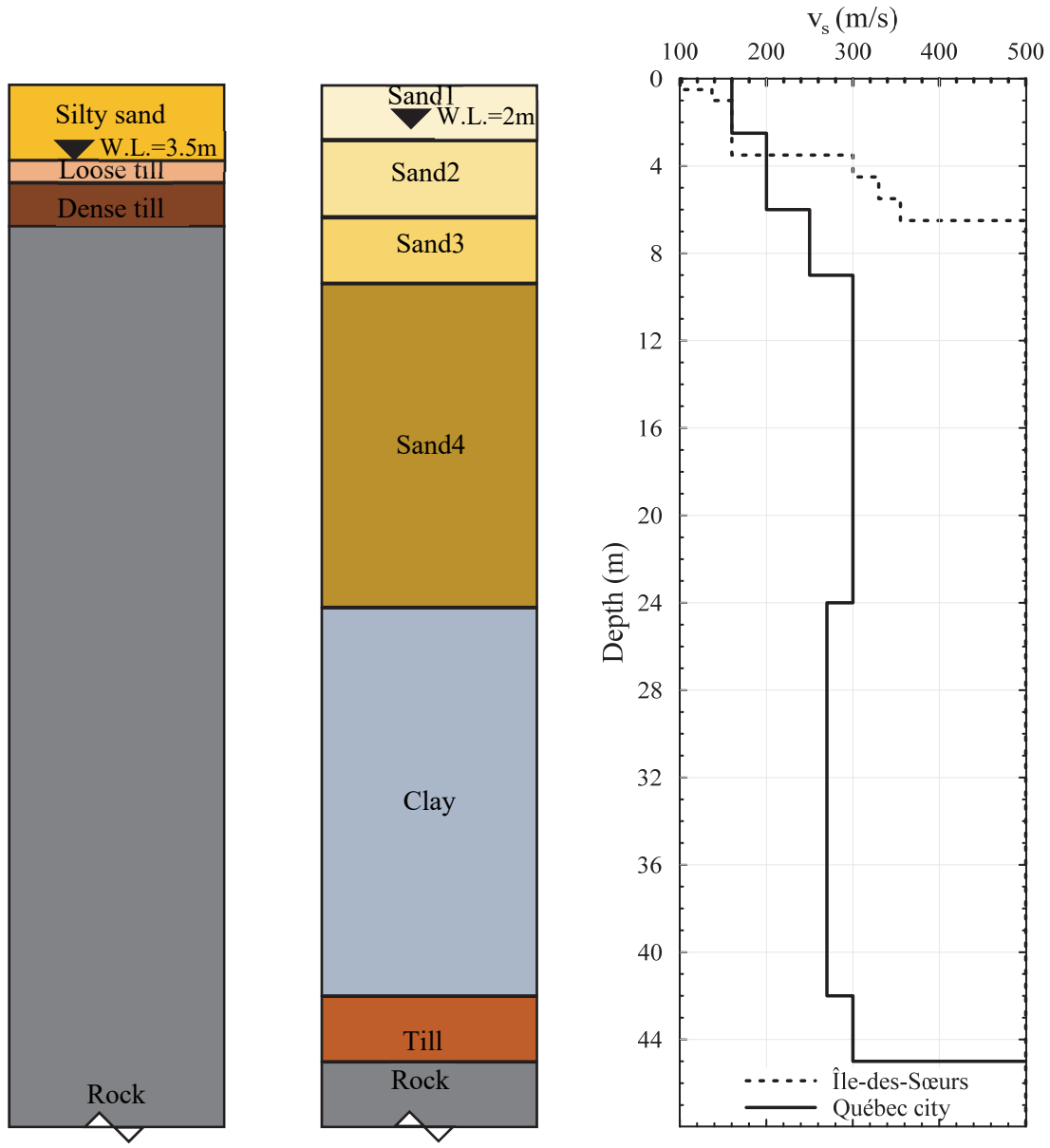

a) Île-des-Sœurs **b)** Québec City **c)** Shear wave velocity (vs).

Figure 0.4 Soil profiles at two different locations within Quebec.

4.4.3. Meshing size

The soil was simulated with 8-node brick elements, and the soil elements are small adjacent to the structure and gradually increase in size as they move away from it. The height of the soil elements affects the transmission of high-frequency shear waves. For this reason, the height of the elements was limited to a maximum height, ΔL (Kuhlemeyer Lysmer 1973), which should be smaller than approximately one-tenth of the wavelength of the input wave.

$$\Delta l \leq \frac{\lambda}{10} \qquad [7]$$

where λ is the wavelength associated with the highest frequency of the input earthquakes. The used earthquake waves have frequency contents of less than 20 Hz and the shear wave velocity of the soil is 100 m/s. wherefore, the soil element size is chosen to be 0.5x0.5x0.5 m surrounding the structure and it gradually increases whenever it goes outward as shown in Figure 4.3b.

4.4.4. Soil-structure interface

When two different stiffness materials had been joined in FLAC, ATTACH and INTERFACE are the two methods that's can deal with this case. In the static analyses, it is more computationally efficient to use the ATTACH command than the INTERFACE command to join sub-grids. However, under some circumstances, it may be necessary to use an interface such as when the structure is uplift which can slip it in response to the float loading. The constitutive model of the interface is defined by a linear Coulomb shear-strength criterion that limits the shear force acting at an interface node. Normal (k_n) and shear stiffnesses (k_s), tensile (T_s), shear strengths (S_s), and a dilation (D) angle are the interface

parameters as shown in Fig.4.5. The shear strength was defined with 2/3 of the friction angle and zero cohesion and tensile for the soil surrounding the structure. The stiffnesses k_n and k_s are set to ten times the equivalent stiffness of the stiffest neighboring zone. The stiffness (expressed in stress-per-distance units) can be determined as:

$$k_n = k_s = 10 \times \left[\frac{K + 4/3 \times G}{\Delta z_{\min}} \right]_{\max} \quad [8]$$

where: K & G are the bulk and shear moduli, respectively; ΔZ_{min} is the smallest width of an adjoining zone in the normal direction (Itasca, 2012).

4.4.5. Material damping

When using simple models, the choice is between Rayleigh damping and hysteretic damping. From some general comparisons between the two approaches, enabling a choice to be made. In general, hysteretic damping is the more realistic of Rayleigh damping, and it entails no reduction in time-step. The hysteretic damping formulation is not a complete constitutive model, but it is used as a supplement to one of the built-in nonlinear models, and not as a primary way to simulate yielding. Hysteretic damping allows strain-dependent modulus and damping functions to be incorporated directly into the FLAC^{3D} simulation. The hysteresis model is developed by noting that the S-shaped curve of modulus versus the logarithm of cyclic strain can be represented by a cubic equation, with zero slopes at both low strain and high strain. The sigmoidal (SIG4) model was adopted to fit the shear modulus degradation and damping curves of the sand during dynamic loading. Thus, the normalized secant modulus ($\overline{G_s}$) can be calculated from the following equation:

$$\overline{G_s} = \frac{\bar{\tau}}{\gamma} = y_0 + \frac{a}{1 + e^{\frac{x_0 - L}{b}}} \quad [9]$$

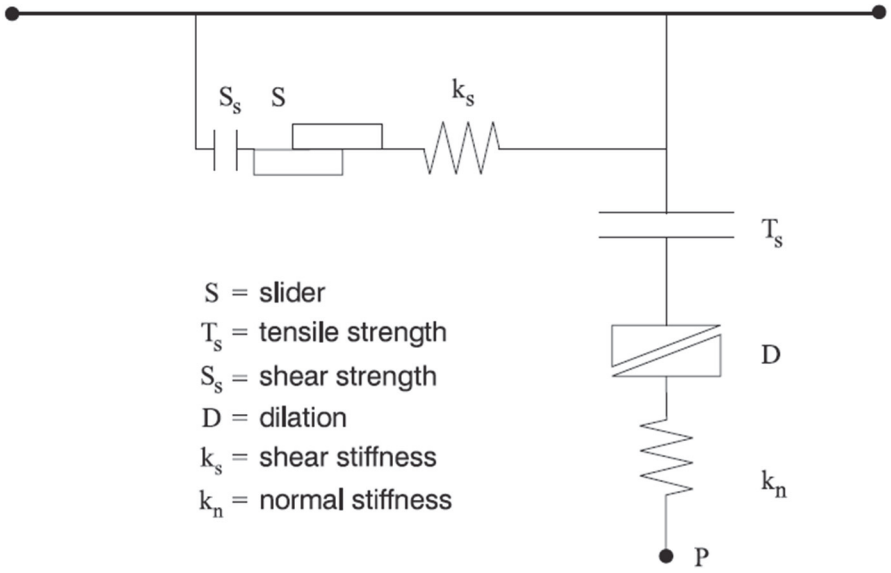

Figure 0.5 Components of the bonded interface constitutive model.

where $(\bar{\tau})$ is normalized shear stress and (L) is the logarithmic shear strain (γ) and the fitted parameters (a, b, x_0, y_0) of the SIG4 model were selected such that they produce shear modulus degradation and damping curves, of all soil deposits. The fitted parameters of the SIG4 model were selected such that they produce shear modulus degradation and damping curves, respectively at the sand upper and lower limits provided by Seed and Idriss (1970).

Additionally, a Rayleigh damping ratio was used, besides the hysteretic damping in operation, to ensure the stability of the numerical solution process at very low strain levels. Therefore, the model has been critically damped by at low value about 0.2% using the natural frequency of oscillation, f_{min}, of 2.5 Hz (vs/4H) to remove high-frequency noise (Itasca, 2012). Both mass and stiffness damping had been used. Also, the shear strain induced in each subsequent cycle of loading increases because the increase of the pore pressure decreases the soil shear stiffness (shear modulus, G). Seed[b] et al. (1975) determined the reduction of the soil shear modulus (G) from the pore-water pressure ratio (R_u) and the maximum shear modulus (G_{max}) using the following equation (Matasovic and Vucetic 1993; Chang et al. 2007):

$$\frac{G}{G_{\max}} = \left(1 - R_u\right)^{0.5} \quad [10]$$

4.4.6. Input earthquake motion

Earthquake records may be classified into three groups according to the frequency content ratio (i.e., the Peak Ground Acceleration (PGA) to Peak Ground Velocity (PGV) ratio): (a) high PGA/PGV ratio when PGA/PGV > 1.2, (b) intermediate PGA/PGV ratio when 1.2 ≥ PGA/PGV ≥ 0.8, (c) low PGA/PGV ratio when PGA/PGV < 0.8 (Tso et al. 1998).In this paper, three different earthquakes with different amplitudes and frequency contents (Table 4.1 and Figs. 4.6) were used to study the effect of the frequency content on the behavior of the underground structure. The used earthquakes are:

i. The Great Hanshin or Kobe earthquake (1995) occurred in the southern part of Japan.
ii. The Loma Prieta earthquake (1989) occurred in Northern California, USA.
iii. The Saguenay earthquake (1988) was one of the largest earthquakes that occurred in northeastern North America in the 20th century.

The three acceleration histories scaled at the same level of PGA which is assumed to be 0.25, 0.5, 1.0g to study the amplitude effect. These earthquakes were used as input motions at the base of the numerical model. A simulated earthquake time history compatible with the 2015 National building code of Canada and with the seismicity of Montreal and Quebec City (Zone 4) developed by Atkinson (2009) was also used in the dynamic analysis as shown in Fig.4.6 (Adams and Atkinson 2003).

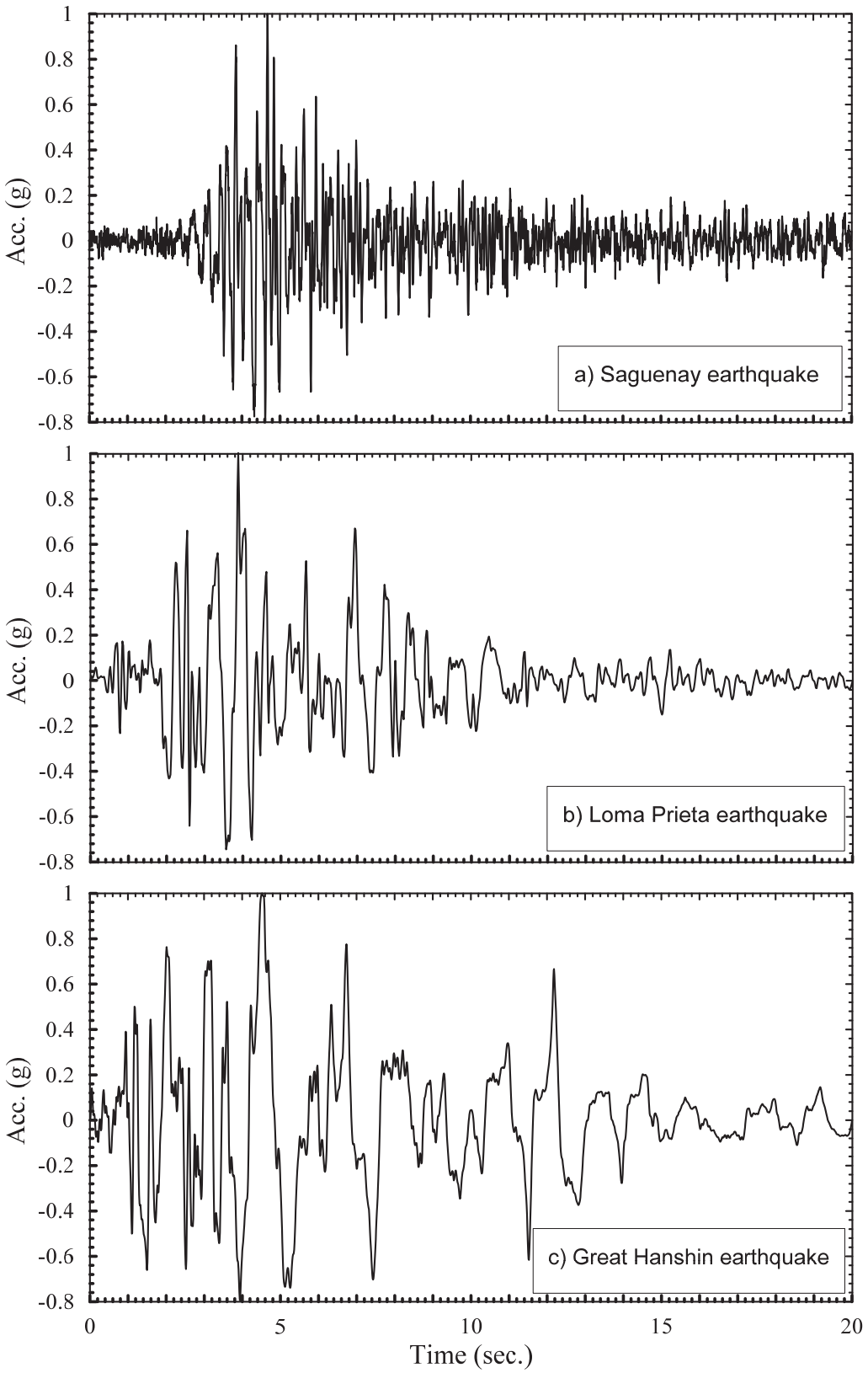
Acc. (g)
a) Saguenay earthquake
b) Loma Prieta earthquake
c) Great Hanshin earthquake
Time (sec.)

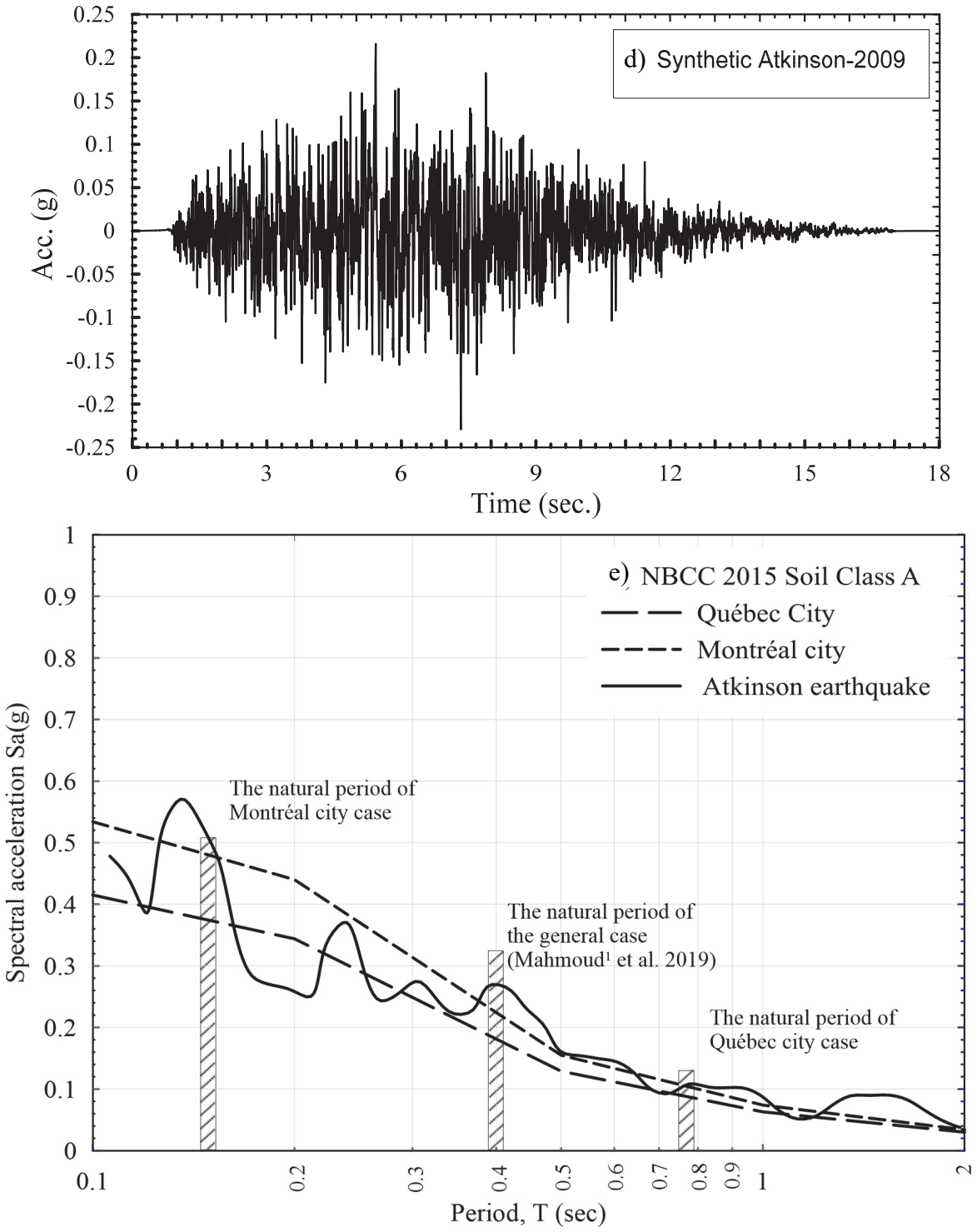

Figure 0.6 Input earthquakes time histories:(a) Saguenay earthquake, (b) Loma Prieta earthquake, (c) Great Hanshin earthquake, (d) Atkinson (2009) “Synthetic 1”; (e) spectral accelerations of the two different sites.

4.4.7. Calibration and validation

Model calibration is the main part of developing the energy-based approach model. In order to use it as a constative model in the current study, the liquefaction parameters should be defined. So the numerical model with the energy-based approach constitutive model has been calibrated by cyclic shear laboratory tests. The liquefiable soils were simulated and calibrated with the experimental results of the direct simple shear test (DSS) to determine their liquefaction parameters (α, β, and a_x). The parameters were determined for each soil type from produce similar shear strain and liquefaction responses as typical cyclic laboratory tests. The liquefaction parameters within the numerical models were adjusted until a reasonable agreement between the laboratory tests and the numerical response was achieved. The liquefaction parameters used in this numerical simulation are listed in Table 4.2. Also, the numerical model was validated with different experimental models. The details and results of calibrated and validated models were explained in Mahmoud[a&b] et al. (2019). In the numerical analyses, acceleration time histories discussed earlier were used as input motions. The earthquake amplitude was multiplied by different factors to study the amplitude factor effect. The acceleration response, excess pore pressure, uplift displacement, and internal forces of underground structures have been carefully studied in all cases considered.

Table 0.1 Characteristics of earthquakes used in this study.

Case	Earthquake characteristics							
	Location	Date	M_w	PGA (g)	PGV (m/s)	a/v (g/m/s)	*f* (Hz)	Classification
a	Quebec (CA)	1988	5.9	0.203	0.0867	2.33	3.644	High
b	Calif. (US)	1989	6.9	0.469	0.469	1.00	1.562	Intermediate
c	Kobe (JP)	1995	6.9	0.611	1.272	0.48	0.75	Low

Table 0.2 Materials parameters used in the numerical simulation.

Properties	Static parameters			Dynamic parameters			Location
	G_0(MPa)	K_0(MPa)	ρ_d(kg/m^3)	α	β	a_x	
Loose Sand	15	40	1500	1.00	0.61	$0.92\gamma^{-0.455}$	General case
Silty sand	25	67	1750	1.05	1.245	$1.02\gamma^{-0.277}$	Case 1 Île-des-Sœurs
Loose till	55	4500	1758	1.03	1.194	$1.35\gamma^{-0.408}$	
Dense till	200	4500	1850			$2.54\gamma^{-0.562}$	
Sand 1	17	45	1535	1.04	1.455	$1.24\gamma^{-0.435}$	Case 2 Québec city
Sand 2	22.6	60	1570			$1.69\gamma^{-0.366}$	
Sand 3	36	96	1600			$3.18\gamma^{-0.456}$	
Sand 4	66	176	1650			$3.68\gamma^{-0.782}$	
Clay	146	4500	1620	0	0	0	
Till	150	4500	1870	0.95	1.42	$4.12\gamma^{-0.798}$	

G_0: initial shear modulus at a confining pressure of 100 kPa; K_0: initial bulk modulus at a confining pressure of 100 kPa; ρ_d: dry density; α, β, and a_x: liquefaction parameters.

4.5.1. Ground motion response

Figures 4.7 show the effects of the earthquake parameters (amplitude and frequency) and liquefaction occurring on the spectra acceleration transfer function ($\mathrm{T.F.} = \frac{\mathrm{Sa(output\ surface)}}{\mathrm{Sa(input\ base)}}$).

In Fig. 4.7a, where the PGA of the three earthquakes are normalized to be 1g, it is found that the decrease of the earthquake frequency has two main effects: (a) it decreases the natural frequency of the soil deposit due to the reduction of shear wave velocity (shear modulus) with acceleration amplitude (strain level); (b) it reduces the peak values because of the increase of soil damping with shear strain. The same thing can be clearly seen in Fig. 4.7b, with the increase of earthquake amplitude, but it can be observed that the effect of the earthquake frequency multiplication is not less than the earthquake amplitude on the ground motion amplification. In Fig. 4.7c, Saguenay earthquake (PGA=0.5g) is applied in two cases "liquefied and not liquefied soil" and it is found that the liquefaction occurring has two main effects: (a) it decreases the natural frequency of the soil deposit (natural period lengthening) due to the soil be more softening; (b) it reduces the peak values because of the increase of soil damping.

Figure 4.8 shows the spectral acceleration response at the ground surface at the two sites in question. It is found that amplification occurred in the case of the Montreal site. However, there are deamplification occurred at the Quebec City site as a result of the damping effect caused by the clay layer and liquefied soil.

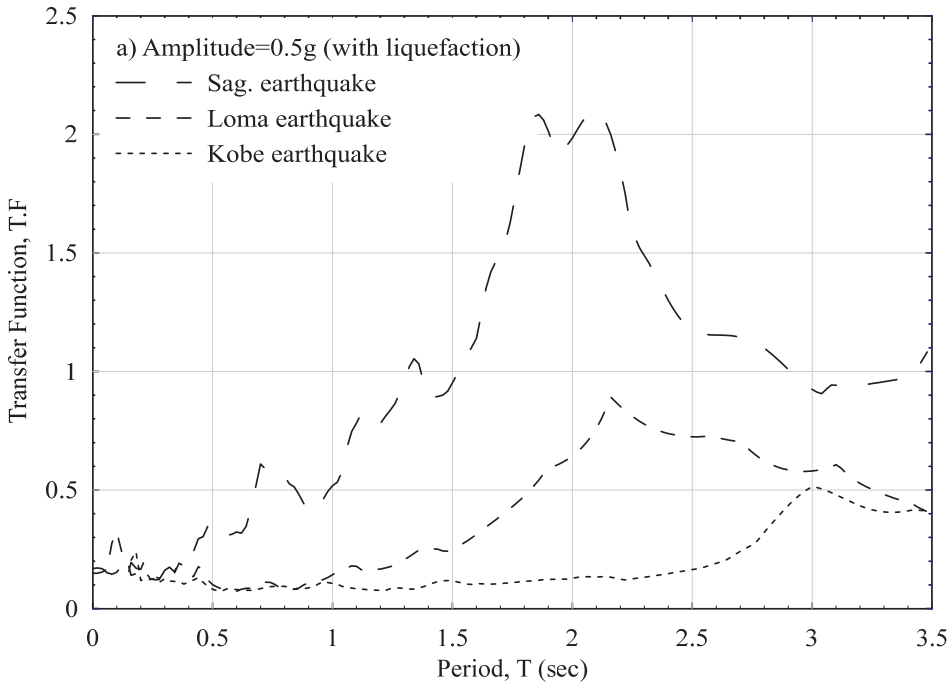
a) Amplitude=0.5g (with liquefaction)
Sag. earthquake
Loma earthquake
Kobe earthquake
Transfer Function, T.F
Period, T (sec)
0
0.5
1
1.5
2
2.5
3
3.5

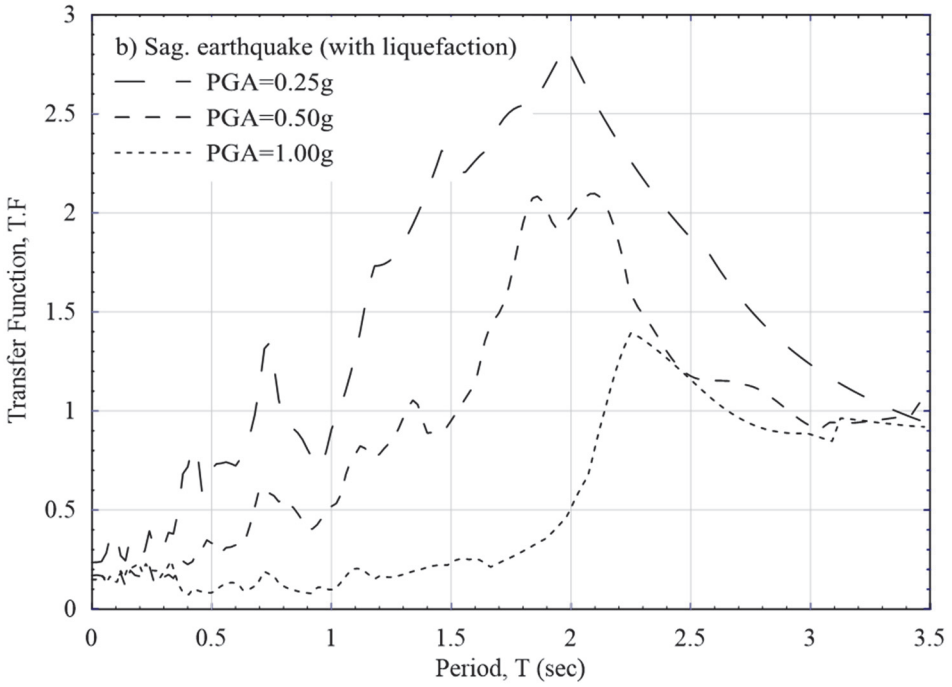
b) Sag. earthquake (with liquefaction)
PGA=0.25g
PGA=0.50g
PGA=1.00g
Transfer Function, T.F
Period, T (sec)
0
0.5
1
1.5
2
2.5
3
3.5

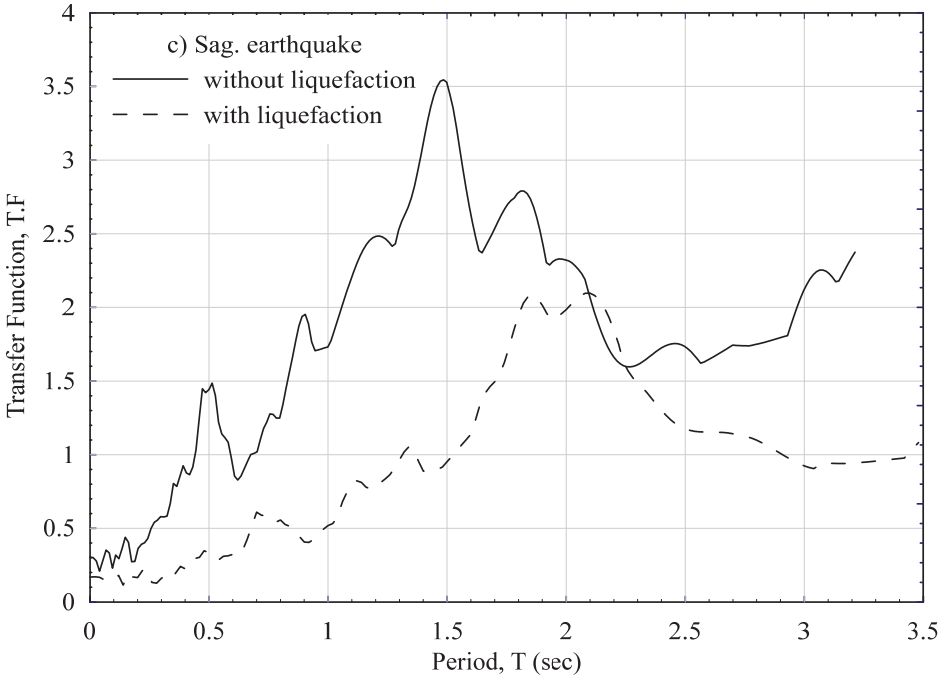

Figure 0.7 Transfer Function of Fourier-Amplitude spectra between the output at the surface to the input at the base: (a) for different frequency contents; (b) for different earthquake amplitudes; (c)liquefaction effect.

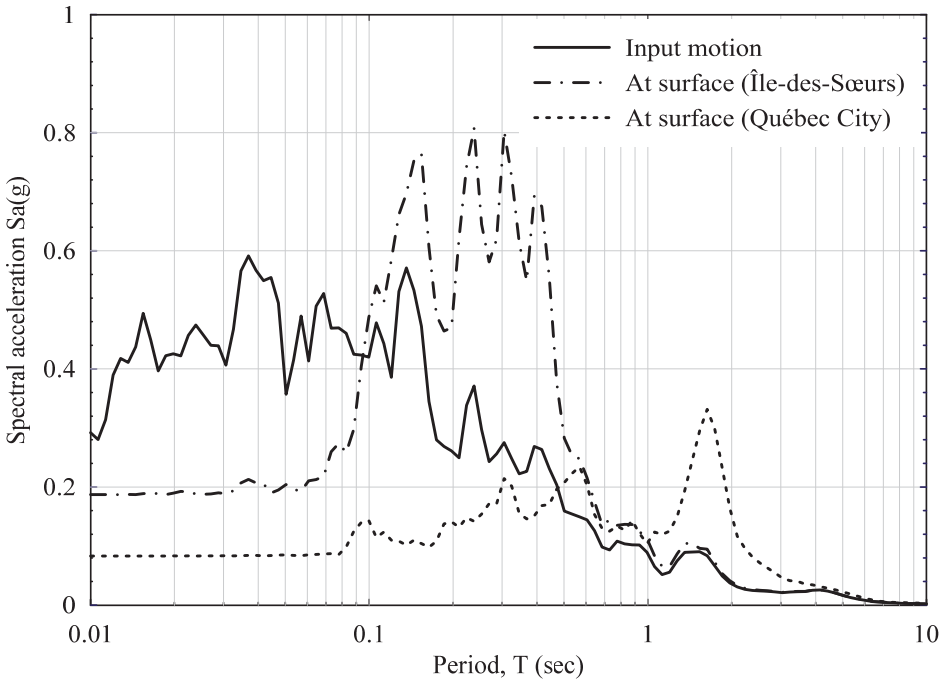

Figure 0.8 Spectral accelerations of the acceleration at the base and at the ground surface for the two study cases.

4.5.2. Excess pore water pressure ratio

Figures 9 show the excess pore pressure ratio time histories of the soil at the base and directly below the structure due to the change in the applied seismic motion. In Fig. 9a., it is can be seen that the amplitude of the Loma-Prieta earthquake has a direct impact on the developed built-up pore water pressure beneath the structure. As expected, the time of liquefaction occurrence decreases with the earthquake amplitude. Soil subjected to an earthquake with PGA=0.25g needs 8.5 sec to liquefy while that exposes to 1.0g earthquake needs only 3 sec to reach the same situation. While as it can be shown in Fig. 9b., the earthquake frequency content is more efficient than the earthquake amplitude where the Kobe earthquake (f=0.75 Hz) needs only 2.0 sec to make the soil liquefy while Loma-Prieta earthquake (f=1.56 Hz) makes the soil liquefy at 3 sec. However, Saguenay earthquake (f=3.33 Hz) can liquefy the soil at 8 sec.

Figures 4.10 shows the variation of the excess pore pressure ratio of the two sites considered in the soil beneath the structure and at the model base. From Figures 4.10a, it is found that the excess pore water pressure ratio at the model base increases to 18% and 29% for Montreal and Quebec City sites, respectively. This difference is due to that the base soil in Montreal is stiffer than that in Quebec City. However, under the structure, as shown in Figures 4.10b, it is found that the excess pore water pressure ratio reaches 20% and 43% for Quebec City and Montreal locations respectively. The coming down in the excess pore water pressure ratio at Quebec City location is the result of the damping process in the clay layer and base liquefied soil. While, in Montreal's location, there was not large liquefaction that occurred at the model base and therefore the seismic motion moved with full strength into the soil beneath the structure which increases the excess pore water pressure ratio.

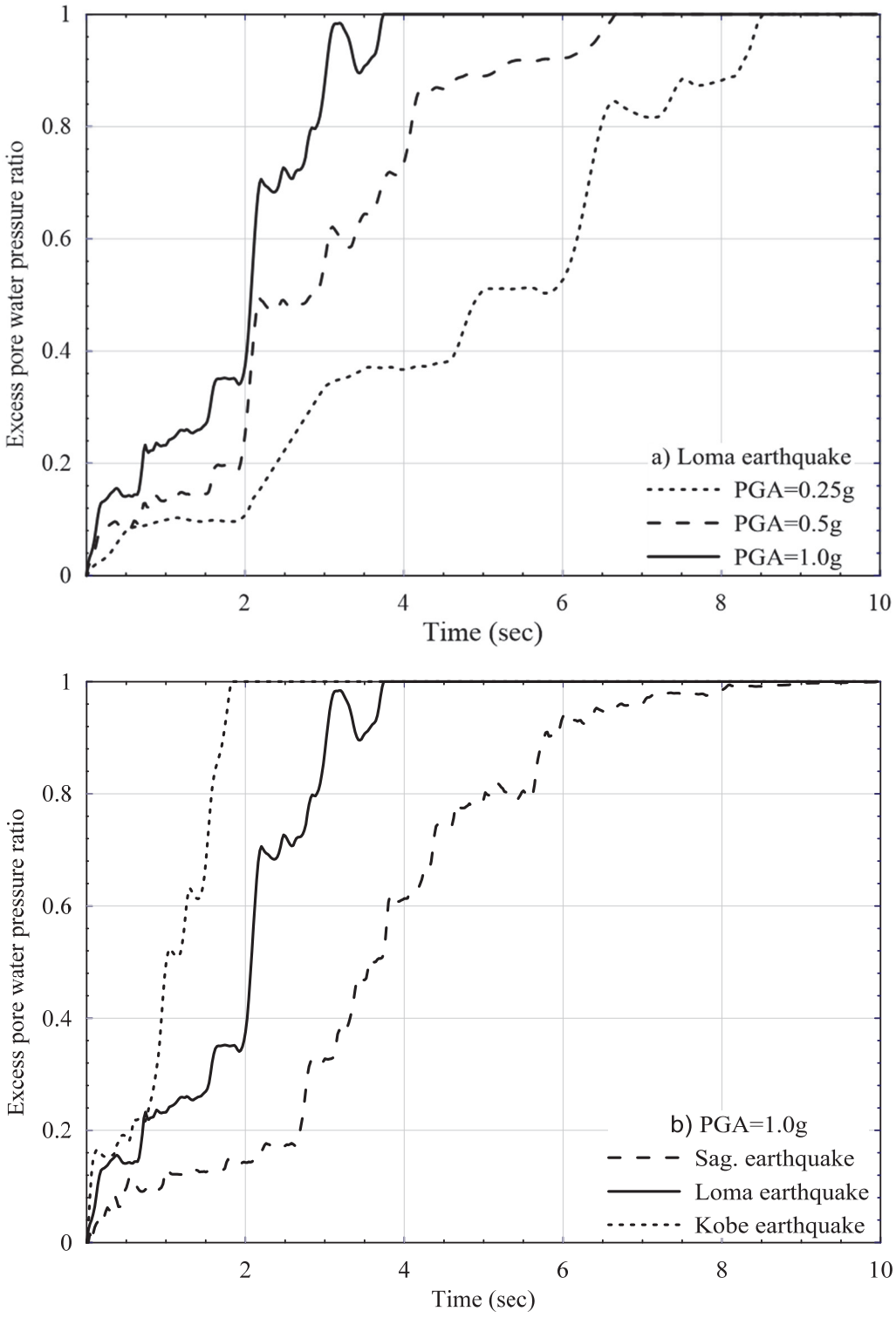

Figure 0.9 Excess pore water pressure ratio time history under the structure with: (a) different PGA (Loma Earthquake); (b) different earthquakes (PGA = 0.5g).

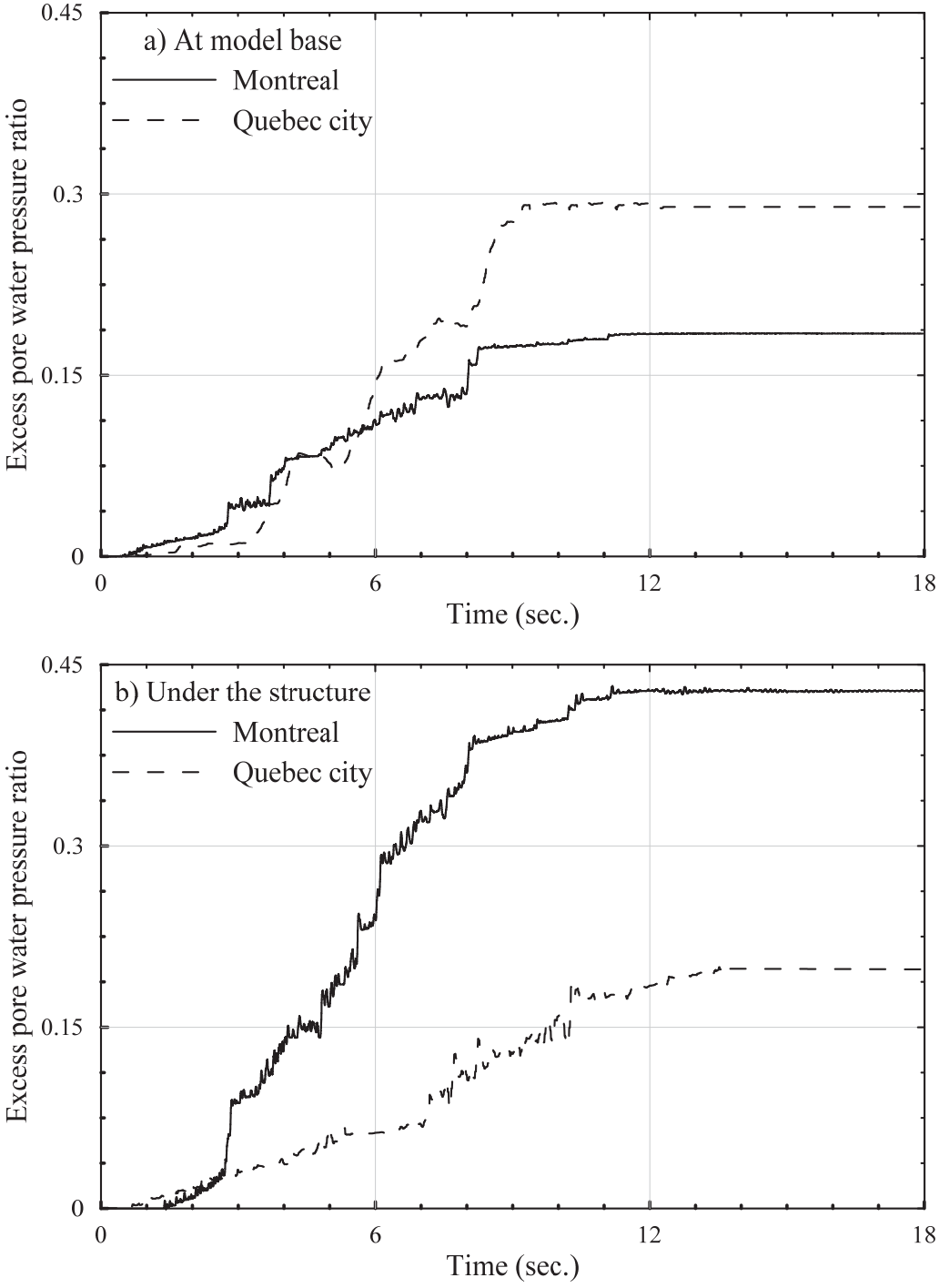

Figure 0.10 Comparing the excess pore water pressure ratio time histories of two study cases: (a) at the model base; (b) at the soil beneath the structure.

4.5.3. Uplift of Underground Structures Liquefaction-induced

A simplified method to predict structures uplift

One of the most serious damages resulting due to soil liquefaction is the underground structures uplift due to increasing the pore pressure (Koseki[b] et al. 1997; Orense 2005; Tobita et al. 2012; Chian et al. 2014; Watanabe et al. 2016; Zhang and Chian 2019). The safety factor against underground structure uplift (F_s) can be derived as follows:

$$F_s = \frac{F_{down}}{F_{up}} \quad [11]$$

where F_{up} and F_{down} are the up and down vertical forces. However, little studies predict the uplift displacement of the buried structure due to liquefaction occurring. Tobita et al. (2008) proposed a simplified method to predict the maximum uplift displacement of underground structures (Δ_1) and surrounding soil settlement (Δ_2). The method was validated with experimental and numerical results (Kang et al. 2014).

Before applying this method in our case study, the following assumptions were formed: (1) There are not soil volumetric change before and after structure uplift, (2) the groundwater table is assumed at the ground surface and kept constant before and after the uplift, and (3) attached forces due to side tubes are neglected. When structure starts moving (F_s=1), the analytical method relies on the existence of a balance between the total vertical weight ($\sum W$) and the surround resistance force ($\sum R$) with a buoyant force acting on the structure ($\sum U$) as shown in Fig.4.11.

$$\sum U = \sum W + \sum R \quad [12]$$

The total vertical weight consists of two main things: the mass of the structure (W_1) and overburden soil above the structure (W_2) as following:

$$\sum \mathrm{W} = W_1 + W_2 = A_1 * \Upsilon_s * H_1 + A_1 * \Upsilon_{sat} * H_2 \quad [13]$$

where A_1 is structure base area, H_1 is the structure height, H_2 is soil above structure height, γ_s is total structure unit weight, and γ_{sat} is soil saturated density. The surround resistance force ($\sum \mathrm{R}$) contains cohesion and/or friction forces between the surrounding soil with the structure (R_1) and overburden soil (R_2) as following:

$$\sum \mathrm{R} = R_1 + R_2 = \rho * H_1 * \sigma'_{v1} * K * \tan\phi' + \rho * H_2 * \sigma'_{v2} * K * \tan\phi \quad [14]$$

where ρ is structure perimeter, σ'_{vI} and σ'_{v} is the average vertical effective stress for surrounding soil and above structure, Ø′ and Ø is the friction angle of the surrounding soil and above structure, and K is static earth pressure. In connection with a buoyant force acting on the structure ($\sum \mathrm{U}$) that splits to hydrostatic buoyant force (U_1) and excess pore water buoyant force (U_2):

$$\sum \mathrm{U} = U_1 + U_2 = \Upsilon_w * A_1 * (H - \Delta_1 - \Delta_2) + \Upsilon_{sub} * A_1 * (H - \Delta_1 - \Delta_2) * R_u \quad [15]$$

where H is the structure base depth, γ_w is the water density, and γ_{sub} is the soil submerged density. In the case of the surrounding soil is totally liquefied (R_u = 1.0) and by offsetting Equation 13, 14 and 15 in Equation 12, The uplift displacement and surround settlement can be calculated by the following method:

$$\Delta_1 + \Delta_2 = \frac{\{H * A_1 * \Upsilon_{sat} - \rho * K * (H_1 * \sigma'_{v1} * \tan\phi' + H_2 * \sigma'_{v2} * \tan\phi) - A_1 * (\Upsilon_s * H_1 + \Upsilon_{sat} * H_2)\}}{(A_1 * \Upsilon_{sat})} \quad [16]$$

Where there are not soil volumetric change, as previously assumed, the uplift displacement and surround settlement can be derived from equal volumes:

$$\Delta_1 * A_1 = \Delta_2 * (A_2 - A_1) \quad [17]$$

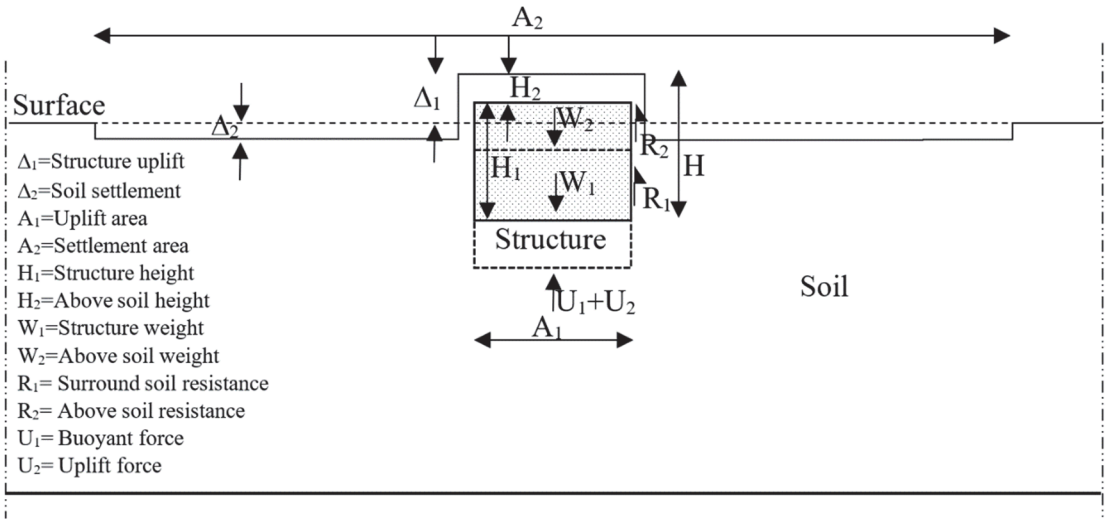

Figure 0.11 Typical diagram of the underground structure cross-section.

Then, from Eqs. (16) and (17), the maximum structure uplift (Δ1) can be given by the following relation:

$$\Delta_1 = \frac{(A_2-A_1)}{A_2} * \frac{H*A_1*\Upsilon_{sat}-\rho*K*(H_1*\sigma'_{v1}*\tan\phi'+H_2*\sigma'_{v2}*\tan\phi)-A_1*(\Upsilon_s*H_1+\Upsilon_{sat}*H_2)}{A_1*\Upsilon_{sat}} \quad [18]$$

where the cross-sectional area of the surrounding settlement soil area is much larger than the uplift area ($A_2 >>> A_1$), so the value of $(A_2-A_1)/A_2$ is expected to be within the unit. Hence, the maximum structure uplift can be calculated by:

$$\Delta_1 = \frac{H*A_1*\Upsilon_{sat}-\rho*K*(H_1*\sigma'_{v1}*\tan\delta+H_2*\sigma'_{v2}*\tan\phi)-A_1*(\Upsilon_s*H_1+\Upsilon_{sat}*H_2)}{A_1*\Upsilon_{sat}} \quad [19]$$

In this study, Figure 4.12a shows the time histories of the structure uplift. It can be obviously seen that the structure started to uplift at about 2, 4, and 8sec. Those times fit with the beginning moment of soil liquefaction occurring at the bottom of the structure as it has been mentioned before in Fig. 4.9b. The structure uplift was not stopped after the end of the earthquake occurring, but it was going on due to the water flow upward which is compatible with previous results (Zhang and Chian 2019). Also, it is clear to see that the structure uplift did not exceed the maximin structure uplift displacement which calculated from equation (19) (Δ_1=0.66m).

Figure 4.12b explains the effect of earthquake frequency (at constant amplitude) on the underground structure uplift. It can be seen that the increase in the earthquake frequency leads to a decrease in the structure uplift. On the other hand, in the two cases studied, the uplift displacement has not been discussed herein as there is no occurrence of full liquefaction (the excess pore water pressure ratio did not reach unity).

4.5.4. Internal forces of the underground structure

Standard methods for underground structure seismic design

AASHTO

According to Standard Practice for Direct Design of Buried Precast Concrete Box Sections and Guide Specifications for LRFD Seismic Bridge Design, seismic effects for underground structures do not need to be considered. Earthquake loads should be considered only where buried structures cross active faults such as unstable ground conditions (e.g. landslides) or large ground deformations (AASHTO 2002).

CHBDC

The Canadian Highway Bridge Design Code adds extra force effects due to earthquake loads by multiplying the static force effects due to self-weight and earth load. The multiplying factor is a vertical component of the earthquake acceleration ratio, A_V, which can be taken as two-thirds of the horizontal ground acceleration ratio, A_H. A_H shall be set equal to the peak ground acceleration, PGA. Amplification of these accelerations shall be considered where a significant thickness of less competent soil overlies rock or firm ground (CHBDC 2014):

$$BM_{dy} = \left(1 + \frac{2}{3} \times PGA\right) \times BM_{st} \qquad [20]$$

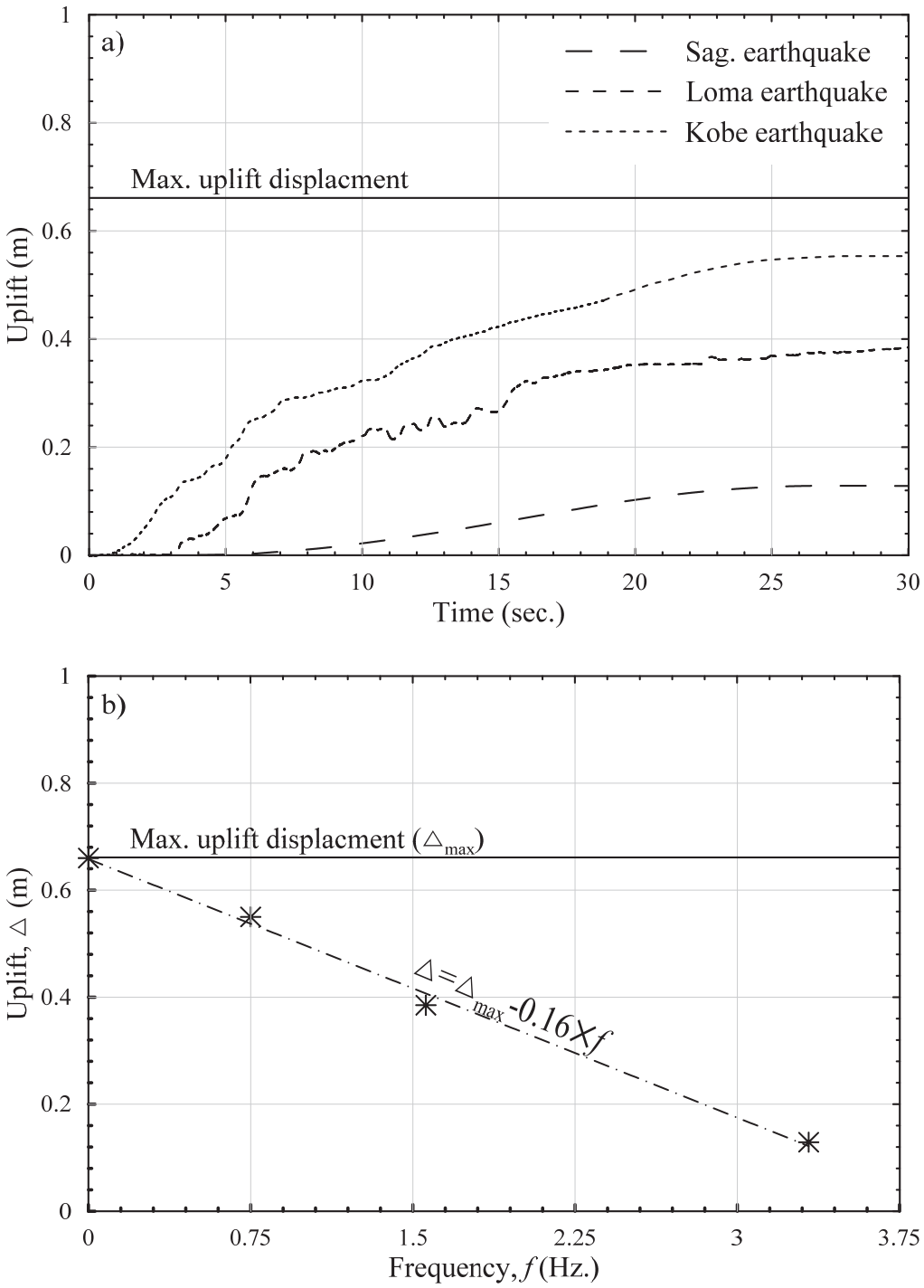

Figure 0.12 (a) Time history of the structure uplift; (b) Relationship between structure uplift and earthquake frequency.

Figs. 4.13 for the static cases (realistic state which W.L.=3.5m and another case which W.L.=0.0m) and dynamic case (after the earthquake application) assuming the loading condition of Montréal seismic zone. It can be seen from Figs. 4.13 that the maximum moment at the static case occurs at the Y-Z section with a value of 16.2 kN.m/m at the edge and a value of 8.1 kN.m/m at the middle of the slab and a value of 8.0 kN.m/m at the middle of the sidewall. At the maximum seismic loading, it is found that in the sidewall increases from 10.5 kN.m/m, while, the moment in the middle of the slab decreases to 6.4 kN.m/m. This reduction is, in fact, resulted from the reverse moment generated from the additional deformations and stresses in the side walls.

Similar to what have been established in the literature [e.g., Liu and Song 2005, Abuhajar[c] et al. 2015], figure 4.14a shows the increase and the decrease in the dynamic bending moment due to seismic loads of the three different earthquakes with the same PGA=0.25g from the numerical model compare to the dynamic bending moment calculated from the CHBDC empirical equation (20). The results low and Intermediate frequency earthquake (Kobe and Loma) are far from the empirical equation results, however, the results of the equation are compatible with the numerical result of the high-frequency earthquake (Saguenay) in the sidewall and wall-slab corner. Take into consideration that there is a simple reduction of the theoretical result than the numerical results because the theoretical method doesn't take the soil liquefaction in the calculations. While, in the middle of the base slab, the empirical equation (20) assumed there is an increase at the moment but actually there is a reduction in the middle slab moment which was not taken into account.

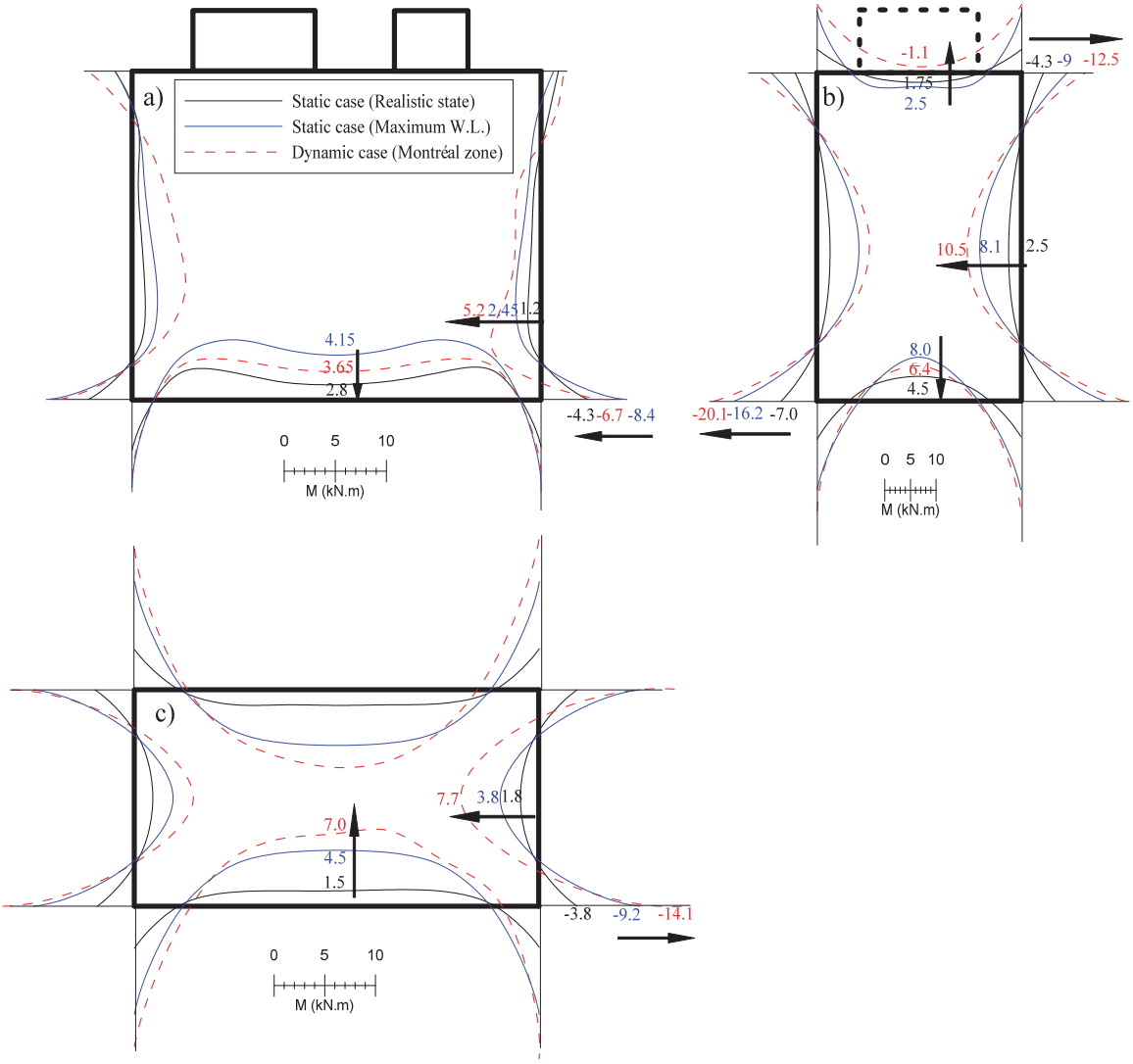

Figure 0.13 Bending moments in static and dynamic phases of analyses in the Montréal city case: (a) X-Z section at C.L.; (b) Y-Z section at C.L.; (c) X-Y section at 2m depth.

Also, it can be observed that the reduction of the earthquake frequency content (3.33 ~ 0.75 Hz) leads to an increase in the sidewall moment by 40 to 60%. For that, it is necessary to add a frequency correlation factor (C_f) to take the effect of earthquakes frequency. This empirical factor (C_f) can be determined from the relation between the earthquake frequency and the difference between numerical and theoretical dynamic internal forces as shown in Fig. 4.14b.

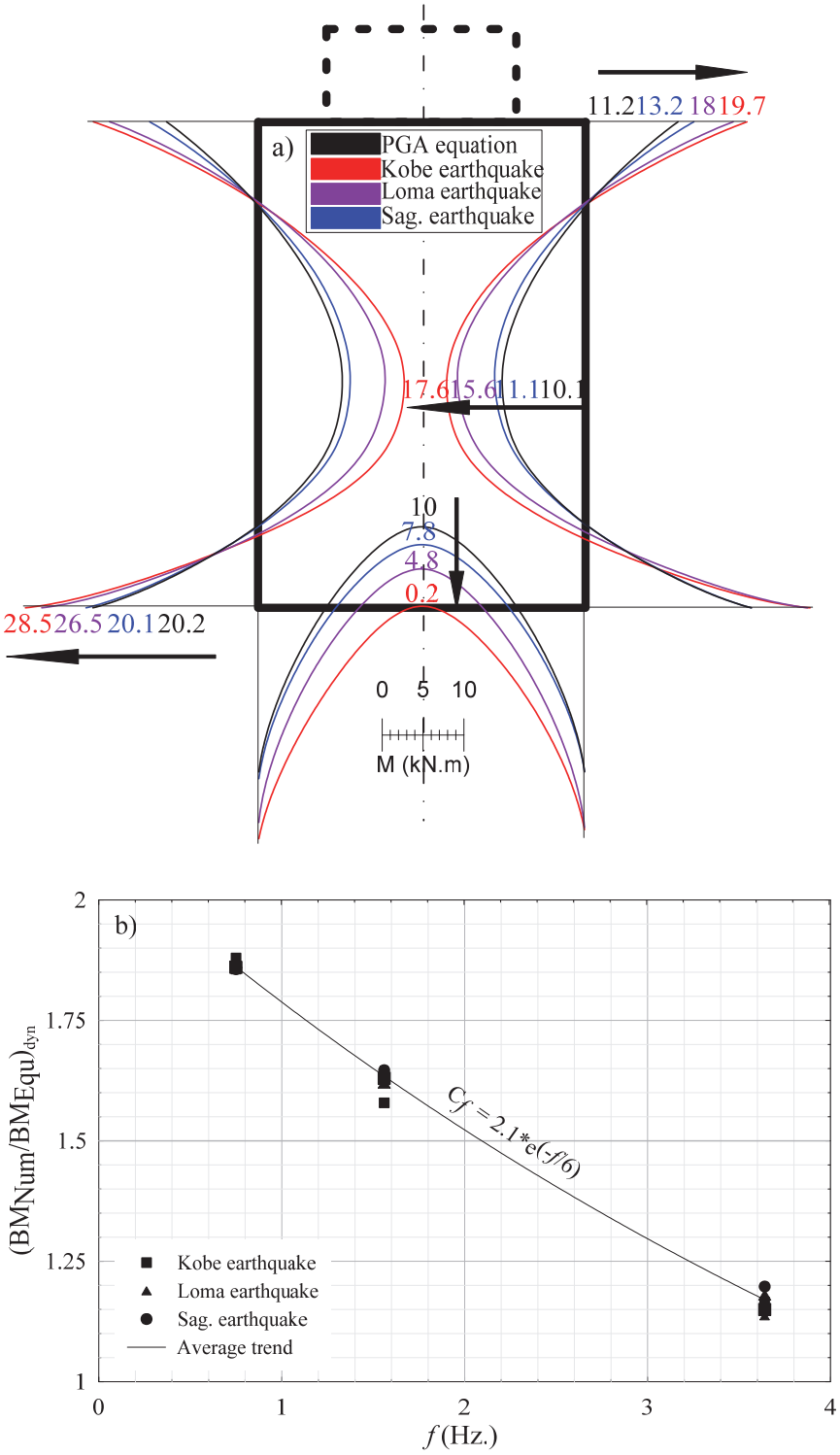

Figure 0.14 Comparing the numerical bending moment at the Y-Z section of the different earthquakes at PGA=0.25g with CHBDC empirical equation.

The modified empirical equation can be given by the following relation:

$$BM_{tot} / BM_{st} = \left(1 + \frac{2}{3} \times PGA\right) \times C_f \quad [21]$$

$$C_f = 2.1 \times e^{-f/6} \quad [22]$$

Figures 4.15 compares the dynamic bending moment of the Y-Z section in the two cases considered. It is already found that the side wall moment increasing in the Montreal site is more than it's in Quebec City site by 10~20%. Where the normalized dynamic bending moment (the dynamic bending moment (BM_{dy}) at a given section is normalized by the static moment (BM_{st}) at the same section) increases to 24~36% and 4~12% for Montreal and Quebec City locations, respectively, as seen in Fig.4.16. These increases are compatible with the increases theoretical calculated from the CHBDC equation and the spectral acceleration equations (Mahmoud[a] et al. 2019) where the increases are 20~44% and 5~14% for Montreal and Quebec City sites, respectively, as seen in Fig.4.16. On the other hand, the reduction of base bending moment is compatible with the increases theoretical calculated from the spectral acceleration equations but it isn't compatible with the increases theoretical calculated from the CHBDC equation. This difference is the result of the CHBDC method assumed there is increasing in the internal force values of all structural elements. While, in fact, there is a reduction in the internal forces of the base slab.

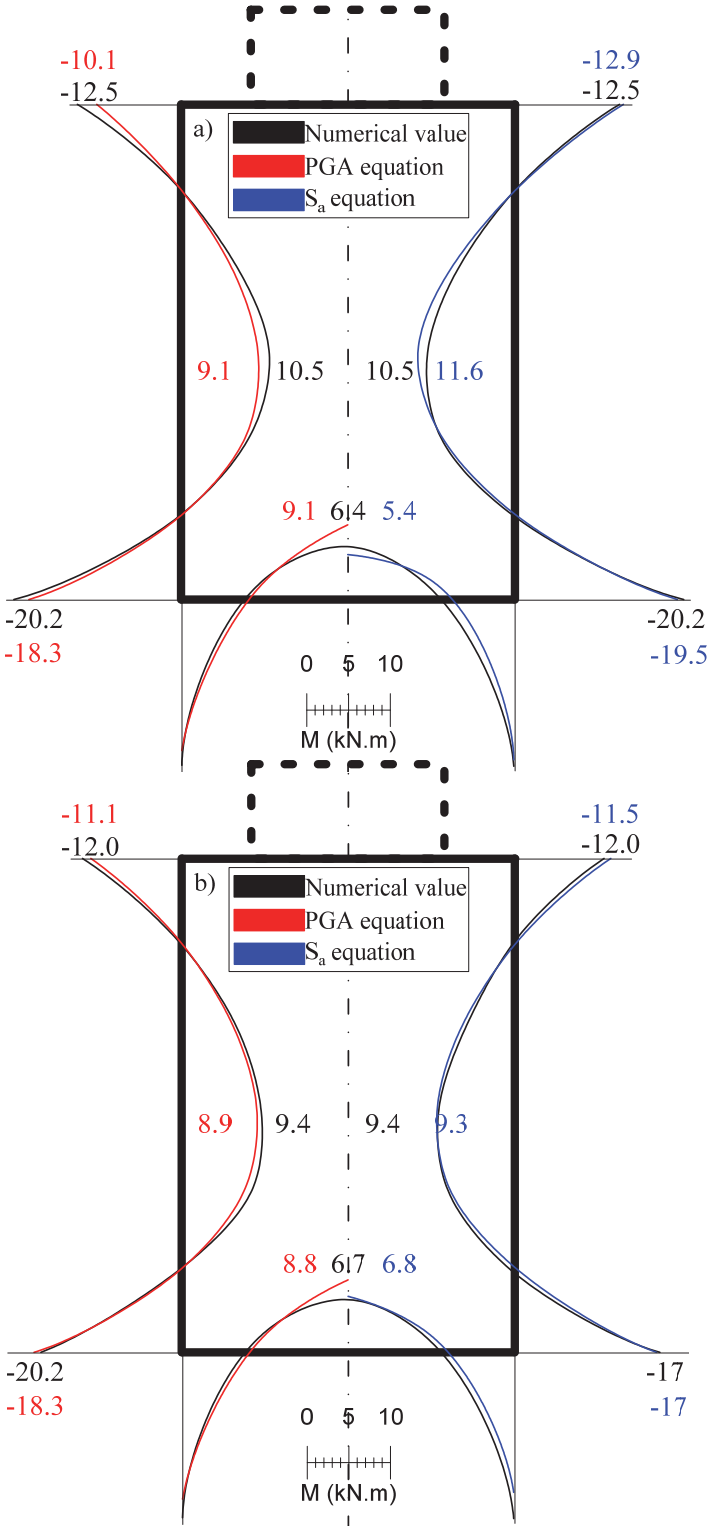

Figure 0.15 Comparing the numerical bending moment at the Y-Z section with empirical equations in: a) Montréal city; b) Quebec City.

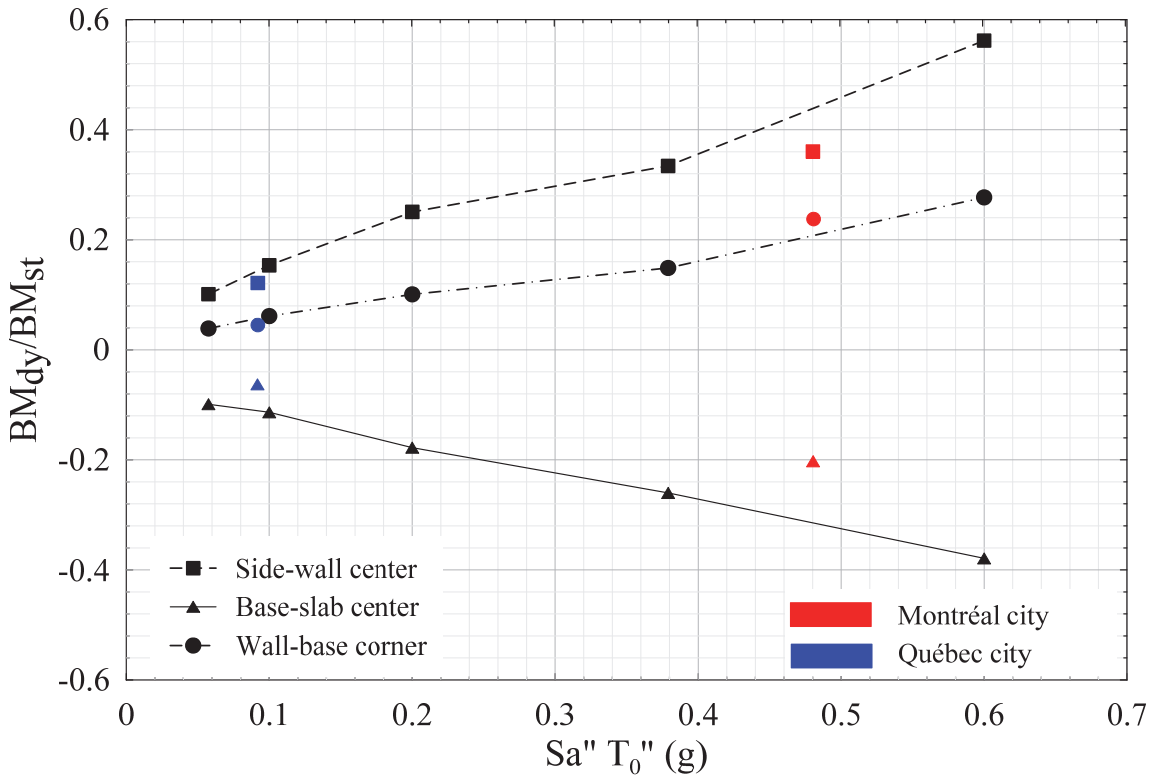

Figure 0.16 Effect of spectral acceleration of the different seismic zones on the bending moments of the Y-Z section (Mahmoud[a] et al. 2019).

4.5. Conclusion

Three-dimensional numerical simulations were conducted in this paper to study the seismic performance of access underground structure to study the effects of the earthquake parameters (i.e., amplitude and frequency) and liquefaction occurring. The energy-based approach was used as a constitutive model to simulate the seismic behavior of the soil. The acceleration response, the excess pore pressure, the structure uplift, and the internal forces of the underground structure (bending moment) were investigated. From the numerical results, the following conclusions can be obtained:

1. When the soil liquefied occurs, the liquefaction works to damping the earthquake power and deamplification the earthquake acceleration.
2. Earthquake amplitude increasing and earthquake frequency decreasing content lead to deamplification of the ground surface accelerations. However, the variation of the earthquake frequency content is more effective than the variation of the earthquake amplitude.
3. The increase of earthquake intensity (whether increase earthquake amplitude or decrease of earthquake frequency content) leads to increment and reduction in the dynamic internal forces of the sidewalls and slab base, respectively.
4. Because of the general reduction in response spectral amplitudes of the earthquakes due to liquefaction occurring, the designer may want to consider a special analysis of site response for liquefiable soil sites to avoid loads change in underground structure design when liquefaction occurs.
5. The empirical equation depended on PGA only is not appropriate for all design cases, so it should utilize a more comprehensive equation to take into account earthquakes spectral amplitudes and liquefaction calculations.

It should be noted that the results presented in this paper are valid for Hydro-Québec underground structures which are installed in the Québec seismic zone, and the specific soil properties that were used. For any other installation structures, seismic zone and different soil conditions similar analysis should be performed.

CHAPTER 5. MÉTHODES D'ATTÉNUATION DU SOULÈVEMENT

Ahmed O. Mahmoud: Ph.D. student, Department of Civil Engineering, Université de Sherbrooke Sherbrooke, Québec, Canada.

Mahmoud N. Hussien: Researcher, Department of Civil Engineering, Université de Sherbrooke, Sherbrooke, Québec, Canada.

Mourad Karray: Professor, Department of Civil Engineering, Université de Sherbrooke, Sherbrooke, Québec, Canada.

Mohamed Chekired: Researcher, Institut de Recherche d'Hydro-Québec, Varennes, Québec, Canada.

Carole Bessette: Direction Encadrement réseau et planification, Hydro-Québec, Montréal, Québec, Canada.

Livius Jinga: Direction Encadrement réseau et planification, Hydro-Québec, Montréal, Québec, Canada.

Date de soumission : Octobre 2019

État de la soumission : en évaluation par le comité de lecture de la revue.

Revue: Computers and Geotechnics.

Titre François: Atténuation du soulèvement des structures souterraines induit par la liquéfaction.

Titre English: Mitigation of liquefaction-induced uplift of underground structures.

Résumé: Le soulèvement dû à la liquéfaction des sols est l'une des manifestations les plus graves de l'instabilité de la structure souterraine lors d'un fort mouvement du sol. La liquéfaction du sol et la réduction du module de cisaillement sous ces structures sont les principaux facteurs de ce phénomène. Dans cet article, le comportement sismique de structures d'accès souterraines enfouies dans des dépôts sableux a été analysé à l'aide du programme de différences finies (FL), qui met l'accent sur les défaillances structurelles lors de tremblements de terre réels. Un nouveau modèle de "liquéfaction", basé sur l'énergie, qui simule le comportement cyclique des matériaux et estime l'accumulation de pression des eaux interstitielles, a été intégré au code numérique en tant que modèle constitutif du sol. De plus, l'élément structurel linéaire a été utilisé pour modéliser la structure souterraine. Plusieurs méthodes d'atténuation ont été modélisées contre la flottation de la structure. Ainsi qu'une nouvelle méthode combinée et ses impacts sur la performance structurelle ont été détaillés ici. Des résultats numériques ont montré que les drains de gravier dissipent efficacement l'excès de pression interstitielles sous la structure. D'autres analyses montrent qu'il est aussi possible d'enfouir plus profondément la structure ou encore d'ajouter sous celle-ci une couche imperméable de façon à augmenter la contrainte effective verticale dans les sols et ainsi diminuer le risque de soulèvement dû à la liquéfaction des sols sous la structure. L'étude s'est concentrée sur l'utilisation d'une nouvelle méthode combinée. Il a été constaté que la combinaison des drains de gravier entourant la structure avec la couche imperméable située sous la structure réduirait efficacement le soulèvement de la structure plus que toute autre méthode séparément.

Mots-clés: structure souterraine; différences finies; liquéfaction; rapport de pression interstitielle en excès; soulèvement; drains de gravier.

Abstract: Buoyancy is one of the most serious manifestations of the underground structure's instability during strong ground motion. Soil liquefaction and reduced shear modulus beneath these structures are the main driving factors of this phenomenon. In this article, the seismic behavior of underground access structures embedded in sandy deposits was analyzed using the two-dimension finite differences (2-FD) program (FLAC) with an emphasis on structural failures under real earthquakes. A new liquefaction model "energy-based approach" which simulates material cyclic behavior and estimates pore water pressure buildup, was incorporated into the numerical code as a constitutive model of the soil. Also, the linear structural element was used to model the underground structure. Several mitigation methods have been modeled against the structure flotation. As well as a new combined method and its impacts on the structural performance have been detailed discussed herein. Numerical results showed that gravel drains would effectively dissipate the excess pore water pressure beneath the structure while increasing the burial depth of the structure and adding an impermeable layer under it would increase the vertical effective stress and therefore detract the ability of excess pore water pressure to push the structure upward. The study focused on using a new combined method. It is found that compiling a gravel drains surround the structure with an impermeable layer beneath the structure would effectively reduce the structural uplift more than any method separately.

***Keywords*:** underground structure; finite difference; liquefaction; seismic zone; excess pore pressure ratio; uplift; gravel drains.

5.1. Introduction

Underground structures are currently used for a wide range of applications from small-scale structures such as pipelines, to mid-sized buried structures like manholes and chambers, to large underground structures including subways and tunnels (Macaulay, 1976). These structures are becoming more and more prevalent in the modern world because of land congestion pressures associated with fast-growing populations (Broere, 2016). During the last century, buried infrastructures were widely used to achieve the necessary insulation and safety required for undergrounding power lines, natural gas pipelines, telecommunication conduits and water mains (Kang, 2010). For example, in Québec, more than 30,000 underground structures for housing power cables and transformers have been installed across the province in recent years (Guérin et al., 2016).

There are many safety risks associated with these structures, especially when they are located in seismic zones. One of the severest of these risks is flotation, which can lead to structures going out of service. A number of underground structures were uplifted due to soil liquefaction during major earthquakes, e.g., Niigata (1964), Kushiro-oki (1993), Niigata Chuetsu (2004), Noto Hanto (2007) and Niigata Chuetsu-oki (2007). Other examples include the subway system in Kobe, damaged in the 1995 Kobe earthquake (Iida et al., 1996), uplifting of underground structures (manholes and underground tanks) in Chile during the 2010 Maule earthquake and the underground tank in San Pedrodel Valle uplifted by approximately 1.2 m (Yasuda et al., 2010). Aydan et al. (2012) reported substantial damage to above and underground structures after the 2011 Christchurch earthquake and its aftershocks. The 2011 Great East Japan (or Tohoku) earthquake caused the uplifting of many infrastructures, such as manholes, emergency water tanks and underground parking garages

(Tokimatsu et al., 2012). More than one hundred manholes were uplifted, indicating the high susceptibility of underground structures to damage caused by soil liquefaction at liquefiable sites. This is not, obviously, the case in buried pipelines as their large overall density and the weight of the overlying soil work on increasing the vertical pressure on the soil beneath and surrounding them, a condition that increases the shear stiffness of these soils and reduces the susceptibility of the pipelines to damage. In contrast, at non-liquefiable soil sites, minimal damage to both manholes and pipelines were reported (Tokimatsu et al., 2011).

In fact, a saturated loose granular soil substantially loses its shear strength and stiffness and is converted from solid to a liquefied state when subjected to strong ground shaking. In situations where an underground structure is found in a liquefiable soil, its lower submerged total density compared to the surrounding soil, together with the buoyant force, causes uplift of the structure (e.g., Zhuang et al. 2016, Otsubo[b] et al. 2016, Wang et al. 2018, Zhang et al. 2019, Haiyang et al. 2019). Many numerical and experimental studies have discussed the seismic behavior of underground structures with the liquefaction of soil (e.g., Ling et al., 2003; Byrne et al., 2004; Yang et al., 2004; Gazetas et al., 2005; Liu and Song, 2006; Kang et al., 2009; Chou et al., 2011; Kang[b] et al., 2013; Zhai, et al., 2014; Zhou et al., 2015; Zhuang et al., 2015; Watanabe et al., 2016). However, few of these studies focused on ways to protect buried structures from damage due to soil liquefaction. Several different remediation methods against liquefaction are generally described. However, a number of these methods are specialized in underground structure protection. The fundamental idea of these methods is to reduce the liquefaction ratio (i.e., the ratio between the excess pore water pressure and the vertical effective stress). In other words, these methods work on: (1) decrease the positive excess pore water pressure under the structure (soil densification or

solidification), keep the groundwater away from the underground structure (lowering the water table), or dissipate the excess pore water pressure (surround drainage gravel); 2) increase the vertical effective stress under the structure by increasing the structure's unit weight or increasing its buried depth; 3) change the structure's geometry by increasing the structure's unit weight by increasing the structure walls thickness or change the structure shape by increase structure width or using pyramidal frustum shape; 4) damping the shear loading from the earthquake by installing surround structural members (eg. sheet piles, geosynthetic; overweight). Some case studies that adopted one or more of these methods are discussed next. Yang et al. (2004), Liu and Song (2006), Cheuk et al. (2008), Tobita et al. (2011), and Jung[b] et al. (2013) used high-density material or increased the density of existing material surrounding the structure to limit the generation of pore water produced by soil liquefaction. Sasaki and Taniguchi (1982), Orense et al., (2002), Yang et al. (2004) and Rasouli et al. (2016) drained the build-up of pore water pressure under and beside the structure caused by earthquake loading by using a gravel drain treatment adjacent to the structure. Chou et al. (2001), Liu and Song (2005), and Bao et al. (2017) injected the soil with cement to strengthen the soil and reduce the water flow by plugging soil pores. Azadi[b] and Hosseini (2010), Saeedzadeh and Hataf (2011), and Chian et al. (2014) increased the underground structure buried depth so as to increase the vertical effective stress and confining pressure. Yasuda et al. (2004) and Rasouli et al. (2015) mitigated the uplift of the underground and the settlement of super surface structures due to seismic liquefaction by the installation of sheet-pile walls around the foundation. Ling et al. (2003), Tupa and Palmeira (2007), Palmeira and Andrade (2010), and Palmeira and Bernal (2015) used the geosynthetic material to mitigate pipeline flotation. Castiglia et al. (2017) stabilized

pipelines in liquefiable soils using concrete weighting. Using a combined method of two of more aforementioned traditional methods has different mitigation effects (e.g. reduce EPWP, raise the effective vertical stress, or damping the shear wave from the earthquake) is more efficient than using one method alone. For example, a combined method of sheet-pile with drain system was helped with significant mitigation the buried structure float by reducing the shear deformation in the enclosed soils and creating drainage paths beside the structure (Tanaka et al. 1995, Hashash et al. 2001, and Liu and Song 2006). So, the paper suggests using a combined method of two conventional methods.

The current study investigates the performance of Hydro-Québec's typical underground access structures under seismic loads. Finite different (FD) models of structures buried in a sandy deposit. The soil was constructed by adopting a new constitutive soil model (energy-based) to simulate soil liquefaction surround the structure using the computer code FLAC. Also, in the study, different mitigation methods mentioned above were used to control excess pore water pressure surrounding the structure, thus preventing uplift of the structure and putting it out of the service. The study focuses on protecting the increased against flotation by changing soil properties around the structure and increasing the depth of buried structures. The paper introduces the use of the gravel drain, impermeable base and sand densification as liquefaction mitigation methods for the protection of underground structures against uplift. The other thing this paper presents is using a combined method from customary mitigation methods in the literature. Before presenting the results of the numerical modelling of the effect of earthquake characteristics on the seismic response of underground structures, we present a detailed description of the numerical model adopted for this study, including a section presenting the validation of the model against previous experimental results.

5.2. Numerical modelling

There are several models that can simulate soil-structure interaction. Most of them are built from the finite element (FE), discrete element (DE) or finite difference (FD) methods. Many programs can model dynamic soil-structure problems but few can simulate soil liquefaction as this requires the differential equations of the solid and fluid phases to be coupled. For example, Kang et al. (2014) used the FLIP (FE) program to study the seismic response of underground structures built in liquefiable soils. Using the program DYNA (FE), Liu and Song (2005 and 2006) incorporated a generalized plasticity model that can simulate soil liquefaction. Zhuang et al. (2015) and Wang et al. (2019) utilized ABAQUS software (FE) in modelling the dynamic properties of liquefiable soil by developing a plasticity-based constitutive model. Zhou et al. (2014) succeeded in predicting the uplift response of an underground structure and the occurrence of liquefaction in saturated sand by PFC3D software (DE). Hu et al. (2018) developed LIQCA software (FE-FD) that can simulate the soil liquefaction process (simultaneous pore pressure build-up and dissipation). Bao et al. (2017) investigated the seismic behavior of underground structure using the fully coupling DBLEVES code (FE-FD). FLAC is a code that can implement coupled effective-stress models (Itasca, 2011). FLAC was successfully utilized in engineering practice to investigate the seismic response of underground structures in liquefiable and non-liquefiable ground (e.g., Yang et al., 2004; Azadi[a&b] and Hosseinia, 2010; Azadi, 2011; Chian and Tokimatsu 2012; Chian et al., 2014; Sun and Dais 2019; Zheng et al., 2019; Sun[a&b] et al., 2019). In this study, FLAC was harnessed for the simulation of the seismic behavior of Hydro-Québec underground structures by using the energy-based as a constitutive model of soil.

5.2.1. Simulation Model

The seismic behavior of underground structures in liquefied soil was investigated using FLAC. The underground structure in question was a typical Hydro-Québec chamber (3.75 × 2.25 × 2.75 m) with two different diameter manholes (i.e., D = 0.5 and 1.0 m) located in the top slab of the structure. For the base case, the structure was assumed to be rectangular with 3.75 m width and 2.75 m height (while 2.25m is the dimension in the longitudinal direction) buried at a depth of 0.5 m, as shown in Fig. 5.1a. This structure is already installed in Montréal, Canada (Hydro-Québec 2019) and has been studied extensively by (Guérin 2015; Tremblay 2017; Tremblay et al. 2017; Tremblay et al. 2018). The depth of the buried structure was varied in the simulations to study the effects of mitigation of the structure against uplift. The thickness of the walls and slabs of the structure were all assumed to be 25 cm. The structure and the two manholes were simulated by linear structural elements. A gravel drains or dense soil with variable thickness was installed around and beneath the structure to decrease the pore water pressure and reduce the uplift deformation of the structure. Also, an impermeable reinforcement base was added beneath the structure to create an overweight to the structure.

5.2.2. Material properties and interface

In this study, the soil layer was assumed to be loose saturated sand 10 m thick overlaying rigid rock. In the static analysis, the soils were represented by the Mohr-Coulomb model implemented in FLAC, and the stresses of the model have been developed due to the gravity loading. Sand parameters used in the numerical analyses (Table 5.1) were determined based on relative density and stress-normalized shear wave velocity (V_{s1}) equal to 20 and 100 m/s, respectively. The shear wave velocity (V_s) then determined from V_{s1} as (Youd et al., 2001):

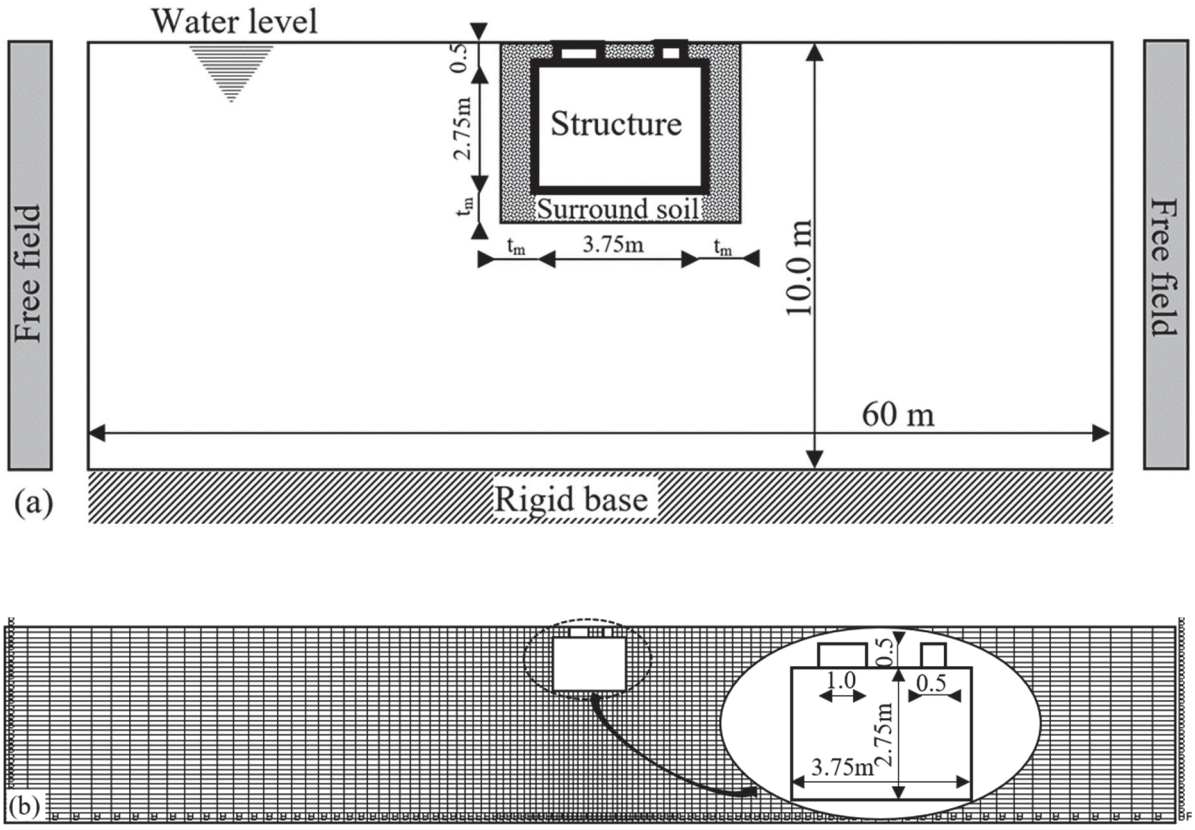

Figure 0.1 a) Illustration of the model and boundary conditions; b) display of meshing size.

$$V_s = V_{s1} \times \left(\frac{\sigma_v^{'}}{P_a} \right)^{0.25} \quad [1]$$

where σ_{v0}' and P_a are the initial effective vertical stress and atmospheric pressure. The maximum shear module (G_0) was determined based on the value of V_s from the elastic relationship between G_0 and V_s, $G_0 = \rho \times V_s^2$, where ρ is the soil density. By assuming a Poisson ratio (υ) of 0.33, the bulk modulus of soil (K_0) was determined from G_0. The structure was assumed to be elastic material with a modulus of elasticity (E_s) and Poisson ratio (υ_s) of 30 GPa and 0.2, respectively (Liu and Song, 2005).

Interface elements are used to connect the structure facing zone in numerical simulations to the adjacent soil zone. The Soil-structure interface is represented as normal and shear springs between two nodes contacting each other and are modelled as linear spring-slider systems (Fig. 5.2). This interface type successfully utilized in the previous studies (Benmebarek et al. 2005; Haldar and Babu 2008; Rayhani and El Naggar 2008; Benmebarek et al. 2008; Hsiung 2009; Mortazavi and Alavi 2013; Abuhajar[a&b] et al. 2015; Lee et al. 2015; Do et al. 2015; Lu et al. 2016; Li and Aubertin 2015; Wu et al. 2016; Lin et al. 2017; Esfeh and Kaynia 2019; Sharaf and Maleki 2019; Sun and Dais 2019; Gong et al. 2019). The interface is modelled with the Mohr-Coulomb constitutive relation. The shear strength at the interface was defined with 2/3 of the friction angle and zero cohesion. The relative interface deformations are controlled by the interface normal (K_n) and shear stiffness (K_s) values, and it should be kept as small as possible to prevent overlapping between materials connected by the interface. So, it is recommended (Itasca 2011) that the stiffness k_n and k_s to be set, as a rule of thumb, at ten times the equivalent stiffness of the stiffest neighboring zone. The preliminary values for the normal and shear interface stiffness (expressed in stress-per-distance units) can be determined from an empirical equation given in the FLAC user's manual (Itasca 2011):

$$k_n = k_s = 10 \times \left[\frac{K + 4/3 \times G}{\Delta z_{\min}} \right]_{\max} \qquad [2]$$

where: K & G are the bulk and shear moduli of the surrounding soil, respectively; ΔZ_{min} is the smallest width of an adjoining zone in the normal direction.

5.2.3. Material damping

Following the dynamic analysis, the hysteretic-type model was developed to simulate the S-shaped curve of modulus versus the logarithm of cyclic strain with zero slopes at both low strain and high strain. The hysteretic models are monotonic within the defined range and have the appropriate asymptotic behavior. Thus, the function is well-suited to represent modulus degradation curves (G/G_{max}). The Sig4 soil model is a type of hysteretic model with a four-parameter model thus it provides more flexibility control in fitting the stiffness and damping data compared to other models. The secant modulus ratio (M_s) can be calculated from the fitting equation (Itasca 2011):

$$M_s = \frac{G}{G_{max}} = y_0 + \frac{a}{1+e^{\frac{x_0-L}{b}}} \quad [3]$$

where L is the logarithmic strain and the fitted parameters (a, b, x_0, y_0) of the SIG4 model were selected such that they produce shear modulus degradation and damping curves, of the sand deposit. There are many previous studies clarified that the experimental curves suggested by Seed and Idriss (1970) gave satisfying results (Wu 2001; El-Mohtar et al. 2013; Chekired et al. 2015). The parameters of the damping model were adopted to fit the shear modulus degradation (Fig. 5.3a) and damping curves (Fig. 5.3b) of the sand during dynamic analyses. Additionally, a Rayleigh damping is used, with components proportional to the mass-proportional (α) and the stiffness-proportional (β) damping constants to ensure the stability of the numerical solution process at very low strain levels. The proportional damping constants can be determined from the critical damping ratio (ξ_{min}) and the natural frequency of oscillation, f_{min} as following:

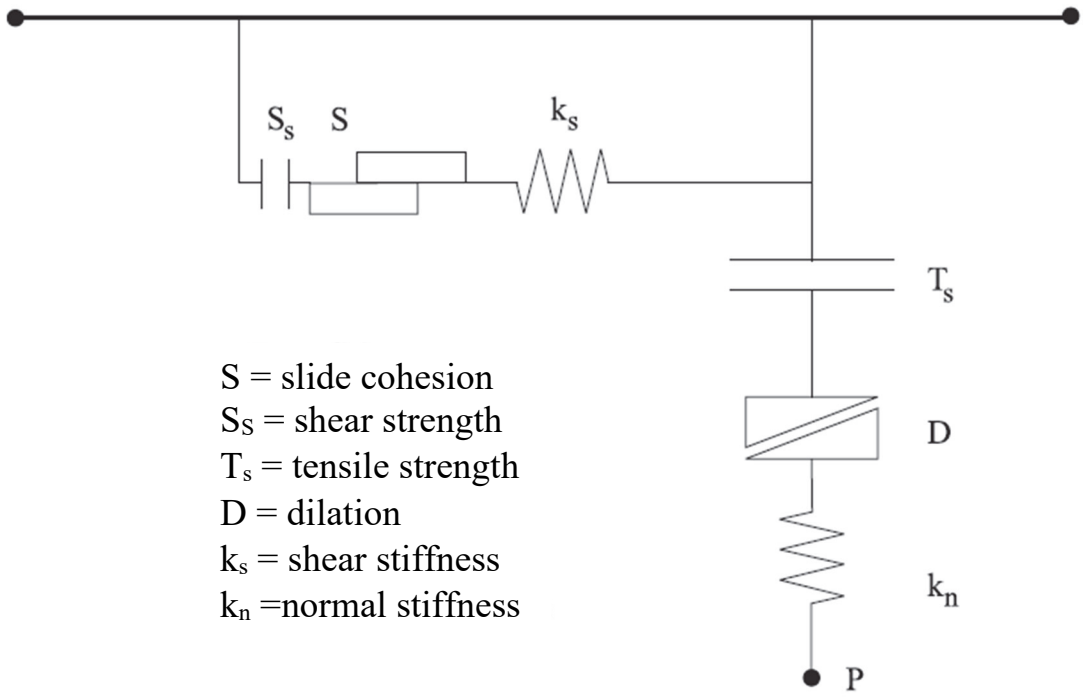

Figure 0.2 Components of the bonded interface constitutive model.

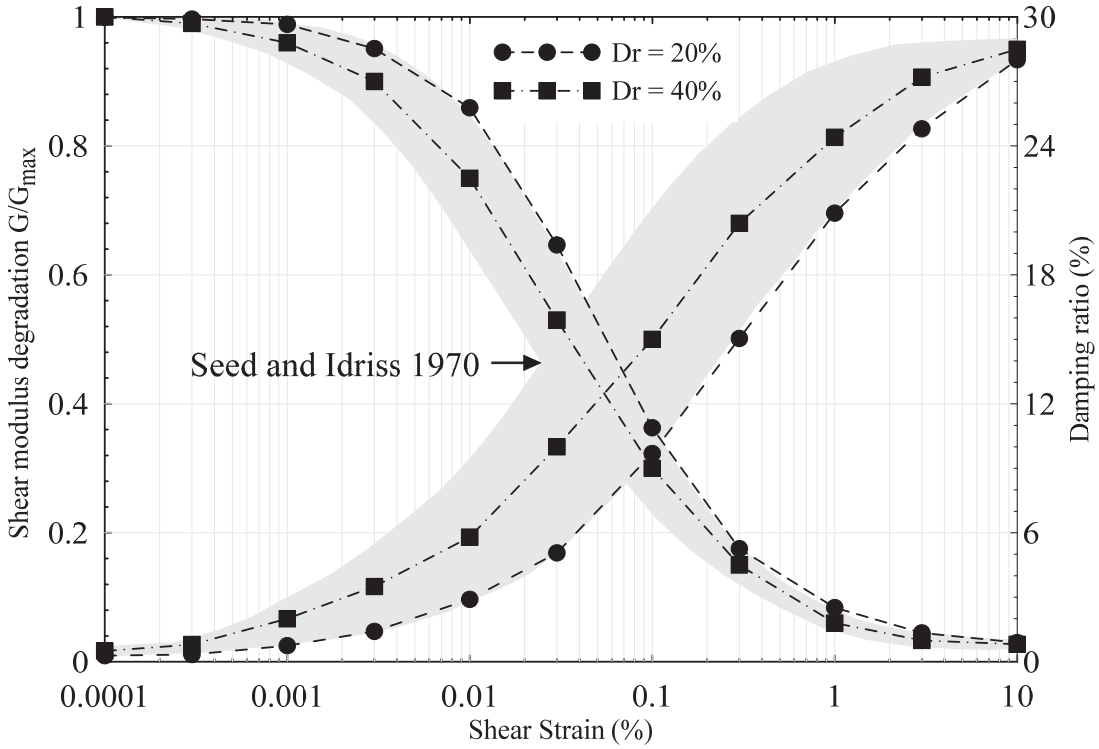

Figure 0.3 Shear modulus reduction and damping ratio curves for sandy soil compared with Seed and Idriss (1970).

$$\alpha = \xi_{min} * 2\pi f_{min} \quad [4]$$

$$\beta = \xi_{min} / 2\pi f_{min} \quad [5]$$

Therefore, the model has been critically damped with a damping ratio of 0.002 and the natural frequency of oscillation, f_{min}, equal to $v_s/4H$ (2.5 and 3.8 Hz at relative density of 20% and 40%, respectively) to ensure the stability of the numerical solution process at very low strain levels as recommended by the FLAC software manual (Itasca, 2011). Also, the shear strain induced in each subsequent cycle of loading increases because the increasing pore pressure decreases the soil shear stiffness (shear modulus, G). Seed[b] et al. (1975) determined the reduction of the soil shear modulus (G) from the pore-water pressure ratio (R_u) and the maximum shear modulus (G_{max}) using the following equation (Matasovic and Vucetic, 1993; Chang et al., 2007):

$$\frac{G}{G_{\max}} = \left(1 - R_u\right)^{0.5} \quad [6]$$

5.2.4. Boundary condition and meshing

In this study, the numerical analyses were performed in two stages. In the first stage (self-weight static analysis), the base boundary between the soil deposit and the bedrock was assumed to be fixed in both horizontal and vertical directions. However, the lateral boundaries were assumed to produce equal displacement in all directions which meant the same level side boundary nodes were moving the same amount and direction. Also, the ground surface was assumed to be flat and free of loadings. As an extreme case, the underground water level was assumed to be at the surface of the ground. In the second stage (seismic analysis), the free-field boundaries are used to represent the lateral extent of the far-field. The assigned

properties and initial conditions are transferred from the main-grid zones adjacent to the free-field boundaries. The free-field boundaries should be placed to minimize wave reflections (Itasca, 2011). The horizontal seismic load was applied at the rigid base boundary as shown in Fig. 5.1a.

The height of the soil elements affects the transmission of high-frequency shear waves. For this reason, the height of the elements was limited to a maximum height, ΔL (Kuhlemeyer and Lysmer 1973), which is less than one-tenth of the wavelength of the input wave:

$$\Delta L \leq \frac{\lambda}{10} \quad [7]$$

where λ is the wavelength associated with the highest frequency of the input earthquake. The selected soil element size was chosen to be 0.25 m around the structure which can allow the spreading of frequency contents up to 40 Hz (the main earthquake frequency is between 0.1 And 25 Hz, which is lower than 40 Hz). The elements gradually increased going outward as shown in Fig. 5.1b.

5.2.5. Input earthquake motion

The Saguenay earthquake (1988) was one of the largest recorded earthquakes in north-eastern North America in the 20th century. This earthquake-induced severe damage to buildings, underground structures and public services (Mitchell et al., 1990 and Tuttle et al., 1990). In this numerical analysis, the earthquake amplitude was multiplied by a constant value to be compatible with the largest seismic zone in Québec as shown in Fig. 5.4b. The earthquake excitation was input at the base nodes as a time-history input acceleration (Fig. 5.4a).

5.2.6. Material calibration and model validation

There is different software with different codes that can simulate the uplift behaviour of underground structures due to soil liquefaction. Almost all of these codes are based on either stress- or strain-based soil constitutive models. Seed and Idriss (1971) and Dobry et al. (1982) were the first proposed strain-based and strain-based procedures, respectively. The main problem of those two procedures is that the calculation of excess pore water pressure associated with one variable (stress or strain) while neglecting the other despite being no less important. While, the energy-based procedures which is one of the closest ways to make a realistic simulation to the soil liquefaction approached to utilize both stress and strain estimate to compute the liquefaction ratio (R_u), unlike other methods (Green, 2001).

The beginning of that method was through Seed and his colleagues at the University of California at Berkeley who developed an energy-based pore pressure generation model as an alternative to the well-known stress-based model (Booker et al.,1976). The motivation for the development of this model was to enable them to use the dissipated energy as a measure of soil liquefaction resistance. Nemat-Nasser and Shokooh (1979) assumed that the pore water pressure build-up is directly related to the amount of seismic energy dissipated in the unit volume of soil by the following relationship:

$$\Delta U = E \times A \times \Delta W \quad [8]$$

where (ΔW) is the amount of energy dissipated in the soil is correlated to the volumetric change (ΔV) by means of constant (A) and modulus of elasticity (E). And, consequently, related to the excess pore-water pressure(ΔU). Davis and Berrill (1982) and Berrill and Davis (1985) also estimated the excess pore water pressure ratio (R_u) from the cyclic energy per unit volume of the soil, as demonstrated by:

$$\frac{\Delta U}{\sigma_{v'}} = \alpha * \left(\frac{\Delta W}{\sigma_{v'}}\right)^{\beta} \quad [9]$$

where α and β are constant parameters that depend on the soil being laboratory tested. In the Geotechnical lab at Sherbrooke University, more recent laboratory test results obtained from the strain-controlled triaxial simple shear T_xSS apparatus by Karray et al. (2015 & 2016) confirmed that the dissipated energy per unit volume during cyclic loading is closely connected to the generated excess pore water pressure. The relationship between dissipated energy and excess pore pressure ratio is:

$$r_u = \alpha \left(\frac{W_s^{0.5}}{a_x} \right)^{\beta} \quad [10]$$

where W_s is the energy dissipated per unit volume of soil divided by the initial effective confining pressure, which is determined by integrating the area bound by stress-strain hysteresis loops as shown in Fig. 5.5, and a_x is a variable parameter that depends on the soil shear strain. To calibrate the liquefaction parameters α, β, and a_x, the applicability of the adopted energy-based approach to study soil behavior under cyclic loading was carried out through the simulation of cyclic simple shear tests on Ottawa sand. The numerical properties and parameters of the sand used in the numerical simulation are listed in Table 5.1. These parameters were determined based on two soils with a relative density equal to 20% and 40%. In the analysis, shear stress was applied to the top of a soil element having a fixed base and free top as a sin wave with constant amplitude and frequency 1.0 Hz. The results of the analysis were compared to the experimental test results in terms of the shear strain time history and excess pore water pressure ratio time history response (Fig. 5.6). The comparative results presented in Fig. 5.6 indicate that the current energy-based model has the capability to reasonably simulate the cyclic behavior of sand.

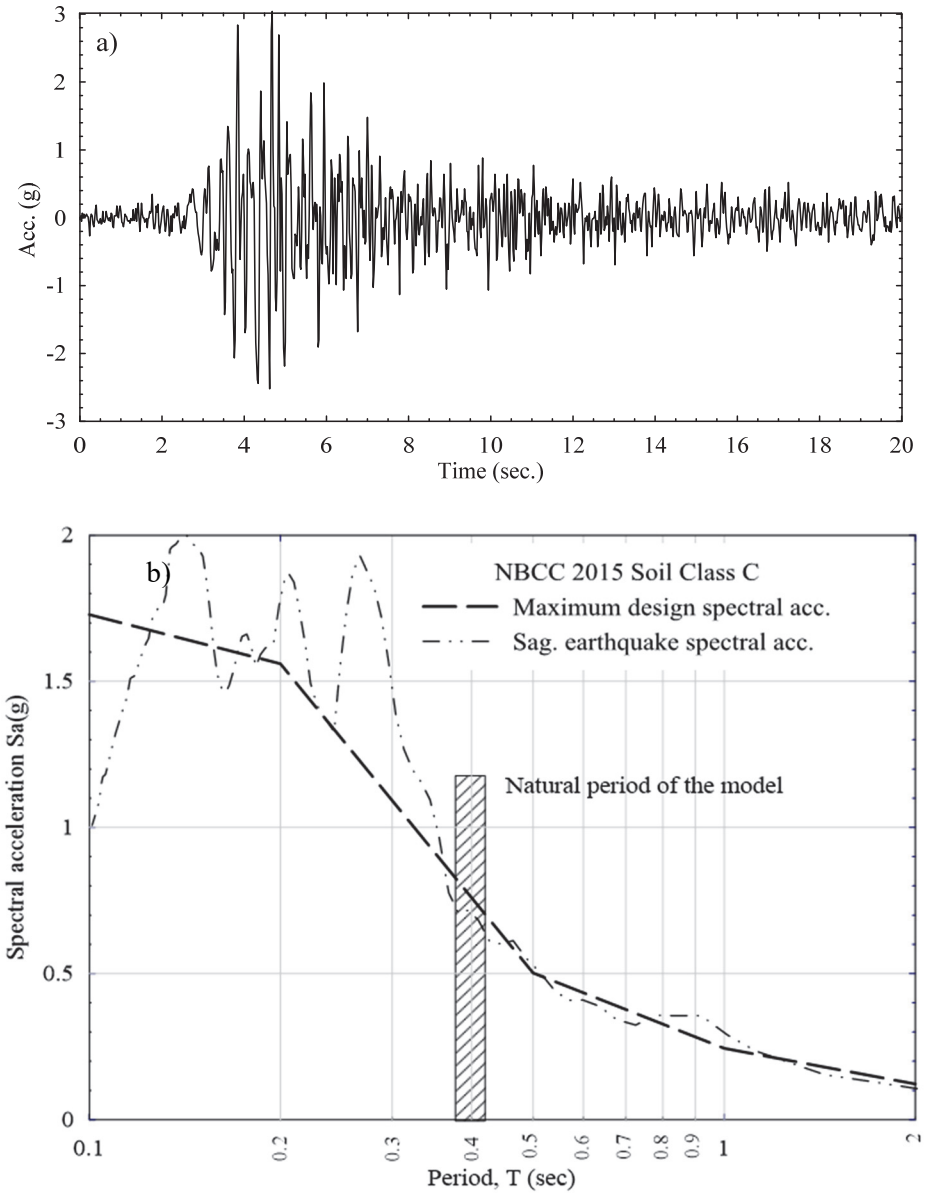

Figure 0.4 a) Acceleration time history of the 1988 Saguenay earthquake; b) comparison between the earthquake spectral acceleration and design spectral acceleration.

Table 0.1 Numerical parameters of materials used in this study

Static soil parameters			Dynamic soil parameters			Structure & interface parameters	
Dr%	20	40	*Dr%*	20	40		
G_0 (MPa)	15	36	α	1.0	1.05	E_s *(GPa)*	30
K_0 (MPa)	40	96	β	0.6	1.5	υ_s	0.2
ρ_d (kg/m^3)	1500	1570	a_x	$0.92\gamma^{-0.455}$	$1.36\gamma^{-0.365}$	ρ_s (kg/m^3)	2500
ϕ_f°	33	35	a	1	1	k_s *(GPa/m)*	0.3
k (m/s)	1e-5	9e-6	b	-0.55	-0.8	k_n *(GPa/m)*	0.3
n	0.43	0.41	x_0	-1.5	-2.25	δ°	23
K_w *(GPa)*	2.2	2.2	y_0	0.001	0.02	Ts	0

G_0: initial shear modulus at a confining pressure of 100 kPa; K_0: initial bulk modulus at a confining pressure of 100 kPa; ρ_d: dry density; ϕ_f°: failure angle of friction; k: soil permeability; K_w: Water modulus; n: porosity; α, β and a_x: liquefaction parameters; *a, b,* x_0 and y_0: hysteretic fitted-parameters; γ: soil shear strain; E_s: structure Young modulus; υ_s: structure Poisson ratio; ρ_s: structure density; k_s and k_n: shear and normal interface stiffness; δ°: friction angle of the interface surface; Ts: tensile bond strength.

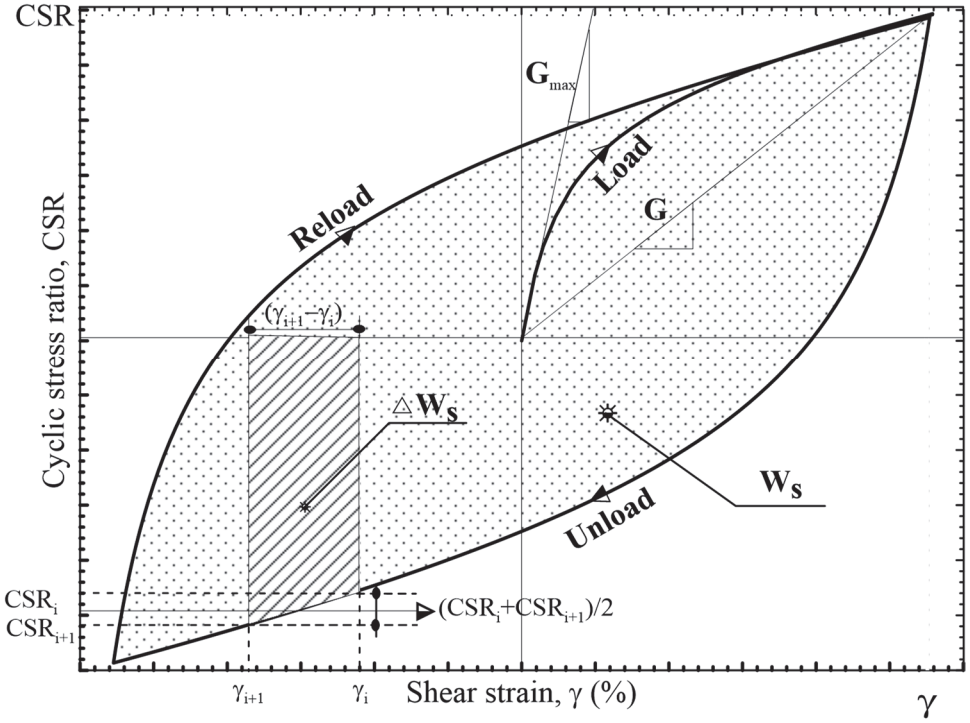

Figure 0.5 Dissipated energy per unit volume for a soil sample in a cyclic shear test determined by integrating the area bound by stress-strain hysteresis loops.

The applicability of the soil constitutive model and the adopted numerical model to the analysis of the seismic behavior of underground structures were examined by simulation of the centrifuge experiments. The first case conducted by Chian et al. (2014) on the seismic performance of a circular tunnel embedded in a uniform horizontal fully loose saturated sand (Dr=20%). The centrifuge experiments were created using a window box. A sine wave acceleration with amplitude 2.2 m/s^2 and frequency 0.75Hz was applied as the seismic load. The sand numerical parameters for the analysis are given in Table 5.1. It is worth mentioning here that because the three grains of sand used in this study had very similar physical properties and particle size distribution curves, the same numerical parameters were used to simulate their behavior in the numerical analyses. From Figs. 5.7a and 5.7b, it can be seen that the buildup of excess pore water pressure ratio, r_u, computed at the tunnel spring line, is very close to its measured counterparts. Also, the final predicted movements were in good agreement with the measured data from the centrifuge tests as shown in Fig. 5.7c. It can, therefore, be concluded that the numerical model adopted in the present investigation adequately simulates the seismic behavior of underground structures.

The second case was previous work by Zhou et al. (2014 and 2015) using a centrifuge and numerical modelling. The prototype contains a clay layer and a sand layer which were 2.5m and 22.5 m, respectively with cubic underground structure with size 10x10x10m at 2.5m depth. Medium saturated sand at a relative density of 40% was used in the experimental work. The general properties of the soil in the model are provided in Table 5.1. The input earthquake motion was based on the Kobe wave, the acceleration recorded at Kobe station during the 1995 Kobe earthquake. the current results are compared with previous results in terms of the excess pore water pressure and structure uplift under seismic loading in Fig.5.8.

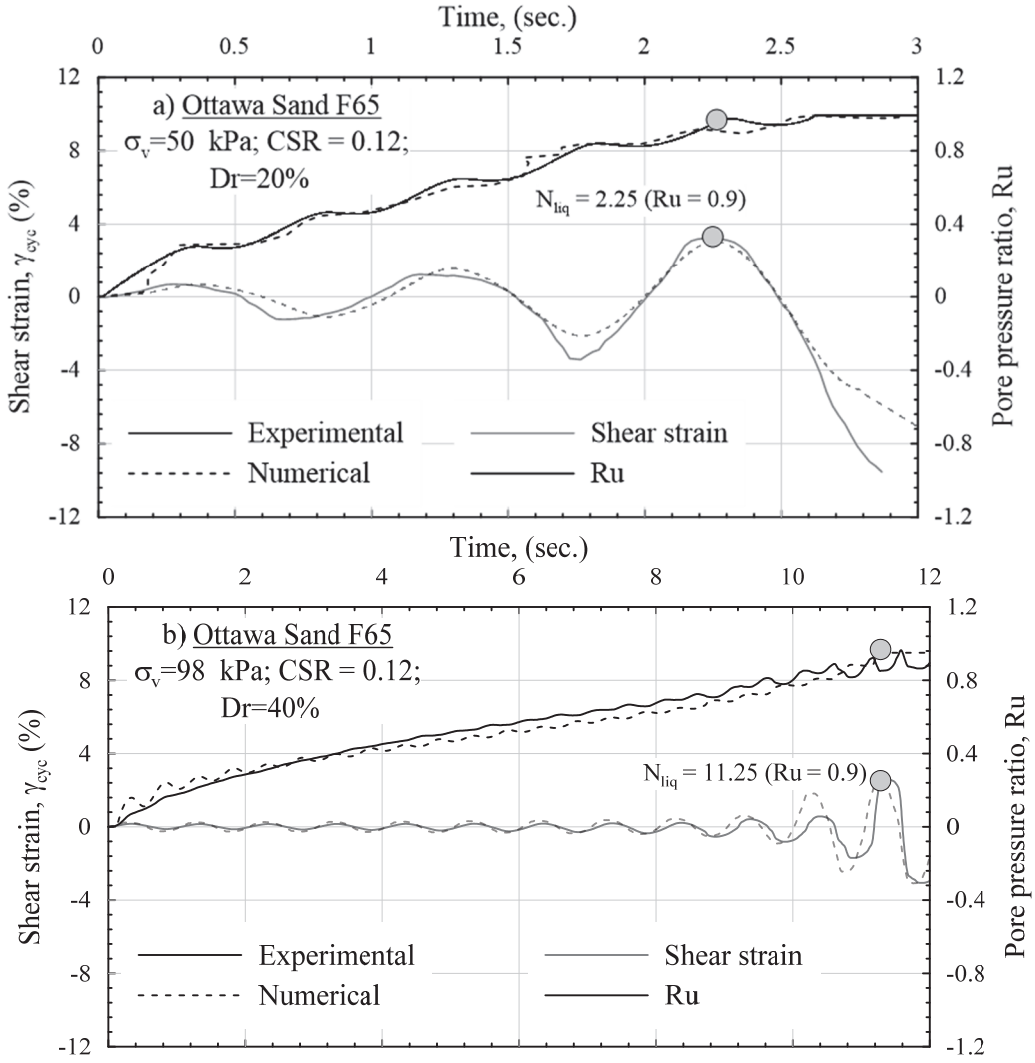

Figure 0.6 Comparison between cyclic direct shear test and current numerical results: (a) Loose sand (relative density = 20%); (b) Medium sand (relative density = 40%).

It is found that there is a significant correspond along the stage of excess pore water pressure, as can be seen in figures 5.8a and 5.8b. Figure 5.8c shows the time histories of the structure uplift for the previous and current models. It can be obviously seen that the structure started to uplift at about 6s when the soil was near to liquefaction occurring (EPWPR near to 0.8) at the bottom of the structure in the two models. The comparison can be considered as good for all practical purposes. Consequently, the analysis model used in this study has reasonable applicability to capture the essential behavior of the structure under seismic excitations.

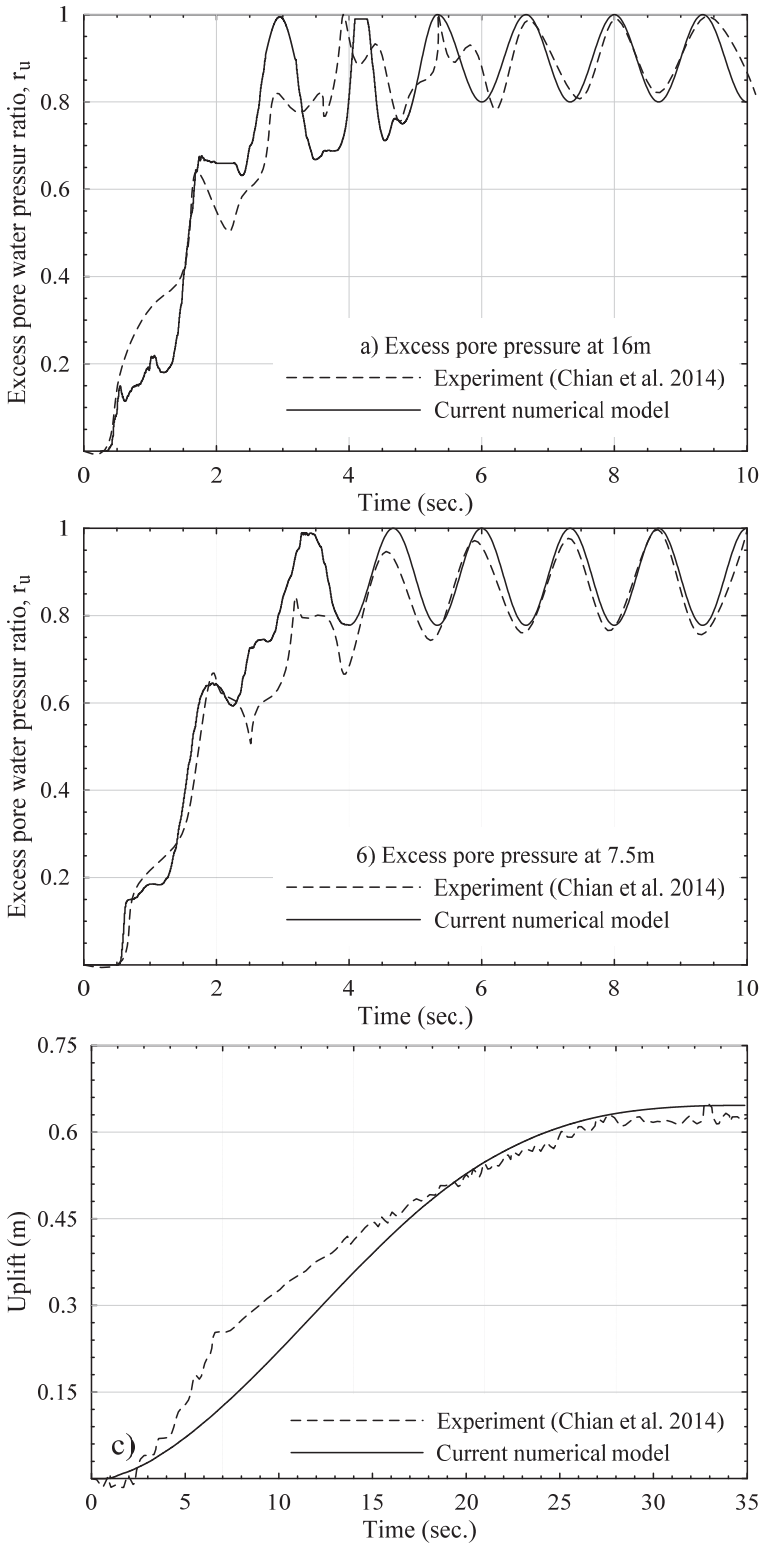

Figure 0.7 Comparing between measured and computed time histories of: (a) R_u at base depth (16m); (b) R_u at spring level (7.5m); (c) structure uplift.

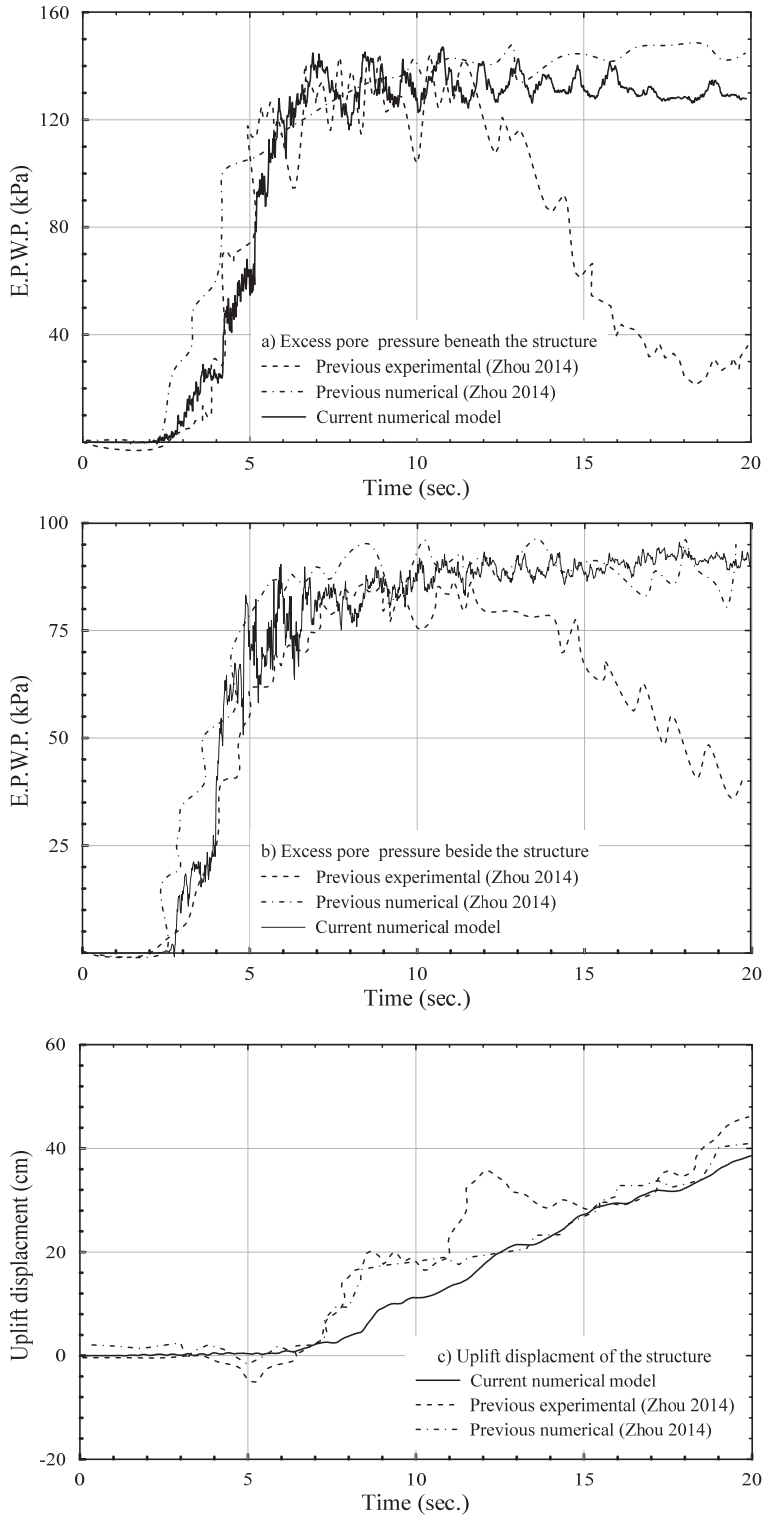

Figure 0.8 Comparing between measured and computed time histories of: (a) excess pore water pressure beneath the structure(m); (b) excess pore water pressure beside the structure (m); (c) structure uplift.

5.3. Results of soil liquefaction in the original model

The buildup of excess pore pressure, as well as the uplift displacement of the underground structures during and after an earthquake, were investigated in order to gain a comprehensive insight into the seismic behavior of the liquefiable soil-structure interaction system. Similar to what has been established in the literature (Liu and Song, 2005; Azadi[a&b] and Hosseini, 2010), the results of the current numerical study showed that when the soil liquefies this leads to a quantity of water that can flow upward as shown in Fig. 5.9a. It is an imbalance of vertical pressures arising from the development of excess pore water pressure beneath the underground structures that leads to the underground structures uplift surrounded by liquefied soil. Often underground structure uplift is accompanied by the surrounding soil settlement as a result of the soil movement as shown in Fig. 5.9b. Where the structure uplift occurrence is evident versus surround soil settlement.

5.3.1. Excess pore water pressure behavior

Figure 5.10a shows the buildup of the excess pore water pressure ratio (EPWPR) of nodes beneath the center of the structure. It was found that the EPWPR was starting to increase by a small rate at the beginning of the earthquake. After 2 seconds and until 5 seconds, it is increased steadily and quickly during this period. The EPWPR under the structure reached 0.8 in the first 5s then it is reached 0.9 at 6s where the uplift began to occur. After that, there was no significant increase in the EPWPR until the end of the earthquake. This trend is compatible with the increase in the energy flux ratio of the earthquake.

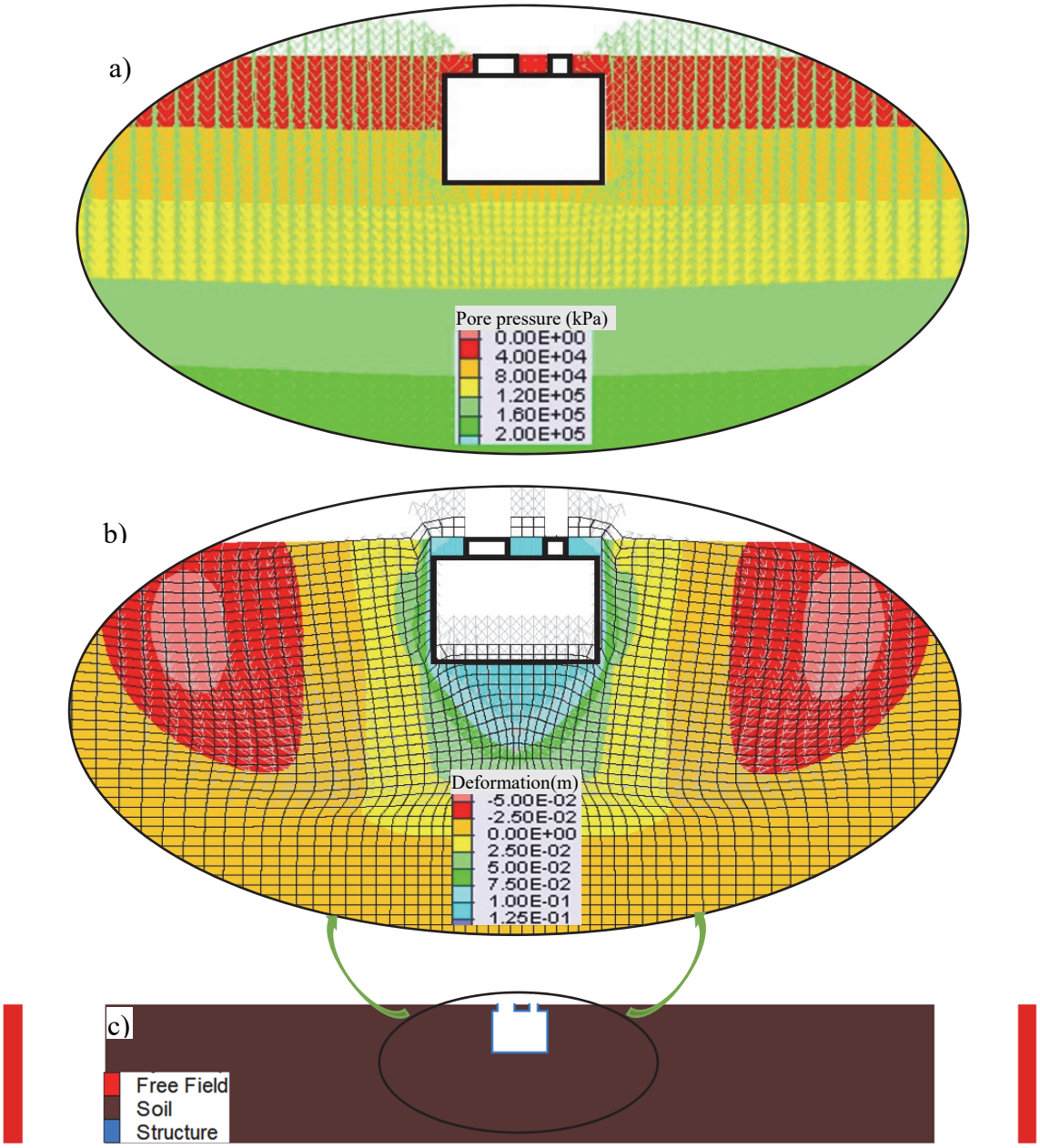

Figure 0.9 Soil liquefaction results a) water flow to the surface b) structure uplift and settlement of surrounding surface.

5.3.2. Uplift behavior

One of the most serious kinds of damage resulting from soil liquefaction is underground structures uplift due to increased pore pressure. Figure 5.10b shows the time histories of the

structure uplift and surrounding ground settlement for this study. When the buried structure is moving up the backfill soil starts flowing from beside the structure to beneath the structure which leads to structure uplift and settlement of the surrounding soil which is compatible with previous studies (Liu and Song, 2005 & 2006; Azadi[a&b] and Hosseini, 2010; Azadi, 2011; Kang et al., 2014). Also, it is clear that soil deformation around the structure created wide circular loops on two sides of the structure which is more clearly in Fig 5.10b. It can be seen that the structure started to uplift at about 6s, when the soil at the bottom of the structure was near liquefaction (EPWPR near 0.9), while the uplift displacement was less severe between near liquefaction and complete liquefaction (EPWPR near 1.0), occurring between approximately 6s and 10s. After that, more severe uplift occurred until the end of the earthquake (about 20s). The structure uplift did not stop after the earthquake ended but continued on, due to the upward flow of water, which is compatible with the previous results (Chian et al., 2014; Hu and Liu, 2017).

5.4. Evaluation of the different uplift mitigation methods

When the soil under structures buried near the surface is liquefied, vertical imbalance stress occurs. This imbalance is the result of the growth of excess pore water pressure beneath the underground structures and the small value of vertical effective stress in this area resulting from the small total density of the structure. Based on the above test results, two different mitigation methods against uplift were suggested. The primary technique, which depends on the reason for the excess water pressure, limits the development of excess pore water pressure under the structure by 1) installation of a layer of drain gravel around the buried structure, which decreases the excess pore water pressure underneath the structure; 2) densification of

the sandy soil surrounding the structure by compaction, which limits the increase of excess pore water pressure. The other technique relies on increasing the vertical effective stress under the structure thereby hindering structure uplift. The underground structures are prefabricated and thus not amenable to any diminution. Therefore, mitigation needs to be addressed by other methods, such as: 1) increasing the depth of the buried structure, as increasing the height of soil above the structure increases the vertical effective stress under the structure; 2) replacing the liquefiable soil layer beneath the structure with an impermeable layer (e.g. plain cement concrete or using an injection method). Various mitigation procedures have been proposed to limit structure uplift. These procedures depend on the methods previously mentioned. The structure was assumed to be buried at variable depths from the ground surface to 1m. The thickness of the surrounding drain gravel and dense sand, as well the impermeable base beneath, were suggested to be 0.25, 0.5, 0.75 and 1.0 m. In addition to this, a new method was used combining the two techniques. In this combined method, an impermeable layer beneath the structure with thickness 25 cm, plus a gravel drain around the structure with thickness 50 cm, was used to control the structure uplift. Figures 5.11 shows the water flow at the different mitigation methods. In case (a), a gravel drain was used to discharge the excess pore water pressure beneath the structure from the surrounding highly permeable drain material. In case (b), the sand deposit surrounding the structure was compacted to increase densification which decreased the generation of excess pore water pressure in this layer. In case (c), the soil layer beneath the structure was injected with concrete to make an impermeable layer so as to prevent water flow to the structure base. Finally, case (d), a combined method (drain gravel and the impermeable base) was used to take advantage of the benefits of both methods. The numerical parameters of the improved soil surround the underground structure summarized in Table 5.2.

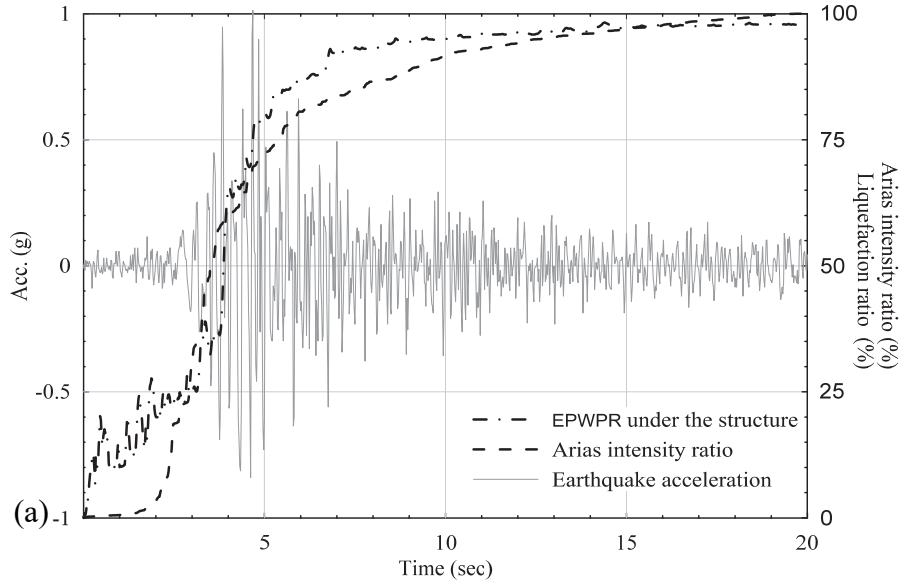

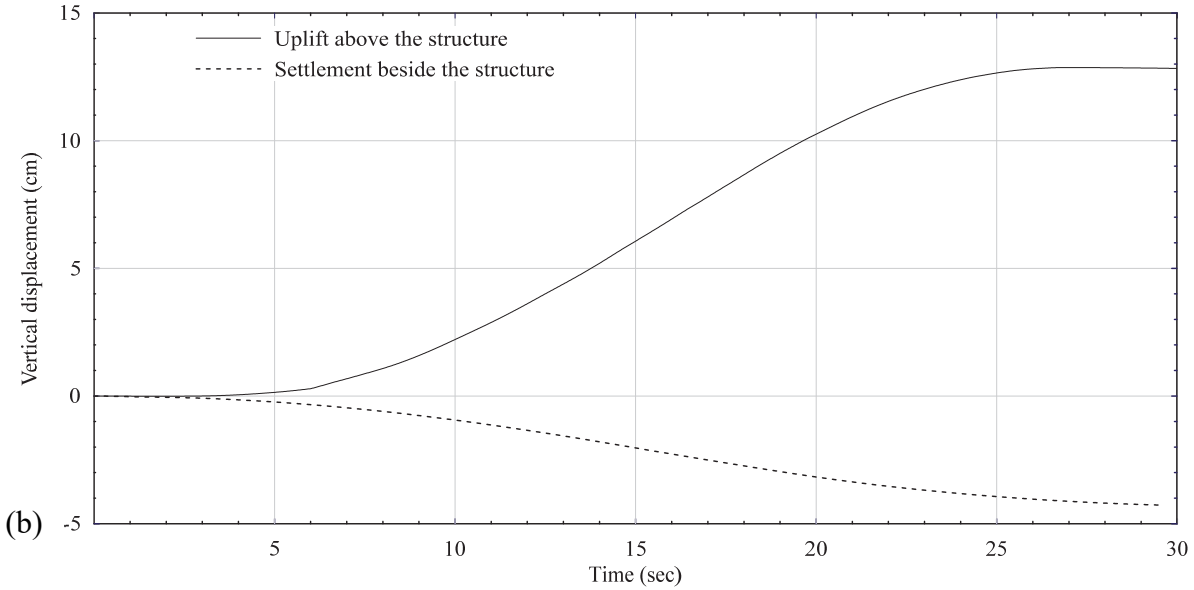

Figure 0.10 Comparison between time histories of (a) excess pore water pressure ratio under the structure in the free field and arias intensity ratio (b) structure uplift and surrounding settlement.

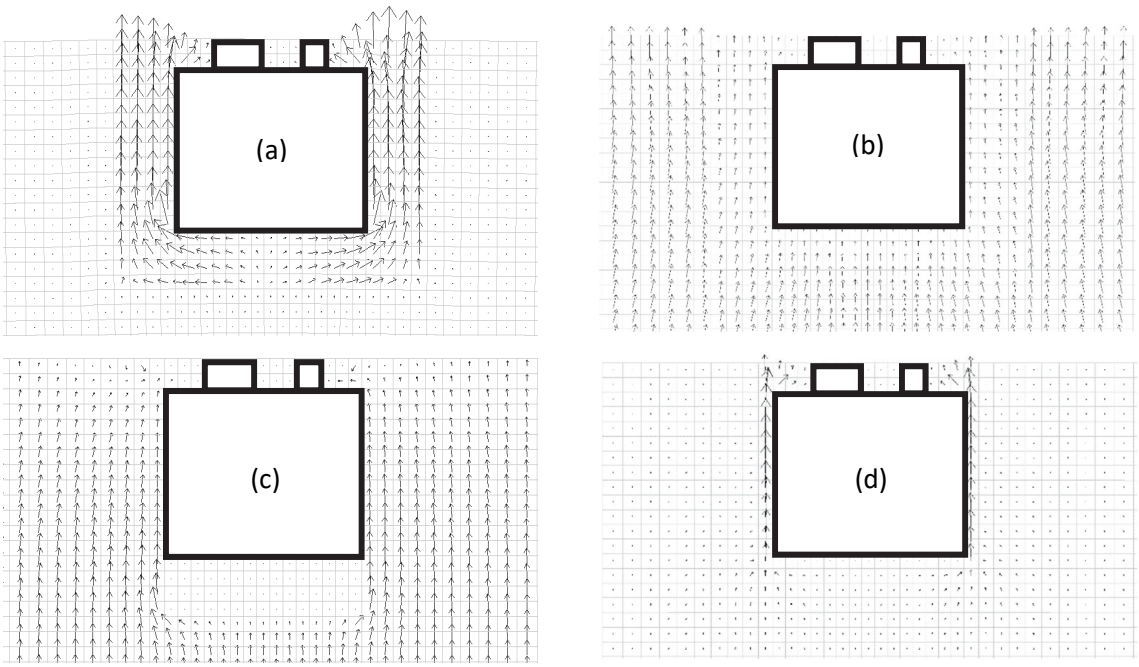

Figure 0.11 Water flow paths with the different mitigation methods: (a) gravel drain; (b) surrounding sand densification; (c) impermeable base; (d) combined method.

Table 0.2 Stabilization materials parameters used in the numerical simulation.

Parameters	Compacted sand	Gravel drain	Impermeable base
G_0 (MPa)	*75*	*150*	*4350*
K_0 (MPa)	*200*	400	*4750*
ρ_d (kg/m^3)	*1700*	*2100*	*2200*
k (m/s)	*0.5e-5*	1e-1	0
$\phi_f°$	*38*	45	-
n	*0.37*	0.25	0

5.4.1. Increasing the buried depth

Increasing the soil layer above the underground structure by increasing the buried depth is one of the most important methods for increasing the safety of structures against flotation. Fig. 5.12 shows the effect of the location of the underground structure on uplift. It can be seen that increasing the depth of the buried structure rapidly decreases the uplift. Despite the increase of excess pore water pressure under the structure with increasing buried depth, as shown in Fig. 5.12, the liquefaction ratio is reduced as a result of the rise of the effective vertical stress beneath the structure. Again, Fig. 5.15a shows that the reduction of uplift is due to a decrease in the degree of liquefaction of the soil with the increase of overburden depth. The increase in effective vertical stress works to balance the vertical stress and therefore, increase the stability of the structure.

5.4.2. Gravel drain

The comparison between the original model and the model with a gravel drain layer for excess pore water pressure ratio time histories under the structure, as well as structure uplift time histories, were utilized to highlight the effectiveness of gravel drains. According to Fig. 5.13a, there was practically no difference between the increment rate of excess pore pressure during the first 5s when the soil was close to liquefaction (EPWPR near to 0.8). After the first 5s, the excess pore water pressure started to flow out. In the case of no mitigation, the structure began to uplift. However, in the case where drain gravel was employed, the excess pore water pressure quickly dissipated and the underground structure barely moved, as shown in Fig. 5.13b.

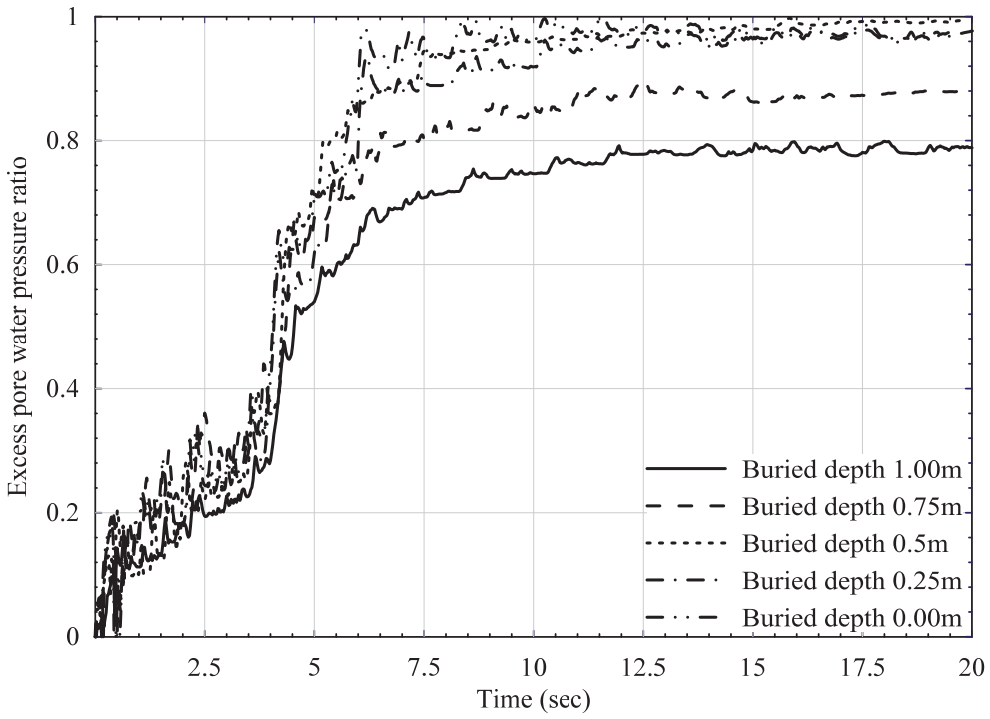

Figure 0.12 Time histories of excess pore water pressure ratio under the structure with different depths.

5.4.3. Impermeable base

The charts in Fig. 5.14 shows the variations in excess pore pressure ratio beneath the structure base at different depths (i.e. from 3.25m to 4.25m). According to Fig. 5.14, as the earthquake time progressed, it gave rise to increased pore pressure with decrease effective vertical stress. Excess pore water pressure was considerable from 2.5 to 5s, which is compatible with arias intensity during this period as shown in Fig. 5.10a. Also, it is interesting to note that the liquefaction ratio reached almost one unit in both the original base and with 0.25m base, where soil liquefaction under cyclic load had occurred, while the liquefaction ratio decreased when the impermeable base was increased.

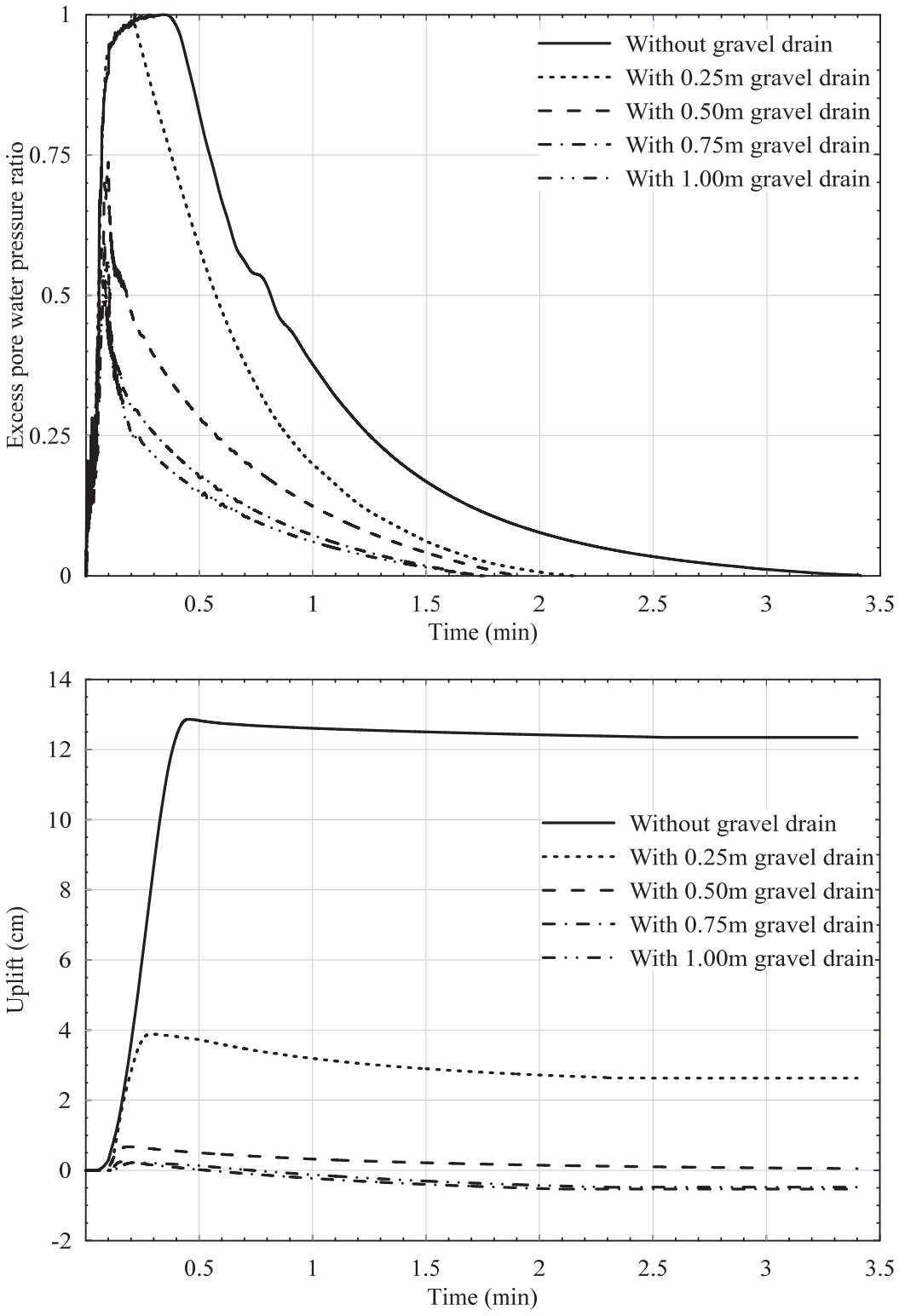

Figure 0.13 Comparison between the model with and without gravel drain (a) excess pore water pressure ratio time histories (b) uplift time histories.

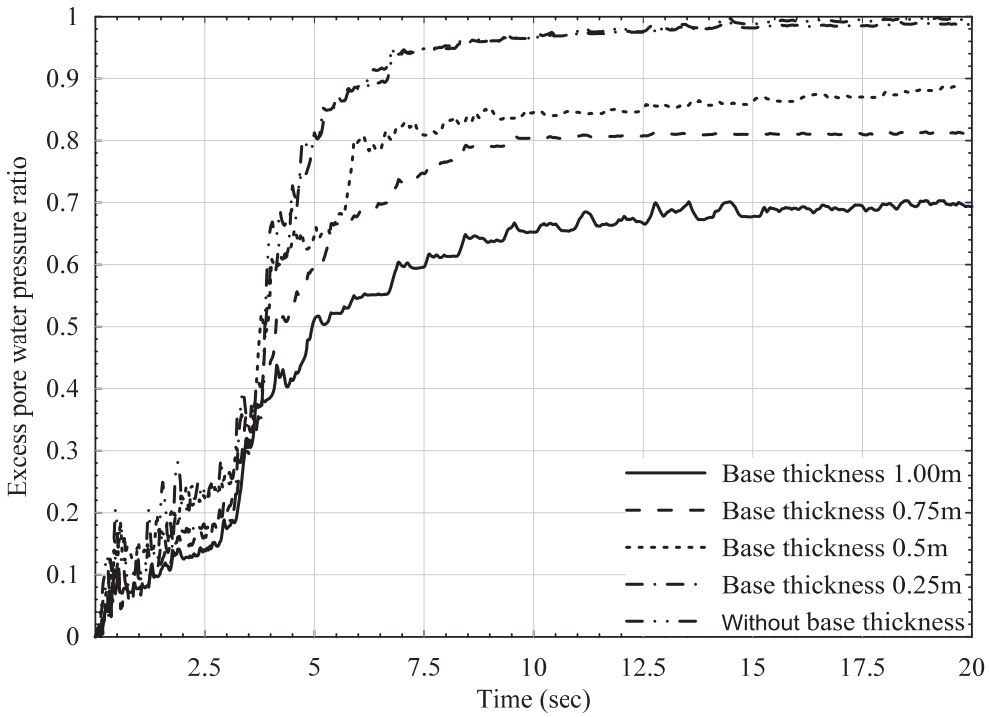

Figure 0.14 Impact of an impermeable base in the time histories of excess pore water pressure ratio under the structure.

5.4.4. Soil densification

The compaction method is the most popular and reliable in the world for preventing damage due to liquefaction. However, compacted sand deposits remain vulnerable to surrounding excess pore pressure, and therefore the drainage method is useful for increasing its resistance to liquefaction (Sasaki and Taniguchi, 1982). In this study, the mitigation method with different thicknesses of compacted sand was used to reduce structure uplift, where the thickness of compacted sand varied from 0.25 to 1 m. Fig. 5.15b shows the effect of different mitigation methods on structure uplift. It can be seen that there was a diminution of structure uplift with an increase in the thickness of the surrounding dense sand but the magnitude of decrease was small in comparison with the drain gravel and impermeable base method.

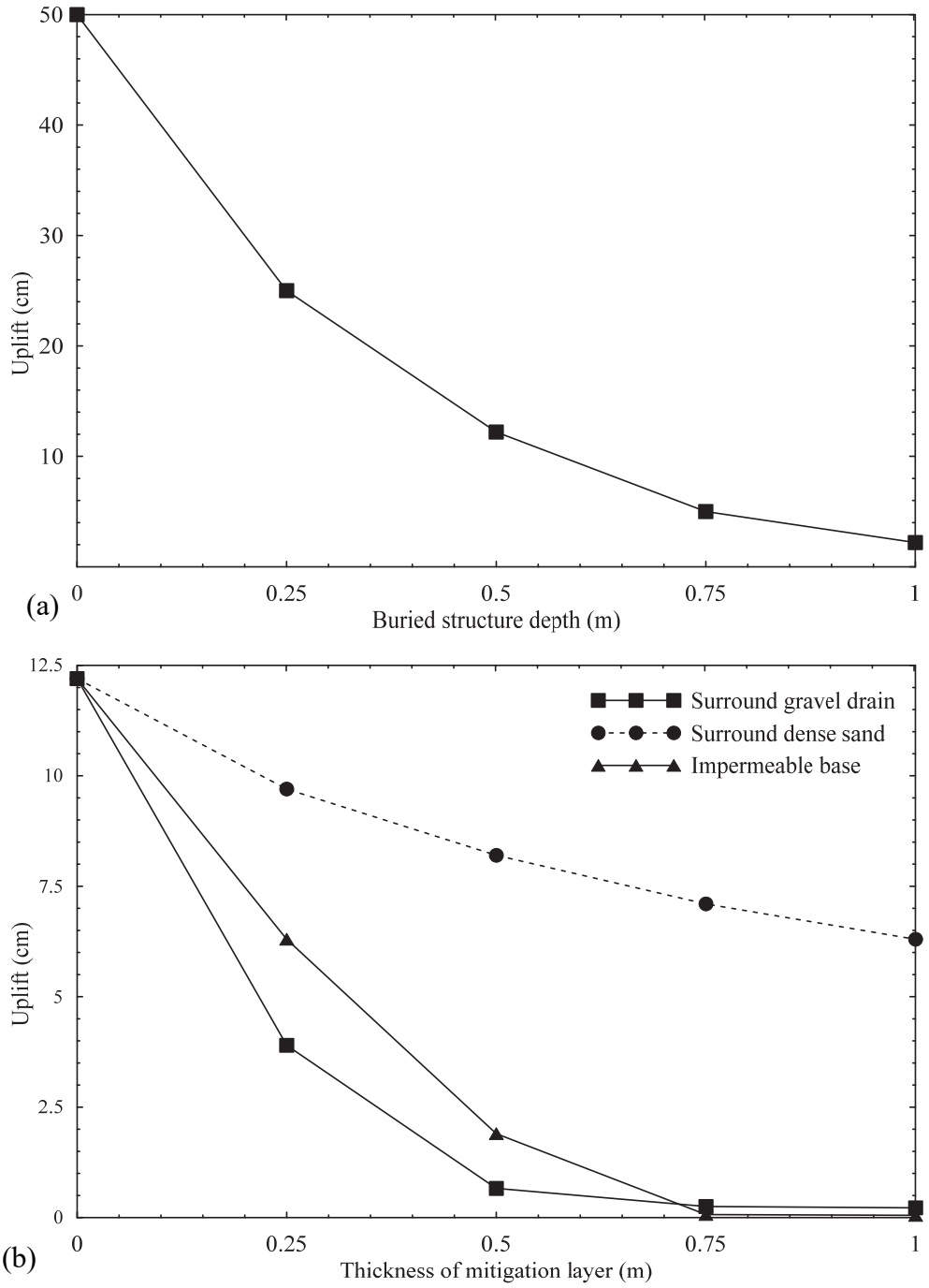

Figure 0.15 Uplift mitigation using different methods (a) change in structure uplift with buried depth (b) change in surrounding or base soil.

5.4.5. Combined method

The main reasons for liquefaction occurring in the soil beneath structures during earthquakes followed by uplift of the structure can be divided as follows: 1) generation of excess pore pressure; 2) the small value of the vertical effective stress. Previous methods attempted to solve these two dilemmas separately, which is not economical. Therefore, in this study, a combined method (by merging drain gravel and impermeable base mitigation methods) was utilized to increase the safety factor for the structure against uplift. In Fig. 5.16a, the excess pore water pressure ratio was reduced by 20% using this method, which means that the liquefaction ratio under the structure did not exceed 0.8. Also, as shown in Fig.5.16b, uplift of the structure was not observed to occur, but consolidation settlement did occur to the structure equal to the approximate amount of the surrounding soil.

Fig. 5.17 shows variations of the vertical deformation of the ground surface for the original structure and the structure with 0.5m layer thickness for the different mitigation methods and 0.25m layer thickness for the new combined method, after the termination of the earthquake. In the original structure case, it is clear that the soil over the structure showed typical uplift, while the soil near the two sides of the structure was a clear settlement. The uplift on the left side was slightly larger than the right side as the manhole on this side was larger. For the cases with mitigation methods, it was observed that the use of drain gravel and an impermeable base dramatically decreased both structure uplift and surrounding settlement but these methods do not eliminate the movement. However, when the combined method of drain gravel and an impermeable base was applied, the structure uplift completely faded.

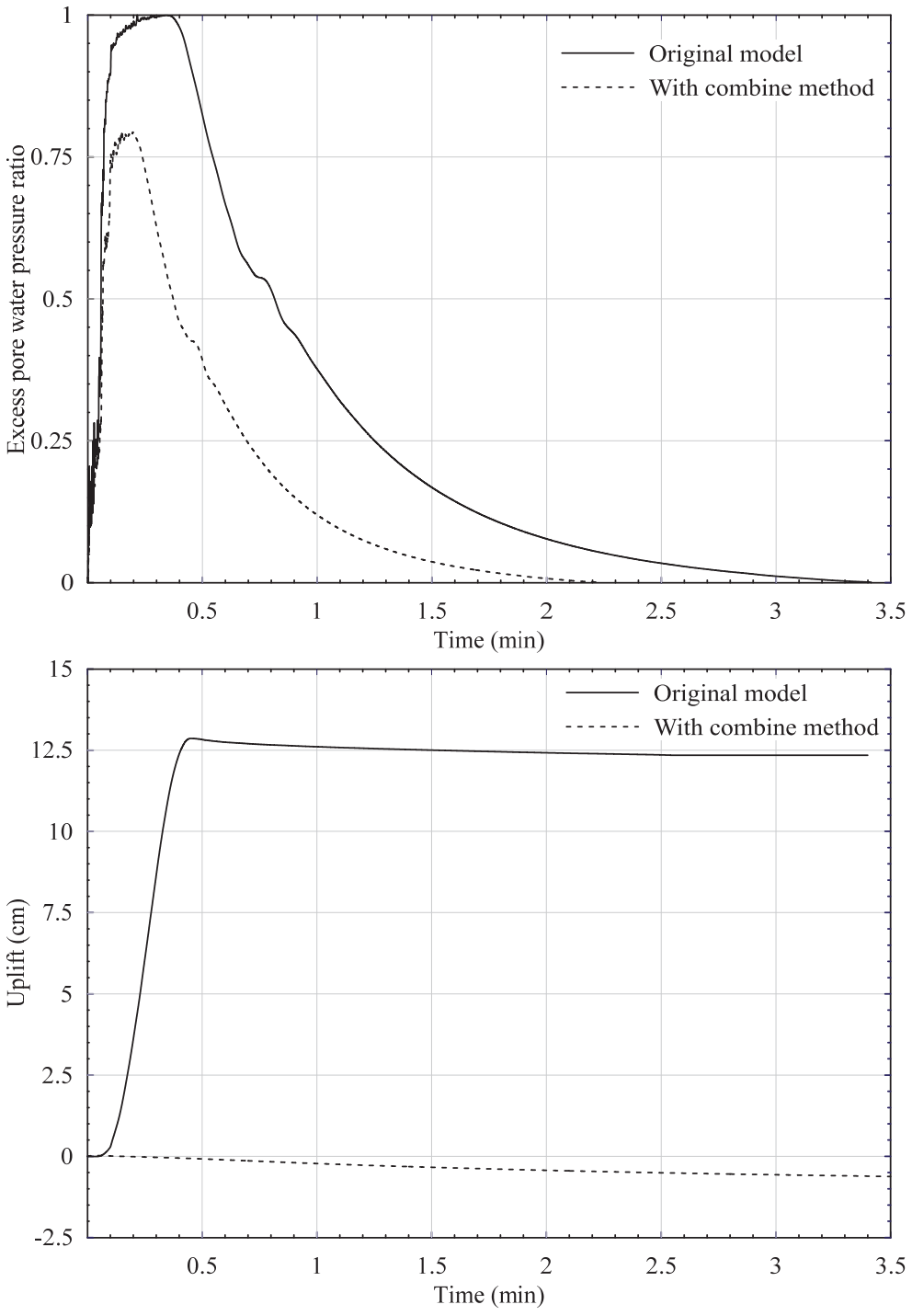

Figure 0.16 Comparison between the original model and the model with combined mitigation method for (a) excess pore water pressure ratio time histories under the structure (b) structure uplift time histories.

Whereas, the typical Hydro-Québec underground chamber uses in electrical power transmission. So, when the structure uplifts liquefaction-induced there is no water leakage occurred. Therefore, there is no limit state to make the structure off-duty. Thus, the underground structure is still serviceable. However, according to CCMTA (2014), when the structure floats, the structure appears protrusion on the ground surface (road surface) which can affect the safety and security of roadways. If the structure notch is longer than 38 mm, this could lead to hazardous conditions for the traffic. In this study, the impermeable base and drain gravel are acceptable methods for mitigating buried structure uplift, while the combined method is the idealistic method to eliminate the underground structure uplifts.

6.1. Conclusions and discussion

The seismic performance of an underground structure in saturated liquefiable soil was investigated using a new liquefaction model "energy-based approach "through a finite difference program. The energy-based model was employed to generate the excess pore water pressure ratio from the soil cyclic shear stress-strain loop under seismic loading. The liquefaction parameters were calibrated with laboratory shear tests and the constitutive model was validated with previous experimental results. The excess pore water pressure and structure uplift were analyzed and several mitigation methods against the liquefaction-induced uplift of underground structures were investigated. From the above analysis, we conclude the following:

a) Underground structures may go out of service due to uplift resulting from earthquake-induced soil liquefaction. The uplift of the structure is caused by the low shear resistance and lightweight of the structure. In addition, the excess pore water pressure beneath the structure surpasses the effective vertical stress.

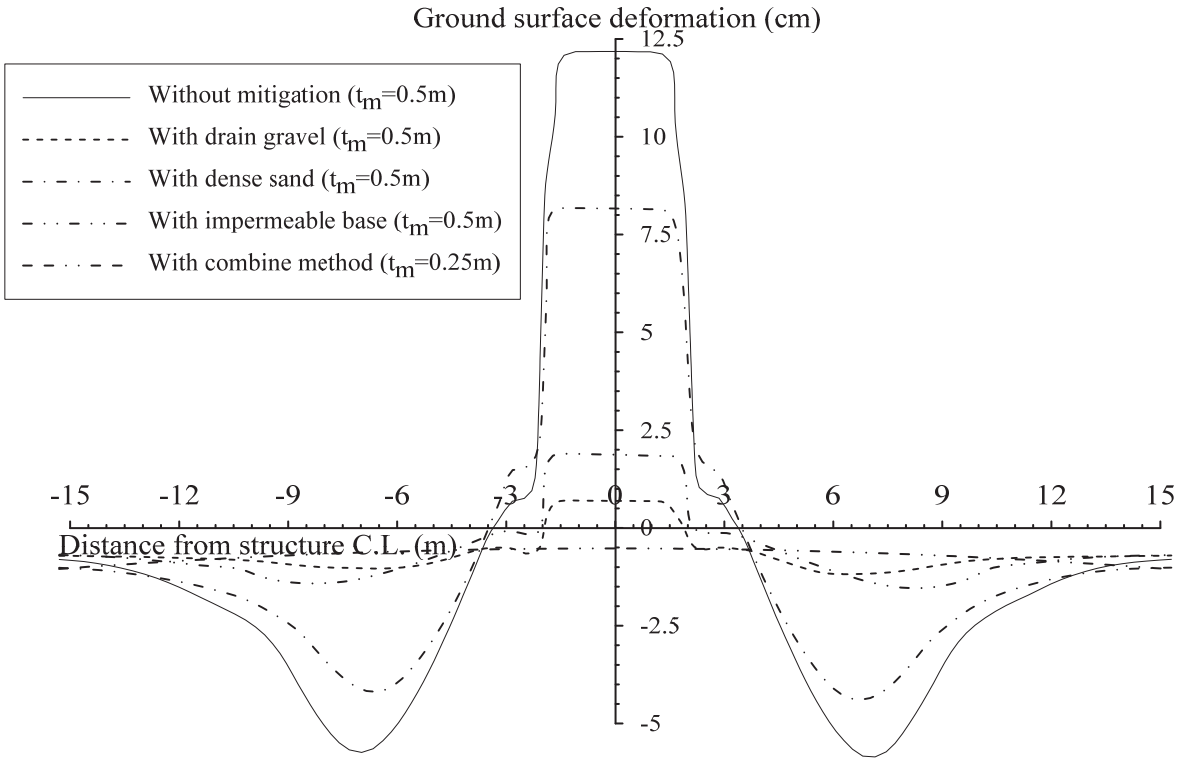

Figure 0.17 Variation in ground surface deformation for different mitigation methods.

b) Increasing the depth of the buried structure increases the safety of the structure against liquefaction due to an increase of overburden on the underground structure which raises the effective vertical stress beneath the structure and therefore reduces the liquefaction ratio.

c) The use of drain gravel around the structure and an impermeable base beneath it was an effective process to mitigate uplift. However, the sand compaction method did not achieve the desired results to ease the pressure beneath the structure and so reduce structure uplift.

d) The combination of mitigation methods (combined method) had the most influence on increasing the safety factor of the underground structure. This combination works to reduce the excess pore water pressure by dissipating it through the surrounding drain layer and increasing the corresponding vertical pressure by using the base impermeable layer, which completely eliminates structure uplift.

CHAPTER. CONCLUSIONS GÉNÉRALES ET RECOMMANDATIONS

Summary and Conclusions

This study closely examines the seismic behavior of the underground structure in liquefied soil (e.g. acceleration response, excess pore water pressure, structure uplift, and internal forces). The structure is a typical access Hydro-Quebec underground chamber which is buried in granular saturated loose soil. 2-D and 3-D numerical models have been constructed to study this phenomenon. There are many methods could be used to simulate soil liquefaction varied from simplified methods to complicated methods. In this study, the energy-based approach has been chosen to simulate the soil behavior at the liquefaction occurring. This method is characterized as a simplified and realistic method. The interface has been used to reproduce the soil-structure interaction. This study divided into two main sections. First section deals with the effect of earthquake characteristics on soil liquefaction and structure behavior resulting. In this section, the numerical model was excited with different real earthquakes compatible with the five seismic zones of Québec. Also, the structural and soil performances were investigated under three different historical earthquakes with similar durations but different frequency contents. The PGA of these earthquakes were modified to be 0.25, 0.5, and 1.0 g to study the amplitude factors. As well, two realistic field study cases have been simulated with realistic earthquake compatible with the two locations. The acceleration response, excess pore pressure, structure uplift and internal forces of underground structures have been carefully studied in this section. The following conclusions can be drawn from the numerical and analytical investigation conducted in this part of the research program:

- Soil liquefaction works on to reduce the PGA and damping the earthquake the intensity of the earthquake because the soil becomes more soften. This case becomes more visible with the increase in the excess pore water pressure ratio.

- This damping decreases the internal forces of the structure members and reduces the liquefaction occurring on the soil upper layers.
- The rise of earthquake intensity leads to an increase and decrease of the sidewalls and slab base internal forces respectively.
- The excess pore pressure ratios increase with the same earthquake's energy flux increasing trends approximately.
- The excess pore pressure ratios beneath the structure are double the value of the free field at the same level.
- Both of earthquake amplitude and frequency have an effect on the soil liquefaction and the peak ground acceleration deamplification.
- The current design internal force equations do not take in the mind the liquefaction occurring. So, the designer may want to consider a special analysis of site response for liquefiable soil sites to avoid more loads in underground structure design when liquefaction occurs.

The second section of this study focuses on finding a procedure to treat the problem related to soil liquefaction especially structure flotation. There are several different treatment methods that could be used to mitigate underground structure uplift. These methods subdivided into two main procedures. The first procedure depends on control of pore water pressure under the structure by: i) drainage of excess pore water pressure surround and beneath the structure by using drain material (gravel); ii) Compact the sandy soil around and under the structure to decrease the excess pore water pressure; iii) Soil injection under the structure; iv) Lowering the water table but this method is very expensive. On the other hand, the second procedure relies on increasing vertical stress-resistant by: i) increase the structure buried depth; increase the unit weight of the structure but, in this case, the structure has fixed dimensions. Therefore, in this study, the above methods have been used to control the effects of liquefaction occurring represented in the structure uplift. The following conclusions can be drawn from the numerical and analytical investigation conducted in this part of the research program:

- Infrastructures could be going out of service as a result of structure moving due to liquefaction occurring. The uplift of the structure is caused by the low shear resistance and lightweight of the structure. In addition, the excess pore water pressure beneath the structure surpasses the effective vertical stress.
- Increase buried depth of the underground structure increase the effective vertical stress and therefore decrease the excess pore water pressure beneath the structure
- Drain gravel around the structure and impermeable base beneath the structure work on relieving excess pore water pressure and increase the effective vertical stress under the structure so those are suitable methods to mitigate structure uplift.
- Combine between two different procedure methods works on decrease the structure movement and increase the factor of safety against uplift. The combination contains one method to reduce the excess pore water pressure and other increase the corresponding vertical pressure under the structure.

Recommendations for Future Work

Through most of the studies carried out in this Ph.D. project, some limitations have been noticed. There are many points that need to consider in the future works, for example:

1. The current study used one homogeneous layer of liquefied sandy soil. However, in fact, the underground structure exists in different types of soil liquefies (such as loose sand and silt) or non-liquefied (such as clay and dense soil). As well the soil profile is mostly different soil layers. So, it is necessary to study the effect of the different soils on the seismic behavior of the underground structure.
2. The movement of vehicles has a significant impact on the load's effect on underground structures. These loads lead to stresses that can’t be underestimated during the structure design. These stresses do not just rely on the moving loads but also the soil type greatly affects the transmission of these loads to the structure especially if the structure is near to the surface as in our case.

3. The soil used in the research was saturated sand. It would be interesting to investigate the effect of saturated and partially saturated sand.
4. The method of installing the underground structure also has important effects on the soil-structure interaction.
5. The effect of freeze-thaw cycles on the underground structures and surrounding soil and the soil-structure interaction.

Résumé et conclusions

Cette étude examine de près le comportement sismique de la structure souterraine dans un sol liquéfié (par exemple, réponse à l'accélération, pression interstitielle, soulèvement de la structure et forces internes). La structure est une chambre souterraine d'accès typique d'Hydro-Québec, enfouie dans un sol meuble, saturé et granulaire. Des modèles numériques 2D et 3D ont été construits pour étudier ce phénomène. Il existe de nombreuses méthodes pour simuler la liquéfaction du sol, allant de méthodes simplifiées à des méthodes compliquées. Dans cette étude, l'approche à base d'énergie a été choisie pour simuler le comportement du sol lors de la liquéfaction en cours. Cette méthode est caractérisée comme une méthode simplifiée et réaliste. L'interface a été utilisée pour reproduire l'interaction sol-structure. Cette étude est divisée en deux parties principales. La première section traite de l'effet des caractéristiques sismiques sur la liquéfaction du sol et du comportement de la structure qui en résulte. Dans cette section, le modèle numérique était excité par différents tremblements de terre réels compatibles avec les cinq zones sismiques du Québec. En outre, les performances de la structure et du sol ont été étudiées sous trois différents séismes historiques de durées similaires, mais avec des contenus de fréquence différents. Les PGA de ces séismes ont été modifiés pour atteindre 0,5, 1,0 et 1,5 g afin d'étudier le facteur d'amplitude. De même, deux études de terrain réalistes ont été simulées avec un séisme réaliste compatible avec les deux sites. La réponse à l'accélération, pression interstitielle, le soulèvement de la structure et les forces internes des structures souterraines ont été soigneusement étudiés dans cette section. Les conclusions suivantes peuvent être tirées des analyses numériques et analytiques menées dans cette partie du programme de recherche:

- La liquéfaction du sol contribue à réduire le PGA et à atténuer l'intensité du séisme, car le sol devient plus ramolli. Ce cas devient plus visible avec l'augmentation du rapport de pression interstitielle.
- Cet amortissement diminue les efforts internes des éléments de la structure et réduit la liquéfaction se produisant sur les couches supérieures du sol.

- L'augmentation de l'intensité des tremblements de terre entraîne une augmentation et une diminution des forces internes des paroi latérale et de la base de la dalle, respectivement.
- Les ratios de pression interstitielle augmentent avec la hausse du flux énergétique du même séisme.
- Les ratios de pression interstitielle sous la structure sont le double de la valeur du champ libre au même niveau.
- L'amplitude et la fréquence des séismes ont un effet sur la liquéfaction du sol et sur la deamplification maximale de l'accélération du sol.
- Les équations de force interne de conception actuelles ne prennent pas en compte la liquéfaction en cours. Le concepteur peut donc envisager une analyse spéciale de la réponse du site pour les sites de sol liquéfiables afin d'éviter des charges supplémentaires lors de la conception de structures souterraines lors de la liquéfaction.

La deuxième partie de cette étude se concentre sur la recherche d'une procédure permettant de traiter le problème lié à la liquéfaction du sol, en particulier la flottation de la structure. Plusieurs méthodes de traitement différentes pourraient être utilisées pour atténuer le soulèvement de la structure souterraine. Ces méthodes sont subdivisées en deux procédures principales. La première procédure dépend du contrôle de la pression d'eau interstitielle sous la structure par: i) le drainage de la pression d'eau interstitielle autour et sous la structure en utilisant un matériau de drainage (gravier); ii) Compacter le sol sableux autour et sous la structure pour diminuer l'excès de pression interstitielle; iii) injection de sol sous la structure ; iv) Abaissement de la nappe phréatique mais cette méthode est très coûteuse. D'autre part, la deuxième procédure consiste à augmenter la résistance verticale aux contraintes verticales: i) en augmentant la profondeur de la structure enterrée; augmenter le poids unitaire de la structure mais, dans ce cas, la structure a des dimensions fixes. Par conséquent, dans cette étude, les méthodes ci-dessus ont été utilisées pour contrôler les effets de la liquéfaction survenant représentée dans le soulèvement de la structure. Les conclusions suivantes peuvent être tirées des analyses numériques et analytiques menées dans cette partie du programme de recherche:

- Les infrastructures pourraient être mises hors service à la suite du déplacement de la structure en raison de la liquéfaction. Le soulèvement de la structure est dû à la faible résistance au cisaillement et à la légèreté de la structure. En outre, la pression interstitielle sous la structure dépasse la contrainte verticale effective.
- Augmenter la profondeur enterrée de la structure souterraine augmenter la contrainte verticale effective et donc diminuer l'excès de pression interstitielle sous la structure
- Le drainage du gravier autour de la structure et de la base imperméable sous la structure permet de réduire l'excès de pression interstitielle et d'augmenter la contrainte verticale effective sous la structure. Ce sont donc des méthodes appropriées pour atténuer le soulèvement de la structure.
- Combiner deux méthodes différentes pour réduire le mouvement de la structure et augmenter le facteur de sécurité contre le soulèvement. La combinaison contient une méthode pour réduire l'excès de interstitielle et une autre pour augmenter la pression verticale correspondante sous la structure.

Recommandations pour des Travaux Futurs

À travers la plupart des études menées dans ce projet de doctorat, des limitations ont été constatées. De nombreux points doivent être pris en compte dans les travaux futurs, par exemple:

1. La présente étude utilise une couche homogène de sol sableux liquéfié. Cependant, en réalité, la structure souterraine existe sous différents types de sol liquéfiés (tels que le sable et le limon) ou non liquéfiés (tels que l'argile et les sols denses). De plus, le profil du sol est constitué principalement de couches de sol différentes. Il est donc nécessaire d'étudier l'effet des différents sols sur le comportement sismique de la structure souterraine.

2. La circulation des véhicules a un impact significatif sur les effets de la charge sur les structures souterraines. Ces chargements entraînent des contraintes qui ne peuvent être sous-

estimées lors de la conception de la structure. Ces contraintes ne reposent pas uniquement sur les charges en mouvement, mais le type de sol également sur la transmission de ces charges à la structure, en particulier si celle-ci est proche de la surface, comme dans notre cas.

3. Le sol utilisé dans la recherche était du sable saturé. Il serait intéressant d'étudier l'effet du sable saturé et partiellement saturé.

4. La méthode d'installation de la structure souterraine a également des effets importants sur l'interaction sol-structure.

5. Effet des cycles de gel-dégel sur les structures souterraines et le sol environnant et sur l'interaction sol-structure.

REFERENCES

AASHTO 2002. Standard specification for highway bridges. American Association of State and Highway Transportation Officials.

Abuhajar[a], O., H. E. Naggar, and T. Newson. 2015. Experimental and numerical investigations of the effect of buried box culverts on earthquake excitation. Soil Dyn. Earthquake Eng. 79 (Part A): 130–148.

Abuhajar[b], O., El Naggar, H., and Newson, T. 2015. Static soil culvert interaction the effect of box culvert geometric configuration and soil properties. Computers and Geotechnics, 69: 219–239.

Abuhajar[c], O., El-Naggar, H and Newson, T. 2015. Seismic soil–culvert interaction. Canadian Geotechnical Journal, 52: 1649–1667.

Adams, J. and Basham, P. 1989. The seismicity and seismotectonics of Canada East of the Cordillera. Geoscience. Canada, 6(1): 3-16.

Adams, J. and Atkinson, G. 2003. Development of seismic hazard maps for the proposed 2005 edition of the National Building Code of Canada. Canadian Geotechnical Journal, 30: 255–271.

Andrews, D.C.A. and Martin, G.R. 2000. Criteria for liquefaction of silty soils. Proceedings of the 12th World Conference on Earthquake Engineering (12WCEE), Paper No. 0312.

Aydan, Ö., Ulusay, R., Hamada, M., and Beetham, D., 2012. Geotechnical aspects of the 2010 Darfield and 2011 Christchurch earthquakes of New Zealand and geotechnical damage to structures and lifelines. Bulletin of Engineering Geology and the Environment, 71 (4):637-662.

Azadi[a], M. and Hosseini, S.M. 2010. Analyses of the effect of seismic behavior of shallow tunnels in liquefiable grounds. Tunnelling and Underground Space Technology, 25: 543–552.

Azadi[b], M. and Hosseini, S.M. 2010. The uplifting behavior of shallow tunnels within the liquefiable soils under cyclic loadings. Tunnelling and Underground Space Technology, 25(2): 158-167.

Azadi, M. 2011. The seismic behavior of urban tunnels in soft saturated soils. Procedia Engineering, 14: 3069-3075.

Bao, X., Xia, Z., Ye, G., Fu, Y., and Su, D. 2017. Numerical analysis on the seismic behavior of a large metro subway tunnel in liquefiable ground. Tunnelling and Underground Space Technology, 66: 91-106.

Beaty, M. and Byrne, P. 1998. An effective stress model for predicting liquefaction behaviour of sand. Geotechnical Earthquake Engineering and Soil Dynamics III, ASCE Geotechnical Special Publication, 75(1):766-777.

Benmebarek, N., Benmebarek, S., and Kastner, R. 2005. Numerical Studies of Seepage Failure of Sand Within a Cofferdam. Computers and Geotechnics, 32:264-273.

Benmebarek, S., Khelifa, T., Benmebarek, N., Kastner, R. 2008. Numerical evaluation of 3D passive earth pressure coefficients for retaining wall subjected to translation. Computers and Geotechnics, 35(1):47–60.

Berrill, J.B., and Davis, R.O. 1985. Energy dissipation and seismic liquefaction of sands: revised model. Soils and Foundations, 25(2): 106–118.

Bo, M. W., Arulrajah, A., Horpibulsuk, S., Leong, M., and Disfani, M. M. 2014. Densification of land reclamation sands by deep vibratory compaction. Journal of Materials in Civil Engineering, 26(8): 06014016.

Booker, J.R., Rahman, M.S., and Seed, H.B. 1976. GADFLEA – A Computer Program for the Analysis of Pore Pressure Generation and Dissipation During Cyclic or Earthquake Loading. EERC 76-24, University of California, Berkeley.

Borja, R. I., and Amies, A. P. 1994. Multiaxial cyclic plasticity model for clays. Journal of Geotechnical Engineering, ASCE, 120(6), 1051-1070.

Boulanger, R.W. and Idriss, I.M. 2006. Liquefaction susceptibility criteria for silts and clays. Journal of Geotechnical and Geoenvironmental Engineering. 132 (11): 1413-1426.

Bray, J.D. and Sancio, R.B. 2006. Assessment of the liquefaction susceptibility of fine-grained soils. Journal of Geotechnical and Geoenvironmental Engineering. 132 (9): 1165-1177.

Broere, W. 2016. Urban underground space: Solving the problems of today's cities. Tunnelling and Underground Space Technology, 55: 245-48.

Byrne, P. M. 1991. A model for predicting liquefaction induced displacement. The Second International Conference on Recent Advances in Geotechnical Earthquake Engineering and Soil Dynamics, St. Louis, Missouri, 2: 1027-1035.

Byrne, P.M., Park, S.S., Beaty, M., Sharp, M., Gonzalez, L., and Abdoun. T. 2004. Numerical modelling of liquefaction and comparison with centrifuge tests. Canadian Geotechnical Journal, 41(2): 193-211.

Cassidy, J.F., Rogers, G.C., Lamontagne, M., Halchuk, S., and Adams, J. 2010. Canada's Earthquakes: "The Good, the Bad, and the Ugly". Geoscience Canada, 37(1): 1-16.

Castiglia, M., Morgante, S., Napolitano, A., and Santucci de Magistris, F. 2017. Mitigation measures for the stability of pipelines in liquefiable soils, The Journal of Pipeline Engineering, 16(3):115–139.

CCMTA 2014. Canadian Council of Motor Transport Administrators. Maintenance and Periodic Inspection Standards. National Safety Code Standard 11.

Chang, W.J., Rathje, E.M., Stokoe, K.H., and Hazirbaba, K. 2007. In situ pore pressure generation behavior of liquefiable sand. Journal of Geotechnical and Geoenvironmental Engineering, 133(8): 921-931.

CHBDC 2014. Canadian Highway Bridge Design Code, Canadian Standards Association. CAN/CSA-S6-14, Mississauga, Ontario.

Chekired, M., Lemire, R., Karray, M., and Hussien, M.N. 2015. Experiment setup for simple shear tests in a triaxial cell: TxSS. 68th Canadian Geotechnical International Conference, Quebec, Canada.

Chen, S., Zhuang, H, Quan, D., Yuan, J., Zhao, K., and Ruan, B. 2019. Shaking table test on the seismic response of large-scale subway station in a loess site: A case study. Soil Dynamics and Earthquake Engineering, 123: 173-184.

Cheuk, C.Y., White, D.J., and Bolton, M.D. 2008. Uplift Mechanisms of Pipes Buried in Sand. Journal of Geotechnical and Geoenvironmental Engineering, 134:154-163.

Chian, S.C. and Tokimatsu, K. 2012. Floatation of Underground Structures during the Mw9.0 Tōhoku Earthquake of 11th March 2011. The 15th World Conference on Earthquake Engineering, in Lisbon, Portugal.

Chian, S.C., Tokimatsu, K., and Madabhushi, S. P. G. 2014. Soil liquefaction–induced uplift of underground structures: physical and numerical modelling. Journal of Geotechnical and Geoenvironmental Engineering, 140(10): 04014057.

Chou, J. C., Kutter, B. L., Travasarou, T., and Chacko, J. M. 2011. Centrifuge modelling of seismically induced uplift for the BART Transbay tube. Journal of Geotechnical and Geoenvironmental Engineering, 137:754-765.

CSCE 2003. Canadian Society of Civil Engineering. Civil infrastructure systems technology road map 2003-2013.

Cubrinovski, M. and Ishihara, K. 2001. Correlation between penetration resistance and relative density of sandy soil. Proceedings of the 15th international conference on soil mechanics and geotechnical engineering, Istanbul, Turkey, 15: 393-396.

Cubrinovski, M., Green, R., Allen, J., Ashford, S., Bowman, E., Bradley, B., Cox, B., Hutchinson, T., Kavazanjian, E., Orense, R., Pender, M., Quigley, M., Wilson, and Wotherspoon, L. 2010. Geotechnical reconnaissance of the 2010 Darfield (New Zealand) earthquake. Bulletin New Zealand Society Earthquake Engineering, 43(4):243-320.

Davis, R.O. and Berrill, J.B. 1982. Energy dissipation and seismic liquefaction in sands. Earthquake Engineering and Structural Dynamics, 10(1): 59-68.

DesRoches, R., Comerio, M., Eberhard, M., Mooney, W., and Rix, G. 2011. Overview of the 2010 Haiti earthquake. Earthquake Spectra, 27(S1): S1-S21.

Do, N.A., Dias, D., Oreste, P., Djeran-Maigre, I. 2015. Behaviour of segmental tunnel linings under seismic loads studied with the hyperstatic reaction method. Soil Dynamic and Earthquake Engineering, 79:108-117.

Dobry, R., Ladd, R. S., Yokel, F. Y., Chung, R. M., and Powell, D. 1982. Prediction of pore water pressure buildup and liquefaction of sand during earthquakes by the cyclic strain method. Building Science Series 138, National Bureau of Standards, Washington, D.C.

El Mohtar, C. S., Drnevich, V. P., Santagata, M., and Bobet, A. 2013. Combined resonant column and cyclic triaxial tests for measuring undrained shear modulus reduction of sand with plastic fines. Geotechnical Testing Journal, 36(4):484-492.

Esfeh, P.K., and Kaynia, A.M. 2019. Numerical modelling of liquefaction and its impact on anchor piles for floating offshore structures. Soil Dynamic and Earthquake Engineering, 127:105839.

Figueroa, J.L., Saada, A.S., Liang, L., and Dahisaria, N.M. 1994. Evaluation of soil liquefaction by energy principles. Journal of Geotechnical Engineering, 120(9):1554-1569.

Gazetas, G. 1984. Seismic response of end-bearing single piles. Soil Dynamic and Earthquake Engineering, 3(2):82-93.

Gazetas, G., Gerolymos, N., and Anastasopoulos, I. 2005. Response of three Athens metro underground structures in the 1999 Parnitha earthquake. Soil Dynamics and Earthquake Engineering, 25: 617-633.

Gong, W., Martin, J.R., Juang, C.H., Dickenson, S.E., and McCullough, N.J. 2019. A hybrid framework for developing empirical model for seismic deformations of anchored sheetpile bulkheads. Soil Dynamic and Earthquake Engineering, 116:192-204.

Green, R.A. 2001. Energy-based evaluation and remediation of liquefiable soils. Ph.D. thesis, Civil Engineering Department, Virginia Polytechnical Institute and State University, Blacksburg, VA.

Green, R.A. and Ebeling, R.M. 2003. Modelling the dynamic response of cantilever earth-retaining walls using FLAC. A.A. Balkema Publishers, Sudbury, ON, Canada, 333-342.

Green, R.A. and Ziotopoulou, K. 2015. Overview of screening criteria for liquefaction triggering susceptibility. Proceedings of the 10th Pacific Conference on Earthquake Engineering, Nov 6-8, Sydney, Australia. Australian Earthquake Engineering Society, Paper No. 35.

Guérin, M. 2015. Analyse comparative entre l'armature d'acier et de polymères renforcés de fibres de verre des structures souterraines en béton armé. Ph.D. thesis, Université de Sherbrooke.

Guérin, M., Mohamed H., and Benmokrane, B. 2016. Fatigue behaviour of concrete underground chambers reinforced with GFRP bars. CSCE annual conference, STR-824:1-9.

Haiyang, Z., Xu, W., Yu, M., Erlei, Y., Su, C., Bin, R., and Guoxing, C. 2019. Seismic responses of a subway station and tunnel in a slightly inclined liquefiable ground through shaking table test. Soil Dynamics and Earthquake Engineering, 116: 371-385.

Haldar, S. and Babu, G. L. S. 2008. Effect of soil spatial variability on the response of laterally loaded pile in undrained clay. Computers and Geotechnics, 35(4):537–547.

Hardin, B.O. and Drnevich, V.P. 1972. Shear modulus and damping in soil: Measurement and parameter effects. Journal of the Soil Mechanics and Foundation Division, ASCE, 98(6): 603-624.

Hashash, Y.M.A., Hook, J.J., Schmidt, B., and Yao, J. 2001. Seismic design and analysis of underground structures. Tunnelling and Underground Space Technology, 16(4):247–93.

He, J. and Chen, W. 2011. The Numerical Experimentation of the Underground Pipeline Anti-To Float in Liquefaction Field with Gravel Draining Water Layer. International Conference on Pipelines and Trenchless Technology (ICPTT), 2011: 1771-1783.

Hsiung, B. C. B. 2009. A case study of behavior of deep excavation in sand. Computers and Geotechnics, 36(4): 665–675.

Hu, J.L. and Liu, H.B. 2017. The uplift behavior of a subway station during different degree of soil liquefaction. Procedia Engineering, 189: 18-24.

Hu, J.L., Chen, Q.H., and Liu, H.B. 2018. Relationship between earthquake-induced uplift of rectangular underground structures and the excess pore water pressure ratio in saturated sandy soils. Tunnelling and Underground Space Technology, 79: 35-51.

Huo, H. 2005. Seismic design and analysis of rectangular underground structures. Ph.D. thesis, Civil Engineering Department, Purdue University.

Hussien, M., Iai, S., and Karray, M. 2018. Analysis of characteristic frequencies of coupled soil-pile-structure systems. International Journal of geomechanics, 18(6): 04018047.

Hydro-Québec 2019. Conversion of the Underground Beaumont–Dorchester Line. Construction work and projects, https://www.hydroquebec.com/projects/beaumont-dorchester-line/documentation.html.

Iai, S., Tsuchida, H., and Koizumi, K. 1986. A new criterion for assessing liquefaction potential using grain size accumulation curve and N-value. Report of the Port and Harbour Research Institute, 25(3): 125-234.

Iai, S., Tsuchida, H., and Koizumi, K. 1989. A liquefaction criterion based on field performances around seismograph stations. Soils and Foundations, 29(2): 52-68.

Iida, H., Hiroto, T., Yoshida, N., and Iwafuji, M. 1996. Damage to Daikai subway station. Soils and Foundations, Japanese Geotechnical Society, Special issue, 283-300.

Itasca Consulting Group. 2011. FLAC: Fast lagrangian analysis of continua in 2-dimensions 7.0.424., manual. Itasca, Minneapolis.

Itasca Consulting Group. 2012. FLAC^{3D}: Fast lagrangian analysis of continua in 3-dimensions 5.01, manual. Itasca, Minneapolis.

Javadi, A.A., Rezania, M., and Mousavi Nezhad, M. 2006. Evaluation of liquefaction induced lateral displacements using genetic programming. Computers and Geotechnics, 33 (4/5): 222-33.

JGS (Japanese Geotechnical Society) 1998. Remedial measures against soil liquefaction. A.A. Balkema, Rotterdam, Netherlands.

Jung[a], J. K., O'Rourke, T. D., and Olson, N. A. 2013. Uplift soil–pipe interaction in granular soil. Canadian Geotechnical Journal, 50: 744-753.

Jung[b], J., O'Rourke, T., and Olson, N. 2013. Lateral soil-pipe interaction in dry and partially saturated sand. Journal of Geotechnical and Geoenvironmental Engineering, 139 (12): 2028-2036.

Kaiser, A., Holden, C., Beavan, J., Beetham, D., Benites, R., Celentano, A., Collett, D., Cousins, J., Cubrinovski, M., Dellow, G., Denys, P., Fielding, E., Fry, B., Gerstenberger, M., Langridge, R., Massey, C., Motagh, M., Pondard, N., McVerry, G., Ristau, J., Stirling, M., Thomas, J., Uma, SR., and Zhao, J. 2012. The Mw 6.2 Christchurch earthquake of February 2011: preliminary report. New Zealand Journal of Geology and Geophysics, 55(1): 67-90.

Kang, G., Tobita, T., Tomisaka, K., and Iai, S. 2009. Centrifuge modelling for uplift of buried structures by liquefaction: a new measure for uplift. Annuals of Disaster Prevention Research Institute, No. 52 B.

Kang, G. 2010. Assessing uplift displacement of buried geotechnical structures in liquefied ground during earthquakes. A Thesis Submitted for the Degree of Doctor of Engineering, Kyoto University.

Kang[a], G., Tobita, T., and Iai, S. 2013. Damage to sewerage systems during the 2004 Earthquake in Niigata-ken Chuetsu. Japan, Engineering Geology, 164 (2013) 230-242.

Kang[b], G., Tobita, T., Kawabata, T., Iai, S., and Ge, L. 2013. Centrifuge modelling and mitigation of manhole uplift due to liquefaction. Journal of Geotechnical and Geoenvironmental Engineering, 139:458-469.

Kang, G., Chung, J., and Iai, S. 2014. Seismic simulation of liquefaction-induced uplift behavior of a hollow cylinder structure buried in shallow ground. Soil Dynamics and Earthquake Engineering, 64: 85-94.

Karray, M., Hussien, M. and Chekired M. 2015. Evaluation of compatibility between existing liquefaction charts in Eastern regions of North America. The 68th Canadian Geotechnical Conference, Québec, Canada.

Karray, M., Hussein, M.N., Chekired, M., and Grenier, S. 2016. Effective Stress Analysis of Liquefaction Potential Using a Novel Approach Based on the Energy Concept – A Case Study. The 69th Canadian Geotechnical Conference. Vancouver, Canada.

Khoshnoudian, F. and Shahrour, I. 2002. Numerical Analysis of the Seismic Behavior of Tunnels Constructed in Liquefiable Soils. Soils and Foundations, 42(6): 1-8.

Koei, N. 2014. Countermeasures for preventing floating of sewer manholes caused by liquefaction (Float-less Method). Japan's International Engineering Consultants No.1, Tokyo, Japan.

Koester, J.P. 1992. The influence of test procedure on correlation of Atterberg Limits with liquefaction in fine grained soils. Geotechnical Testing Journal, 15(4): 352-360.

Koseki[a], J., Matsuo, O., Ninomiya, Y., and Yoshida, T. 1997. Uplift of sewer manhole during the 1993 Kushiro-Oki earthquake. Soils and Foundations, 37(1): 109-121.

Koseki[b], J., Matsuo, O., and Koga, Y. 1997. Uplift behavior of underground structures caused by liquefaction of surrounding soil during earthquake. Soils and Foundations, 37:97-108.

Kovacs, P. 2010. Reducing the risk of earthquake damage in Canada: Lessons from Haiti and Chile. The Institute for Catastrophic Loss Reduction, Toronto, Ontario, Canada.

Kramer, S. L. and Elgamal A. W. 2001. Modelling Soil Liquefaction Hazards for Performance-Based Earthquake Engineering. PEER Report 2001/13, University of California, California, USA.

Kuhlemeyer, R.L. and Lysmer, J. 1973. Finite element method accuracy for wave propagation problems. Journal of Soil Mechanics and Foundations, Div. ASCE, 99: 421-427.

Kutter, M., Chou, S., and Travasarou, A. 2008. Centrifuge Testing of the Seismic Performance of a Submerged Cut-and-Cover Tunnel in Liquefiable Soil. Geotechnical Earthquake Engineering and Soil Dynamics IV, DOI: 10.1061/40975(318)204.

Lamontagne, M., Halchuck, S., Cassidy, J.F., and Rogers, G.C. 2007. Significant Canadian Earthquakes 1600–2006. Geological Survey of Canada.

Lecomte, E., Pang A., and Russell J. 1998. La tempête de verglas de 1998, Document de recherche de l'IPSC.

Lee, J. S., Chae, H. G., Kim, D. S., Jo, S. B., and Park, H. J. (2015). Numerical analysis of inverted T-type wall under seismic loading. Computers and Geotechnics, 66: 85-95.

Li, L., and Aubertin, M. 2015. Numerical analysis of the stress distribution in backfilled trenches with inclined walls. Indian Geotechnical Journal, 45(3): 278-290.

Lin, H., Liu, T., Li, J., and Cao, P. 2013. Simple generation technique of complex geotechnical computational model. Mathematical Problems in Engineering, 2013: 1-8.

Lin, Y-L., Li, Y-X., Yang, G-L., and Li, Y. 2017. Experimental and numerical study on the seismic behavior of anchoring frame beam supporting soil slope on rock mass. Soil Dyn Earthq Eng. 98:12–23.

Ling, H., Mohri, Y., Kawabata, Y., Liu, H., Burke, C., and Sun, L. 2003. Centrifugal Modelling of Seismic Behavior of Large-Diameter Pipe in Liquefiable Soil. Journal of Geotechnical and Geoenvironmental Engineering, 129: 1092-1101.

Liu, H. and Song, E. 2005. Seismic response of large underground structures in liquefiable soils subjected to horizontal and vertical earthquake excitations. Computers and Geotechnic, 32: 223-244.

Liu, H. and Song, E. 2006. Working mechanism of cutoff walls in reducing uplift of large underground structures induced by soil liquefaction. Computers and Geotechnic, 33: 209–221.

Lu, Y., Wang, Z., and Chong K. 2005. A comparative study of buried structure in soil subjected to blast load using 2D and 3D numerical simulations. Soil Dynamics and Earthquake Engineering, 25: 275-288.

Lu, Y., Marshall, A.M., and Hajirasouliha I. 2016. A simplified nonlinear sway-rocking model for evaluation of seismic response of structures on shallow foundations. Soil Dyn Earthq Eng, 81:14-26.

Macaulay, D. 1976. Underground. Boston: Houghton Mifflin Company.

Mahmoud[a], A., Hussien, M., Karray, M., Chekired, M., Bessette, C., and Jinga, L. 2020. Implementation of the energy-based approach as a soil constitutive model in seismic analyses of underground structures. Tunnelling and Underground Space Technology, in processing.

Mahmoud[b], A., Hussien, M., Karray, M., Chekired, M., Bessette, C., and Jinga, L. 2020. Mitigation of liquefaction-induced uplift of underground structures. Computer and Geotechnics, in processing.

Marcuson, W.F., Hynes, M.E., and Franklin, A.G. 1990. Evaluation and use of residual strength in seismic safety analysis of embankments. Earthquake Spectra. 6(3): 529-572.

Marsh, J. H. 2001. The Canadian encyclopedia. Hurtig Publishers, Edmonton, AB, Canada.

Martin, G.R., Finn, W.D.L., and Seed, H.B. 1975. Fundamentals of liquefaction under cyclic loading. Journal of the Geotechnical Engineering Division, ASCE, 101(5): 423-439.

Matasovic, N. and Vucetic, M. 1993. Cyclic characterization of liquefiable sands. Journal of Geotechnical and Geoenvironmental Engineering, 119(11): 1805–1822.

Mitchell, D., Tinawi, R., and Law, T. 1990. Damage caused by the November 25, 1998 Saguenay earthquake. Canadian Geotechnical Journal, 17(3): 338–365.

Mortazavi, A, and Alavi, F.T. 2013. A numerical study of the behavior of fully grouted rockbolts under dynamic loading. Soil Dynamics and Earthquake Engineering. 54: 66-72.

Moss, R.E.S. and Chen, G. 2008. Comparing liquefaction procedures in the U.S. and China. Proceedings of the 14th World Conference on Earthquake Engineering. Beijing, China, October 12-17.

Naesgaard, E. 2011. A hybrid effective stress – total stress procedure for analyzing soil embankments subjected to potential liquefaction and flow. Ph.D. thesis, Civil Engineering Department, The University of British Columbia, Vancouver, Canada.

Natural Resources Canada, 2015. Simplified seismic hazard map for Canada. Available at: (http://www.seismescanada.rncan.gc.ca/hazard-alea/simphaz-en.php).

Nemat-Nasser, S. and Shokooh, A. 1979. A unified approach to densification and liquefaction of cohesionless sand in cyclic shearing. Canadian Geotechnical Journal, 16(4): 659-678.

Oral, S. 2014. Effective Stress Based Constitutive Modelling and Assessment of Seismic Pile-Soil Interaction in Liquefiable Soils. Ph.D. Thesis. Orta Doğu Teknik Üniversitesi, Ankara.

Orense, P., Morimoto, I., Yamamoto, Y., Yumiyama, T., and Yamamoto, K. 2003. Sugawara Study on wall-type gravel drains as liquefaction countermeasure for underground structures. Soil Dynamics and Earthquake Engineering, 23(1): 19-39.

Orense, R. P. 2005. Assessment of liquefaction potential based on peak ground motion parameters. Soil Dynamics and Earthquake Engineering. 25(3): 225-240.

Osouli A., and Zamiran S. 2017. The effect of backfill cohesion on seismic response of cantilever retaining walls using fully dynamic analysis. Computer and Geotechnics, 89:143–152.

Otsubo[a], M., Goto, S., Akima, T., and Hayashida, T. 2016. Practical application of mitigation measures for existing underground lifelines subjected to liquefaction. Japanese Geotechnical Society Special Publication, 2(22): 835-839.

Otsubo[b], M., Towhata, I., Hayashida, T., Shimura, M., Uchimura, T., Liu, B., Taeseri, D., Cauvin, B., and Rattez, H. 2016. Shaking table tests on mitigation of liquefaction vulnerability for existing embedded lifelines. Soils and Foundations, 56(3): 348-364.

Palmeira, E. M., and Andrade, H. K. P. A. 2010. Protection of buried pipes against accidental damage using geosynthetics. Geosynth. Int., 17(4): 228-241.

Palmeira, E.M., Bernal, D.F. 2015. Uplift resistance of buried pipes anchored with geosynthetics. Geosynth Int, 22:149-160.

Paramasivam, B., Dashti, S., and Liel, A. 2019. Impact of Spatial Variations in Permeability of Liquefiable Deposits on Seismic Performance of Structures and Effectiveness of Drains. Journal of Geotechnical and Geoenvironmental Engineering, 145(8): 04019030.

Polito, C., Green, R.A., Dillon, E., and Sohn, C. 2013. Effect of load shape on relationship between dissipated energy and residual excess pore pressure generation in cyclic triaxial tests. Canadian Geotechnical Journal, 50:1118-1128.

Potter, S.H., Becker, J.S., Johnston, D.M., and Rossiter, K.P. 2015. An overview of the impacts of the 2010-2011 Canterbury earthquakes. International Journal of Disaster Risk Reduction 14: 6–14.

Puebla, H., Byrne, M., and Phillips, P. 1997. Analysis of complex liquefaction embankments prototype and centrifuge models. Canadian Geotechnical Journal, 34:641–657.

Qiao, L., Yuan, C., Miyajima, M., and Zhai, E. 2008. Shake-Table Testing and FLAC Modelling of Liquefaction-Induced Slope Failure and Damage to Buried Pipelines. Geotechnical Earthquake Engineering and Soil Dynamics IV: 1-10.

Rasouli, R., Towhata, I., and Hayashida, T. 2015. Mitigation of seismic settlement of light surface structures by installation of sheet-pile walls around the foundation. Soil Dynamic and Earthquake Engineering, 72:108-118.

Rasouli, R., I. Towhata, and T. Akima. 2016. Experimental evaluation of drainage pipes as a mitigation against liquefaction-induced settlement of structures. Journal of Geotechnical and Geoenvironmental Engineering, 142(9): 04016041.

Rayhani, M. H. T. and El Naggar, M. H. 2008. Numerical Modelling of Seismic Response of Rigid Foundation on Soft Soil. International Journal of Geomechanics, 8(6):336–346.

Robertson, P.K. and Wride, C.E. 1998. Evaluating cyclic liquefaction potential using the cone penetration test. Canadian Geotechnical Journal, 35(3): 442–459.

Saeedzadeh, R. and Hataf, N. 2011. Uplift response of buried pipelines in saturated sand deposit under earthquake loading. Soil Dynamics and Earthquake Engineering, 31(10): 1378–1384.

Sasaki, Y. and Taniguchi, E. 1982. Shaking table tests on gravel drains to prevent liquefaction of sand deposits. Soils and Foundations, 22(3): 1-14.

Sasaki, T. and Tamura, K. 2004. Prediction of liquefaction-induced uplift displacement of underground structures, 36th Joint Meeting US-Japan Panel on Wind and Seismic Effects, 36: 191-198.

Sassa, S. and Takagawa, T. 2019. Liquefied gravity flow-induced tsunami: First evidence and comparison from the 2018 Indonesia Sulawesi earthquake and tsunami disasters. Landslides, 16(1): 195-200.

Seed, H. B. and Idriss, I. M. 1970. Soil moduli and damping factors for dynamic response analyses. Report No. EERC 70-10, Earthquake Engineering Research Center, Univ. of California, Berkeley, California.

Seed, H. B. and Idriss, I. M. 1971. Simplified procedure for evaluating soil liquefaction potential. Journal of the Geotechnical Engineering Division, ASCE, 97(9): 1249–1273.

Seed[a], H. B., Idriss, I. M., Makdisi, F., and Banerjee, N. 1975. Representation of irregular stress time histories by equivalent uniform stress series in liquefaction analyses. Rep. No. UCB/EERC 75-29, Earthquake Engrg. Res. Ctr., University of California, Berkeley, Calif.

Seed[b], H.B., Martin, P. P., and Lysmer, J. 1975. The generation and dissipation of pore water pressures during soil liquefaction. Earthquake Engineering Research Center, University of California, Berkeley, Report No. EERC 75-26.

Seed, H. and Idriss, I. 1982. Ground motions and soil liquefaction during earthquakes: engineering monographs on earthquake criteria, structural design, and strong motion records. MNO-5, Earthquake Engineering Research Institute, Oakland, California.

Seed, H. B., Idriss, I. M., and Arango, I. 1983. Evaluation of liquefaction potential using field performance data. Journal of Geotechnical and Geoenvironmental Engineering, ASCE, 109(3): 458-482.

Seed, H. B., Tokimatsu, K., Harder, L. F., and Chung, R. M. 1985. The influence of SPT procedures in soil liquefaction resistance evaluations. Journal of Geotechnical and Geoenvironmental Engineering., ASCE, 111(12): 1425-1445.

Seed, R B., Cetin, K.O., Moss, R.E.S., Kammerer, A., Wu, J., Pestana, J., Riemer, M., Sancio, R.B., Bray, J.D., Kayen, R.E., and Faris, A. 2003. Recent advances in soil liquefaction engineering: a unified and consistent framework. Keynote presentation, 26th Annual ASCE Los Angeles Geotechnical Spring Seminar, Long Beach, CA.

Sharaf, H., and Maleki, Y.S. 2019. Evaluation of the lateral displacements of a sandy slope reinforced by a row of floating piles: A numerical-experimental approach. Soil Dyn Earthq Eng. 122:148-170.

Shirahama, Y., Yoshimi, M., Awata, Y., Maruyama, T., Azuma, T., Miyashita, Y., Mori, H., Imanishi, K., Takeda, N., Ochi, T., Otsubo, M., Asahina, D., and Miyakawa, A. 2016. Characteristics of the surface ruptures associated with the 2016 Kumamoto earthquake sequence. central Kyushu, Japan. Earth Planets Space, 68:191.

Sun, Q., and Dais, D. 2019. Seismic behavior of circular tunnels: Influence of the initial stress state. Soil Dyn Earthq Eng. 126:105808.

Sun[a], Q. and Dias, D., and Sousa L. 2019. Impact of an underlying soft soil layer on tunnel lining in seismic conditions. Tunnelling and Underground Space Technology, 90: 293–308.

Sun[b], Q., Dias, D., Guo, X., and Li, P. 2019. Numerical study on the effect of a subway station on the surface ground motion. Computers and Geotechnics, 111:243-254.

Sunitsakul, J. Dynamic Behavior of Silty Soils, Oregon State University, Corvallis (2004).

Tanaka, H., Kita, H., Iida, T., Saimura, Y. 1995. Countermeasure against liquefaction for buried structures using sheet pile with drain capacity. Earthquake geotechnical engineering. Rotterdam, The Netherlands: Balkema, 999-1004.

Technical Committee on Earthquake Resistant Design of Sewage Lifelines, 2004. Urgent Proposal for Reconstruction of Sewage Lifelines. Committee Report. (in Japanese).

Technical Committee on Earthquake Resistant Design of Sewage Lifelines, 2008. Earthquake Resistant Design of Sewage Lifelines. Committee Report. (in Japanese).

Tobita, T., Iai, S., Kang, G., Konishi, Y., and Harazono, S. 2008. Simplified method for estimation of the maximum uplift displacement of a manhole during earthquakes, Journal of applied mechanics, 11: 587-594.

Tobita, T., Kang, G., and Iai, S. 2011. Centrifuge modelling on manhole uplift in a liquefied trench. Soils and Foundations, 51(6):1091-1102.

Tobita, T., Kang, G., and Iai, S. 2012. Estimation of liquefaction induced manhole uplift displacements and trench-backfill settlements. Journal of Geotechnical and Geoenvironmental Engineering, 138(11): 491-499.

Tokimatsu, K., Tamura, S., Suzuki, H., and Katsumata, K. 2011. Quick report on geotechnical problems in the 2011 Tohoku Pacific Ocean Earthquake. Technical Report, Center for Urban Earthquake Engineering, Tokyo Institute of Technology, Tokyo.

Tokimatsua, K., Tamurab, S., Suzukia, H., and Katsumata K. 2012. Building damage associated with geotechnical problems in the 2011 Tohoku Pacific earthquake. Soils and Foundations, 52(5): 956-974.

Tremblay, S. P. 2017. Développement d'une procédure non intrusive basée sur la propagation des ondes élastiques pour l'évaluation de l'état des structures en béton enfouis du réseau de distribution d'Hydro-Québec. Ph.D. thesis, Université de Sherbrooke.

Tremblay, S. P., Karray, M., Chekired, M., Bessette, C., & Jinga, L. 2017. Inspection of the lids of shallowly buried concrete structures based on the propagation of surface waves. Journal of Applied Geophysics, 136:19-34.

Tremblay, S. P., Karray, M., Chekired, M., Bessette, C., & Jinga, L. 2018. Inspection of the lids of shallowly buried concrete structures based on the propagation of surface waves-PART II. Journal of Applied Geophysics, 148:55-69.

Tso, W.K., Zhu, T.J., and Heidebrecht, A.C. 1992. Engineering implications of ground motion A/V ratio. Soil Dynamics and Earthquake Engineering 11:133-144.

Tupa, N., Palmeira, E.M. 2007. Geosynthetic reinforcement for the reduction of the effects of explosions of internally pressurised pipes. Geotextiles and Geomembranes Journal, 25(2):109-127.

Tuttle, M., Law, K. T., Seeber, L., and Jacob, K. 1990. Liquefaction and ground failure induced by the 1988 Saguenay, Quebec. Canadian Geotechnical Journal, 27(5): 580-589.

Uenishi, K. and Sakurai, S. 2000. Characteristic of the vertical seismic waves associated with the 1995 Hyogo-kenNanbu (Kobe), Japan earthquake estimated from the failure of the Daikai underground station. Earthquake Engineering and Structural Dynamics, 29(6): 813-822.

Unutmaz, B. 2014. 3D liquefaction assessment of soils surrounding circular tunnels. Tunnelling and Underground Space Technology, 40: 85–94.

USGS. 2010. United States Geological Survey. M5.2 - Ontario-Quebec border region, Canada.

Wang, W.S. 1979. Some findings in soil liquefaction. Water Conservancy and Hydroelectric Power Scientific Research Institute, Beijing, China.

Wang, Z.L. 1990. Bounding Surface Hypoplasticity Model for Granular Soils and Its Applications. Ph.D. Thesis. Faculty of the Graduate School of The University of California, Davis.

Wang, Z.L. 2001. Simulation of Earthquake Performance of a Waterfront Slope Using Fully Coupled Effective Stress Approach. FLAC and Numerical Modelling in Geomechanics, Proceedings of the 2nd International FLAC Conference, Lyon, France, 101-108.

Wang, Z., Lu, Y., Hao, H., and Chong K. 2005. A full coupled numerical analysis approach for buried structures subjected to subsurface blast. Computers and Structures, 83: 339–356.

Wang, K., Brennan, A.J., Knappett, J.A., Robinson, S., and Bengough, A.G. 2018. Centrifuge modelling of remediation of liquefaction-induced pipeline uplift using model root systems. Physical Modelling in Geotechnics, 1265:1270.

Wang, J., Ma, G., Zhuang, H. Dou., Y., and Fu, J. 2019. Influence of diaphragm wall on seismic responses of large unequal-span subway station in liquefiable soils. Tunnelling and Underground Space Technology, 91:102988.

Watanabe, K., Sawada, R., and Koseki, J., 2016. Uplift mechanism of open-cut tunnel in liquefied ground and simplified method to evaluate the stability against uplifting. Soils and Foundations, 56(3): 412-426.

Welsh, J.P. and Burke, G.K. 1991. Jet grouting-uses for soil improvements. Geotechnical Engineering Congress, ASCE Geotechnical Special Publication, 27(1): 334–345.

Welsh, J.P. 1997. State of the art of grouting in North America. Ground Improv., 2(1):11-15.

Wood, J.H. 2004. Earthquake design procedures for rectangular underground structures. Earthquake Commission Research Foundation, EOC Project No .1/470.

Wu, G. 2001. Earthquake-induced deformation analyses of the upper San Fernando Dam under the 1971 San Fernando earthquake. Canadian Geotechnical Journal, 28:1-15.

Wu, J.J., Li, Y., Cheng, Q.G., Wen, H., and Liang X. 2016. A simplified method for the determination of vertically loaded pile-soil interface parameters in layered soil based on FLAC3D. Frontiers of Structural and Civil Engineering, 10(1):103-111.

Xia, Z., YE, G., WANG, J., YE, B., and ZHANG, F. 2010. Numerical analysis on the influence of thickness of liquefiable soil on seismic response of underground structure. J. Shanghai Jiaotong Univ. (Sci.), 15(3): 279-284.

Xie, Q., Da Gama, C., Yu, X., and Chen, Y. 2013. A Parametric Study of Interface Characteristics in a Buttress Retaining Wall. Electronic Journal of Geotechnical Engineering, 18:1477-1492.

Yamaguchi A., Mori T., Kazama M., and Yoshida N. 2012. Liquefaction in Tohoku district during the 2011 off the pacific coast of Tohoku earthquake. Soils and Foundations, 52(5):811-829.

Yang, D., Naesgaard, E., Byrne, P.M., Adalier, K., and Abdoun T. 2004. Numerical model verification and calibration of George Massey Tunnel using centrifuge models. Canadian Geotechnical Journal, 41: 921-942.

Yang, j. and Wang, H. 2012. Seismic response analysis of shallow utility tunnel in liquefiable soils. International Conference on Pipelines and Trenchless Technology (ICPTT): 1606-1618.

Yasuda, S., Tanaka, H., Tatsuta, M., and Yamashita, J. 2004. Several Shaking Table Tests and Analyses on the Effect of Countermeasures by Sheet Piles against Liquefaction-induced Floatation of a Buried Duct, Proc. of 3rd International Conference on Earthquake Geotechnical Engineering, 638-643.

Yasuda, S. 2005. Survey of recent remediation techniques in Japan, and future applications. Journal of Earthquake Engineering, Special Issue, 9(1): 151-186.

Yasuda, S., Verdugo, R., Konagai, K., Sugano, T., Villalobos, F., Okamura, M., Tobita, T., Torres, A., and Towhata, I. 2010. Geotechnical damage caused by the 2010 Maule, Chile earthquake. International Society for Soil Mechanics and Geotechnical Engineering, 4(2): 16-27.

Yoshida, M., Miyajima, M., and Kitaura, M. 2008. Experimental study on mitigation of liquefaction-induced flotation of sewerage manhole by using permeable recycled materials packed in sandbags. The 14th World Conference on Earthquake Engineering, October 12-17, Beijing, China.

Youd, T.L., Idriss, I.M., Andrus, R.D., Arango, I., Castro, G., Christian, J.T., Dobry, R., Finn, W.D.L., Harder, L.F., Hynes, M.E., Ishihara, K., Koester, J.P., Liao, S.S.C., Marcuson, W.F., Martin, G.R., Mitchell, J.K., Moriwaki, Y., Power, M.S., Robertson, P.K., Seed, R.B., and Stokoe, K.H., 2001. Liquefaction resistance of soils: summary report from the 1996 NCEER and 1998 NCEER/NSF Workshops on evaluation of liquefaction resistance of soils. Journal of Geotechnical and Geoenvironmental Engineering, ASCE 127(10): 817-834.

Youd, T. L. and Carter, B.L. 2005. Influence of Soil Softening and Liquefaction on Spectral Acceleration, Journal of Geotechnical and Geoenvironmental Engineering, 131(7): 811-825.

Yue, Q. and Li, J. 2007. Seismic analysis of utility tunnel considering wave passage effect. 4th International Conference on Earthquake Geotechnical Engineering, Paper No. 1369.

Zhai, E., Davis, C. A., Yan, L., and Hu, J. 2014. Numerical simulations of geotechnical centrifuge modelling of seismic earth pressures on an underground restrained structure. Int. Efforts in Lifeline Earthquake Engineering, ASCE, Reston, VA, 369-376.

Zhang, Z. and Chian, S. C. 2019. Importance of sidewall friction on manhole uplift during soil liquefaction. Soil Dynamics and Earthquake Engineering, 119:51–61.

Zheng, G., Yang, P., Zhou, H., Zeng, C., Yang, X., He, X., and Yu, X. 2019. Evaluation of the earthquake induced uplift displacement of tunnels using multivariate adaptive regression splines. Computers and Geotechnics, 113:103099.

Zhou, J., Wang, Z., Chen, X. and Zhang, J. 2014. Uplift mechanism for a shallow-buried structure in liquefiable sand subjected to seismic load: centrifuge model test and DEM modelling, Earthquake Engineering and Engineering Vibration, 13(2): 203–214.

Zhou, J., Jiang, J., and Chen X. 2015. Micro-and macro-observations of liquefaction of saturated sand around buried structures in centrifuge shaking table tests. Soil Dynamics and Earthquake Engineering, 72: 1-11.

Zhuang, H., Hu, Z., Wang, X. and Chen, G. 2015. Seismic responses of a large underground structure in liquefied soils by FEM numerical modelling, Bulletin of Earthquake Engineering, 13:3645–3668.

Zhuang, H., Chen, G., Hu, Z., and Qi, C. 2016. Influence of soil liquefaction on the seismic response of a subway station in model tests. Bulletin of Engineering Geology and the Environment, 75(3):1169–1182.

APPENDIX A

The Novelty of the Study and Feild Application

The thesis presents a particular problem of soil-structure interaction linked to the liquefaction of soils, one of the consequences of which is the risk of uplifting buried structures. The research framework purposes to develop empirical relationships applicable to practice to allow Hydro-Québec, which has many underground electrical chambers, to better design them or to assess whether they risk being damaged by a major earthquake across Quebec. These relationships, based on 3D numerical simulations using software FLAC^{3D}, make it possible to determine the dynamic amplification of shear forces and bending moments according to the value of spectral acceleration. It also analyzed various mitigation methods to reduce the risk of uplift due to liquefaction for such buried structures.

The thesis is clear and original, particularly with regard to the following points:

1. Adopting a new constitutive soil model (energy-based) to simulate soil liquefaction surround the structure using the computer code FLAC;
2. Taking into account the earthquake effect in different seismic zones in Quebec and its influence on the Excess pore-water pressures leading ultimately to the liquefaction of soils and structure uplift;
3. The development of empirical relationships to quantify the dynamic amplification of shear forces and bending moments according to the value of spectral acceleration. These relationships could be readily applicable for the purposes of the preliminary design of underground electrical chambers;
4. The development of an analytical equation to predict the maximum uplift of the underground structure due to soil liquefaction;
5. Analysis of various uplift mitigation methods to counter or limit the structure movement due to soil liquefaction.

APPENDIX B

Numerical Simulation Flow Chart and Liquefaction Code

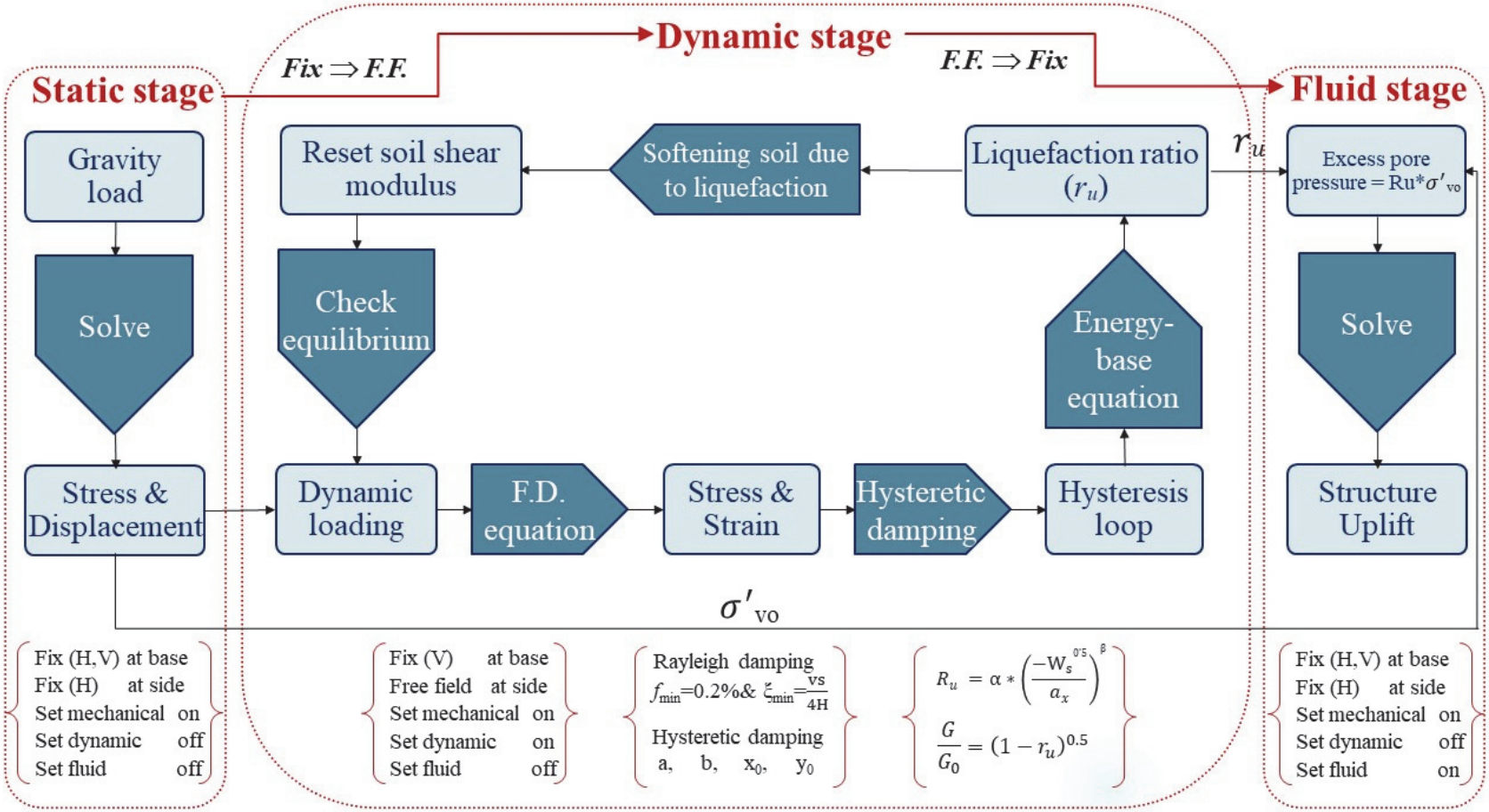

FLAC^{3D} Code to Calibrate the Liquefaction Parameters of the Constitutive Model "Energy-Based Approach" Using Triaxial Simple Shear Test (TxSS).

```
;;;;title "simple shear";;;;;
new
conf dynamic
conf fl
set fish autocreate on
set fish safe on
;;geometry;;
gen zone cylinder  p0(0,0,0) p1(0.315,0,0) p2(0,0,-0.20) p3(0,0.315,0) size 10 5 10 ;r 1.1 1 1
gen zone reflect dd 0 dip 90
gen zone reflect dd 90 dip 90
;;Boundary conditions;;
fix z y range      z 0
fix x y z  range     z -0.20
;;;;;;
apply nstress -0.5e5 range cylinder end1 (0,0,0)  end2  (0,0,-0.20)  radius 0.32 &
cylinder end1 (0,0,0)  end2  (0,0,-0.20)  radius 0.31 not
apply szz -0.5e5 range z 0
apply szz -0.5e5 range z -0.20
;;ini zdis -0.05 grad 0 0 -0.05;range z 0
;;;;;Material & interfaces (first step)
model mech elas
prop bulk 4.5e9 shear 4e7
ini dens 1540
;;;;;
;model fluid fl_iso
;ini sat 1.0
;ini ftens 0
```

```
;prop poros 0.44
;ini fdens 1000
;ini pp 0
;ini fmod 2e9
;;;;;;;
set dy off
set fl off
solve
save static
;;;;;
ini state 0
ini xdis 0 ydis 0 zdis 0
ini xvel 0 yvel 0 zvel 0
set dy on
def init
loop k (1,5)
loop i (1,40)
loop j (1,10)
z=-0.20+0.04*float(k)-0.02
t=2*3.14*float(i)/40-0.0785
r=0.0315*float(b)/10-0.01575
x=r*cos(float(t))
y=r*sin(float(t))
zp0=z_near(x,y,z)
z_extra(zp0,1) = 0 ;;z_sxz(zp0)
z_extra(zp0,2) = 50000 ; z_szz(zp0)+z_pp(zp0)+1
z_extra(zp0,20)= z_extra(zp0,2)
z_extra(zp0,4) = z_pp(zp0)
z_extra(zp0,3) = z_prop(zp0,"shear")
```

```
z_extra(zp0,5)=0.025          ;;;;;;gammamax
end_loop
end_loop
end_loop
end
@init
;;;
ini damp hyst sig4 1 -0.45 -1.925 0.000  ;;;; Hysteretic damp
set dyn damp ray 0.002 2.0  ;;;; Rayleigh damping
;;;; load
def setup
global freq = 0.1 ;Hz
global ampl = 6e3
global omega = 2.0 * pi * freq
end
def wave
wave = ampl* sin(omega * dytime)
;wave = ampl* cos(omega * dytime)
end
apply sxz 1 his @wave range z 0
;apply xvel 1 his @wave range z 0
@setup
;;;;;;;
;table 1 read koba.acc
;apply xvel 0.275 his table 1  range z 0
;;;;;
def tmax
loop nstep (1,5000)
loop k (1,5)
```

```
loop i (1,40)
loop j (1,10)
kk=-0.20+0.04*float(k)-0.02
t=2*3.14*float(i)/40-0.0785
r=0.315*float(b)/10-0.01575
ii=r*cos(float(t))
jj=r*sin(float(t))
zp3=z_near(ii,jj,kk)
global p_gp1 = gp_near(ii, jj, kk)
global p_gp2 = gp_near(ii, jj, kk+0.04)
global zp111 = z_near(0.15,0.15,-5)
xtable(i+100*J+10000*k+1,nstep)=100*((gp_xdisp(p_gp2)-gp_xdisp(p_gp1))/0.04)
z_extra(zp3,15) = abs(xtable(i+100*J+10000*k+1,nstep))        ;;;;;;gamma
ytable(i+100*J+10000*k+1,nstep)=z_sxz(zp3)/50000     ;CSR
z_extra(zp3,6)=(xtable(i+100*J+10000*k+1,nstep)-xtable(i+100*J+10000*k+1,nstep-1))    ;shear strain
z_extra(zp3,7)=((ytable(i+100*J+10000*k+1,nstep)+ytable(i+100*J+10000*k+1,nstep-1))/2) ;shear stress
z_extra(zp3,8) =z_extra(zp3,6)*z_extra(zp3,7)      ;;;; stress*strain
z_extra(zp3,9)= z_extra(zp3,9)+ z_extra(zp3,8)    ;;;; EN SOMME
if z_extra(zp3,9) < 0 then
z_extra(zp3,9)=0
end_if
if z_extra(zp3,15) > z_extra(zp3,14) then
z_extra(zp3,14) = z_extra(zp3,15)
end_if
z_extra(zp3,16)=0.92*((z_extra(zp3,14))^(-0.455))     ;;;;;;;ax
if z_extra(zp3,16) > 2 then
z_extra(zp3,16)=2
end_if
if z_extra(zp3,16) < 0.8 then
```

```
z_extra(zp3,16)=0.8
end_if
z_extra(zp3,10)=( 1.0*((z_extra(zp3,9))^0.5/z_extra(zp3,16))^0.61)    ;;;Ru
if z_extra(zp3,10) > 0.90 then
z_extra(zp3,10)=0.90
end_if
z_prop(zp3,"shear")= z_extra(zp3,5)*((1-z_extra(zp3,10))^0.5)  ;;; soften
if z_prop(zp3,"shear") < 1e6 then
z_prop(zp3,"shear") = 1e6
end_if
z_extra(zp3,11)= z_extra(zp3,4)+(abs(z_extra(zp3,2)*z_extra(zp3,10)))
z_extra(zp3,12)= (abs(z_extra(zp3,2)*z_extra(zp3,10)))
z_extra(zp3,13)=(z_sxz(zp3)-z_extra(zp3,1))
pp111= z_extra(zp111,11)
ru111= z_extra(zp111,10)
prod111= z_extra(zp111,6)
prod112= z_extra(zp111,7)
prod113= z_extra(zp111,8)
prod114= z_extra(zp111,9)
gmax111= z_extra(zp111,14)
g111= z_extra(zp111,15)
ax111= z_extra(zp111,16)
zp3=z_next(zp3)
end_loop
end_loop
end_loop
command
step 100
end_command
```

```
end_loop
end
hist add dytime
hist add zone sxz 0,0,-0
hist add gp xvel 0,0,-0
hist add gp xacc 0,0,-0
hist add fish @ru111
hist add fish @prod111
hist add fish @prod112
hist add fish @prod113
hist add fish @prod114
hist add fish @gmax111
hist add fish @ax111
hist add fish @prod111
hist add fish @prod112
hist add fish @prod113
hist add fish @prod114
hist add fish @g111
his add unbal
@tmax
Save dynamic
```